

CYCLOSTATIONARY SPECTRUM SENSING TECHNIQUES FOR COGNITIVE RADIO

A DISSERTATION

*Submitted in partial fulfillment of the
requirements for the award of the degree
of*

INTEGRATED DUAL DEGREE

(Bachelor of Technology and Master of Technology)

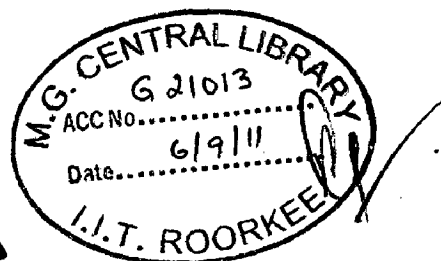
in

ELECTRONICS AND COMMUNICATION ENGINEERING

(With Specialization in Wireless Communication)

By

HEMANT SAGGAR



**DEPARTMENT OF ELECTRONICS AND COMPUTER ENGINEERING
INDIAN INSTITUTE OF TECHNOLOGY ROORKEE
ROORKEE -247 667 (INDIA)**

JUNE, 2011


CANDIDATE'S DECLARATION

I hereby declare that the work presented in this dissertation report entitled, "CYCLOSTATIONARY SPECTRUM SENSING TECHNIQUES FOR COGNITIVE RADIO", towards the partial fulfilment of the requirements for the award of the degree of **Integrated Dual Degree** (Bachelor of Technology and Master of Technology) in Electronics and Communication Engineering with specialisation in **Wireless Communication**, submitted in the Department of Electronics and Computer Engineering, Indian Institute of Technology, Roorkee (INDIA), is an authentic record of my own work carried out during the period from May 2010 to June 2011, under the guidance of **Dr. D.K. MEHRA, Professor, Department of Electronics and Computer Engineering, Indian Institute of Technology Roorkee.**

I have not submitted the matter embodied in this dissertation for the award of any other Degree or Diploma.

Date: 30/6/2011

Place: Roorkee



HEMANT SAGGAR

CERTIFICATE

This is to certify that the above statement made by the candidate is correct to the best of my knowledge.

Date: 30.06.11

Place: Roorkee



Dr. D.K.MEHRA

Professor,

E & C Department,

IIT Roorkee,

Roorkee-247667 (INDIA)

ACKNOWLEDGEMENTS

After undertaking an eventful year long journey of working on the thesis, I would like to congratulate and thank all those who have helped and supported me in the process. First and foremost, I would like to express my deep sense of respect and gratitude towards my guide **Professor Daljit Kumar Mehra**, who has been a consistent source of guidance and motivation for my work. He is a teacher par excellence and his sincerity and knowledge of the subject have always been a source of inspiration for me. I am greatly indebted to him for his constant encouragement and invaluable advice whenever I approached him, and I wish him the very best for future.

I would also like to thank all the faculty of the E&C department who helped me build the foundation of knowledge and indirectly helped my work in many ways. Special thanks are also due to the lab assistants in the signal processing lab for cheerfully bearing with my 'consistent' lab timings.

The pace of this work would have been much slower had all my friends not been there to cheer me and keep a spirit of friendly competition alive. Most of all I would like to thank my mother, father and sister for being a truly loving and understanding family. Finally I thank God for helping to make it all possible.

HEMANT SAGGAR

ABSTRACT

A cognitive radio by virtue of its ability to sense and adapt to the dynamic spectrum scenario, can increase the spectral efficiency. In order to be non-invasive, a cognitive radio must adhere to strict benchmarks in the quality of spectrum sensing for primary users of a band. Thus, spectrum sensing has a major role to play in cognitive radio. Many algorithms have been proposed to enable spectrum sensing such as energy detection and cyclostationary detection. IEEE 802.22, the first standard for cognitive radio devices, imposes strict requirements for the detection and false alarm probability on all spectrum sensing devices at SNR up to -20 dB. This requires use of robust spectrum sensing techniques.

Energy detection is the simplest and near optimum technique that is widely used for spectrum sensing. However, its performance is drastically affected by uncertainty in noise variance due to SNR wall [1]. Cyclostationary detection can exploit spectral correlation present in most modulated signals to reliably detect signals even at low SNR. All general QAM signals exhibit distinct cyclic frequencies depending on their carrier frequency, baud rate etc. which can help to distinguish between the SOI (Signal of Interest) and interference.

The filter structures for optimum MMSE estimation of cyclostationary signals are frequency shift (FRESH) filters. The theory of cyclic Wiener filtering theory, developed by Gardner [2], forms the basis of LCL (Linear Conjugate Linear) filtering used in FRESH filters. By adding appropriately frequency shifted versions of a cyclostationary signal, FRESH filters can provide significant gains for cyclostationary detection. Hence, it is intuitive to apply FRESH filters for spectrum sensing in the cognitive radio context. For upcoming wireless standards like Wi-MAX and LTE, OFDM (Orthogonal Frequency Division Multiplexing) is used because of the advantage of multicarrier transmission. Spectrum sensing for OFDM signals is especially challenging due to the cancellation of cyclostationary features and efficient detection algorithms for OFDM need to be developed.

This thesis presents a comparative analysis between cyclostationary and energy detection and proposes FRESH filter based detection for cyclostationary spectrum sensing, with supporting simulation results. For spectrum sensing in OFDM, it develops an optimal Neyman-Pearson detector for induced cyclostationarity in CP-OFDM and shows that the proposed detector outperforms energy and cyclostationary detection techniques in the detection performance.

LIST OF ABBREVIATIONS

ASIC	Application Specific Integrated Circuit
AWGN	Additive White Gaussian Noise
BA-FRESH	Blind Adaptive Frequency Shift
BPSK	Binary Phase Shift Keying
CAF	Cyclic Autocorrelation Function
CFAR	Constant False Alarm Rate
CP	Cyclic Prefix
CP-OFDM	Cyclic Prefixed Orthogonal Frequency Division Multiplexing
CSD	Cyclic Spectral Density
DOA	Direction of Arrival
DTV	Digital Television
DVB	Digital Video Broadcasting
FDM	Frequency Domain Multiplexing
FRESH	Frequency Shift
IFFT	Inverse Fast Fourier Transform
ISI	Inter Symbol Interference
LMS	Least Mean Squares
LTE	Long Term Evolution
MF	Matched Filter
MMSE	Minimum Mean Square Error
MSE	Mean Square Error
OFDM	Orthogonal Frequency Division Multiplexing
P_d	Probability of Detection
PDF	Probability Density Function

P_f	Probability of False Alarm
PSD	Power Spectral Density
QAM	Quadrature Amplitude Modulation
QPSK	Quadrature Phase Shift Keying
RLS	Recursive Least Squares
ROC	Receiver Operating Curves
SCD	Spectral Correlation Density
SCF	Spectral Correlation Function
SNR	Signal to Noise Ratio
SOI	Signal of Interest
WiMAX	Worldwide Interoperability for Microwave Access
WLAN	Wireless Local Area Network
R_{xx}^α	Cyclic Autocorrelation Function of x at cyclic frequency α
$R_{xx}^{\alpha*}$	Conjugate Cyclic Autocorrelation Function of x at cyclic frequency α
S_{xx}^α	Cyclic Spectral Density of signal x at cyclic frequency α
$S_{xx}^{\alpha*}$	Conjugate Cyclic Spectral Density of signal x at cyclic frequency α
$g(t)$	Pulse Shaping Waveform
N_c	Number of subcarriers in OFDM
α	Cyclic Frequency
σ_x^2	Variance of x

LIST OF FIGURES

- Figure 1.1: Dynamically changing spectrum scenario for a cognitive radio with black dots representing spectrum opportunities [3].
- Figure 1.2: The cognition cycle [4].
- Figure 2.1: ROC curves for energy detection for different SNR and N (number of samples).
- Figure 2.2: SNR walls in energy detection for noise uncertainty of 1 dB, 0.1 dB and 0.01 dB ($P_f=0.1$, $P_d=0.9$).
- Figure 2.3: Plot of cyclic spectral density of BPSK signal versus α and f/f_s .
- Figure 2.4: Plot of conjugate cyclic spectral density of BPSK signal versus α and f/f_s .
- Figure 2.5: Cyclic autocorrelation function of BPSK signal.
- Figure 2.6: Conjugate cyclic autocorrelation function of BPSK signal.
- Figure 2.7: Alpha profile of BPSK signal.
- Figure 2.8: Variation of false alarm probability with threshold λ for cyclostationary detection.
- Figure 2.9: Comparison of probability of detection curves of cyclostationary detection, energy detection, and energy detection with 1dB noise uncertainty for 800 received samples of BPSK signal.
- Figure 3.1: Structure of a LCL FRESH filter.
- Figure 3.2: Structure of an adaptive FRESH filter using LMS algorithm.
- Figure 3.3: Structure of a blind adaptive FRESH filter.

- Figure 3.4: Two branch blind adaptive FRESH filter.
- Figure 3.5: Time averaged MSE of the two branch LMS blind adaptive FRESH filter.
- Figure 3.6: Six branch blind adaptive FRESH filter.
- Figure 3.7: Comparison of time averaged mean square error for the six branch and two branch LMS blind adaptive FRESH filter for three values of step size μ .
- Figure 3.8: Comparison of probability of detection curves for different techniques with $N=400$ samples.
- Figure 3.9: Comparison of probability of detection curves for different techniques with $N=800$ samples.
- Figure 3.10: Comparison of probability of detection curves for different techniques with $N=1600$ samples.
- Figure 3.11: Comparison of probability of detection curves for different techniques with $N=3200$ samples.
- Figure 3.12: Comparison of probability of detection curves for different techniques with 0dB interference.
- Figure 3.13: Comparison of probability of detection curves for FRESH filter based detection in AWGN with 800 samples and with BPSK interference at 0dB INR with 30800 samples.
- Figure 4.1: OFDM transmitter and receiver block diagram.
- Figure 4.2: Theoretical probability of detection curves for energy detection with $N=400$ samples.
- Figure 4.3: Normalised CAF of an OFDM signal at lag 1.
- Figure 4.4: Normalised CAF of a CP-OFDM signal at lag 64.

- Figure 4.5: Normalised CAF of an OFDM signal using time domain rectangular pulses.
- Figure 4.6: Normalised CAF of an OFDM signal at lag 1 using RC shaping with 100% excess bandwidth.
- Figure 4.7: Normalised CAF of a CP-OFDM signal at lag 64 using RC pulse shaping with 100% excess bandwidth.
- Figure 4.8: FRESH filter to detect an RC shaped CP-OFDM signal with $1/T=640$ Hz.
- Figure 4.9: Comparison of probability of detection curves for cyclostationary detection and FRESH filter based detection for $N=3200$ samples.
- Figure 4.10: Comparison of probability of detection curves for cyclostationary detection and FRESH filter based detection for $N=6400$ samples.
- Figure 4.11: Comparison of probability of detection curves for cyclostationary detection and FRESH filter based detection for $N=9600$ samples.
- Figure 4.12: Generation of induced cyclostationarity in OFDM by mapping of subcarriers.
- Figure 4.13: Normalised CAF for OFDM signal with induced cyclostationarity at $p/T_s = 24300$ Hz.
- Figure 4.14: Comparison of probability of detection curves for energy detection and optimal detectors for cyclic prefix and induced cyclostationarity in CP-OFDM for 400 samples and $M=3$.
- Figure 4.15: Comparison of probability of detection curves for energy detection and optimal detectors for cyclic prefix and induced cyclostationarity in CP-OFDM for 400 samples and $M=5$.

CONTENTS

CANDIDATE'S DECLARATION	i
CERTIFICATE	i
ACKNOWLEDGEMENTS	ii
ABSTRACT	iii
LIST OF ABBREVIATIONS	iv
LIST OF FIGURES	vi
Chapter 1: Introduction	1
1.1. Cognitive Radio.....	1
1.1.1. Issues in Cognitive Radios	4
1.2. Spectrum Sensing Techniques.....	7
1.3. FRESH Filters	8
1.4. Motivation and Problem Statement	9
1.5. Organisation of the report.....	10
Chapter 2: Spectrum Sensing Techniques	13
2.1. Energy Detection	14
2.1.1. Effect of Uncertainty in Noise Variance	19
2.2. Cyclostationary Signal and its Properties.....	21
2.2.1. Cyclostationarity in Digital Modulated Signals	23
2.2.2. Simulation Example 1: Cyclostationarity in BPSK	24
2.3. Cyclostationary Spectrum Sensing.....	28
2.3.1. Simulation Example 2: Comparison of Cyclostationary & Energy Detection..	31
Chapter 3: FRESH (Frequency Shift) Filters For Spectrum Sensing	35

3.1. Cyclic Wiener Filtering	36
3.2. Adaptive Fresh Filters	41
3.2.1. LMS Adaptive FRESH Filter	41
3.2. Blind Adaptive FRESH Filter	42
3.3. FRESH filter based Spectrum Sensing	44
3.3.1 Signal Detection	44
3.3.2 Spectrum Sensing	49
3.3.3 Signal Detection with Interference Signal Present.....	54
Chapter 4: Spectrum Sensing for OFDM signals.....	57
4.1 Orthogonal Frequency Division Multiplexing (OFDM)	58
4.2 Energy Detection	59
4.3 Cyclostationary Detection	62
4.3.1. Excess Bandwidth	65
4.4 FRESH Filter based Detection	68
4.5 Induced Cyclostationary Detection	71
4.5.1. Induced Cyclostationarity	72
4.5.2. Optimal Detector for Induced Cyclostationarity in OFDM	75
4.5.3. Simulation Results for Optimal Detection in OFDM.....	80
Chapter 5: Conclusion and Future Work.....	83
Appendix A: Cyclic Frequencies in Digital Modulated Signals.....	87
Appendix B: Derivation of the Co-variance Matrix of the Optimum Detector for Induced Cyclostationarity in CP-OFDM.....	91
Bibliography	95

Chapter 1

Introduction

The 7th of September 1987 is a day in the history of wireless communication that charted its future for decades to come. It was on this day that the European Union approved the introduction of a unified system for communication codenamed GSM(Global System for Mobile Communications), a technology that spearheaded the development of wireless services and devices, and exposed us to the immense opportunities and concomitant challenges that lay in harnessing its potential for future. Starting from the need to communicate information over a long range, our needs in the present day have risen exponentially to include voice, data and multimedia communication. This spiralling need has imposed an immense pressure on a precious resource, the radio spectrum. While this has led to many frequency bands being overused, such as the ISM band, studies [5] suggest that many frequency bands remain underutilized i.e. they remain free from their primary users for a substantial amount of time. This opportunity can be exploited to serve the growing demand for spectrum by allowing unlicensed users to transmit their own data on licensed bands with the precondition that the quality of service (QoS) of primary transmission is not compromised in any way. Such kind of opportunistic spectrum access forms the basis of a *cognitive radio*.

1.1. Cognitive Radio

Joseph Mitola coined the term ‘Software Defined Radio’, while pursuing his doctoral dissertation work at KTH Sweden in 2000 [6]. He called these radios up to 80% programmable beyond the antenna output terminals and thus capable of doing RF, IF, baseband and bitstream operations using high speed Analog to Digital to Analog (A/D/A) converters and microprocessors. Subsequently he extended the concept of a Software Radio to ‘Cognitive Radio’ [7],[8] as follows,

“ (A cognitive radio is) a radio frequency transceiver designed to intelligently detect whether a particular segment of the radio spectrum is in use, and to jump into (and out of) the

temporarily unused spectrum very rapidly, without interfering with the transmission of other authorized users”.

Such an intelligent radio would be able to learn about the network condition and structure. It could detect unused frequency bands and allow unlicensed to opportunistically access licensed bands without causing any interference to the primary user. This would intuitively improve the spectrum utilization. In the terminology of cognitive radio, users who do not have not obtained prior permission for accessing a band are referred to as secondary users while the authorized users of a band are called primary users. Studies have suggested that while most frequency bands are licensed to primary users, many of these like military, marine communication, amateur radio etc. remain highly underutilized giving rise to a virtual scarcity in spectrum [5]. Fuelled by such revelations along with exponentially increasing number of wireless devices in the market like cordless telephones, remote surveillance cameras, the interest in cognitive radios has been growing at an amazing pace. Cognitive radios require unlicensed users who want to use the licensed bands opportunistically, to be highly adaptive in their parameters like frequency of operation, modulation technique, power allocation etc. Figure 1.1 shows the opportunistic scenario in which a cognitive user operates.

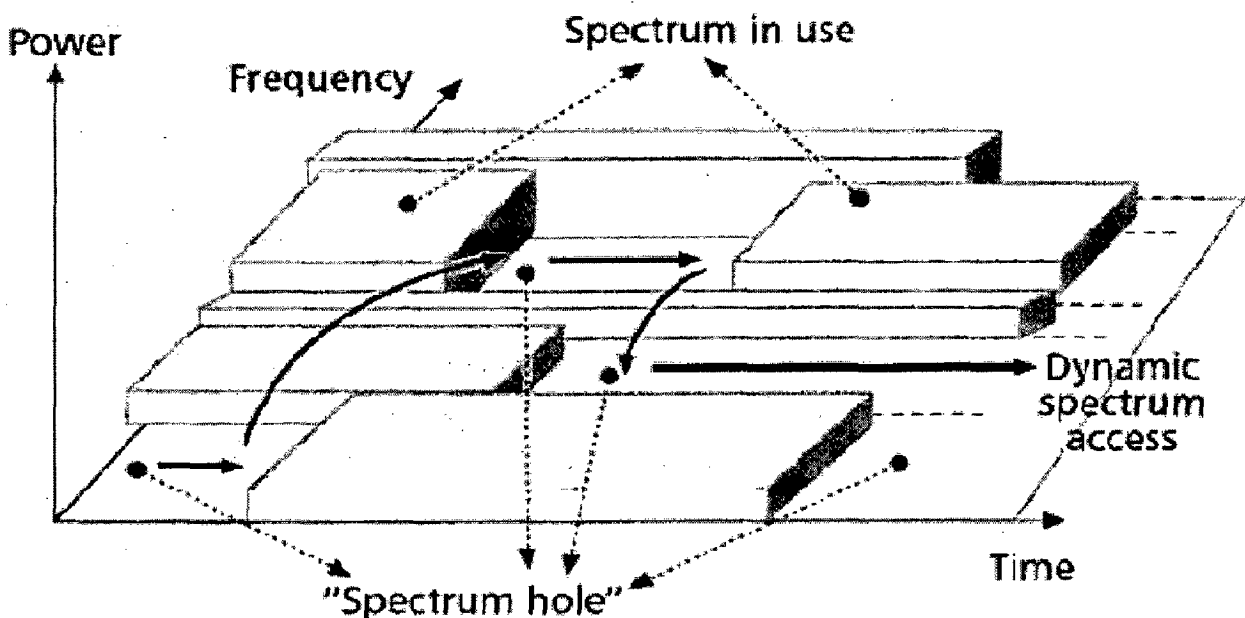


Figure 1.1: Dynamically changing spectrum scenario for a cognitive radio with black dots representing spectrum opportunities [3].

Haykin [4] states that a Cognitive Radio has to perform three basic tasks as listed below.

- (1) Radio-scene analysis: This consists of two main tasks, namely,
- Estimation of interference temperature of the radio environment;
 - Detection of spectrum holes.

The interference temperature in a band is a measure of the total RF interference present at the receiver with no primary signal present. This helps define a limit on the maximum interference power a band can accommodate without adversely affecting the primary transmission. Following the measurement of interference temperature, the RF spectrum is categorized as either *white* or *black* depending on whether it is occupied by high power signals or contains only ambient noise signals. This categorization may be performed through many methods such as the MTM-SVD (Multi Taper Method Singular Value Decomposition) [9], energy detection [10], and cyclostationary detection [11]. A *white* spectrum signifies a spectrum opportunity. This task of detecting *spectrum holes* or vacant spaces in the spectrum is called *Spectrum Sensing*.

- (2) Channel identification: This consists of the following two tasks, namely,
- Estimation of channel-state information(CSI)
 - Prediction of channel capacity for use by the transmitter.

Channel state information can be estimated at the receiver by using pilot transmission or semi-blind approaches. Subsequently the channel coefficients must be tracked at the receiver through a mathematical model such as Kalman or particle filter. The estimate of CSI must be fed back to the transmitter to enable adaptive modulation.

- (3) Transmit power control and dynamic spectrum management: Once the spectrum holes have been identified and their CSI estimates are available, a cognitive radio transmitter must choose its transmission bands accordingly and dynamically adjust them as and when the RF scenario changes. It also needs to optimise the transmit power in each band, in sync with the interference temperature limit for that band.

While the first two tasks are performed by the cognitive receiver, the third is performed at the transmitter. Figure 1.2 shows the different stages of cognitive cycle emphasizing the role of a feedback channel from the receiver to transmitter for conveying various channel parameters.

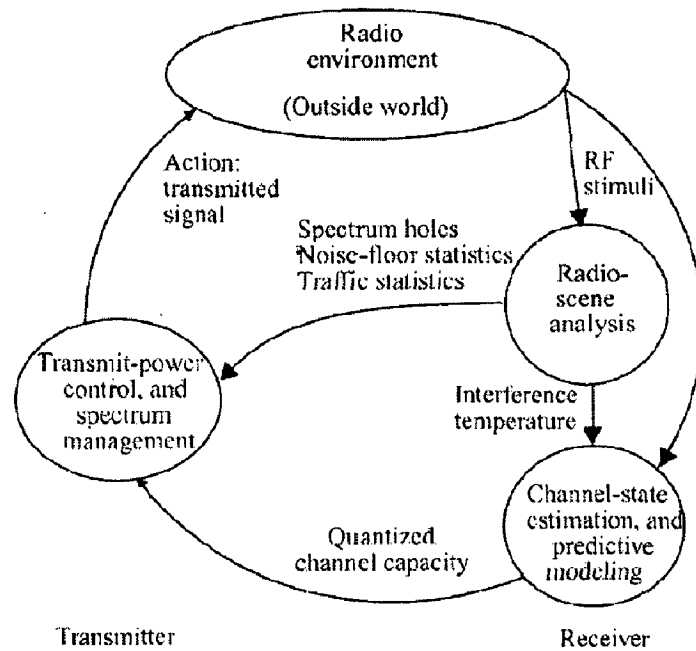


Fig. 1.2: The cognition cycle [4]

1.1.1. Issues in Cognitive Radios

A cognitive radio must be adaptive, reconfigurable, intelligent and flexible enough to detect different kinds of primary transmissions like BPSK, QPSK, and QAM and also switch between them as the channel conditions demand. Because the location of *spectral holes* in frequency and time is continuously changing a cognitive radio must have the ability to selectively transmit on any given set of frequency bands from a wideband range as the primary transmission requires. In this context, OFDM (Orthogonal Frequency Division Multiplexing) is a multi carrier modulation technique that lends itself naturally to such adaptive modulation. OFDM offers the ability to selectively modulate those subcarriers with data where a spectral hole is currently available while leaving other subcarriers untouched. It is also possible to use *bit-loading* in OFDM by which the bit-rate for a specific subcarrier can be optimised according to its SNR [4]. OFDM has already been adopted as the PHY layer for many kinds of standards eg.DVB, DAB, IEEE 802.11a/g/n WLAN standards and the 802.16 Wi-MAX standard.

Reliable detection of spectrum holes, or spectrum sensing, is currently a major challenge for cognitive radios because of its overarching need in implementing a secondary system with a pre-existing legacy system without harming the latter. The following text presents briefly the major issues that are pertinent to cognitive radio.

Spectrum Sensing

Spectrum sensing is the task of obtaining awareness about spectrum usage and the presence of primary users in a given geographical area. This may be accomplished using geo-location database, beacons or local spectrum sensing at the cognitive radios. Although spectrum sensing is traditionally understood as measuring the signal energy present over the spectrum, in the context of cognitive radios it assumes a much bigger and challenging role that includes information about what kind of signals occupy the spectrum including their modulation, carrier frequency, bandwidth etc. To optimally utilize spectrum opportunities, spectrum sensing may be performed across multiple dimensions like time, frequency, code and angle. Since a high QoS (Quality of Service) must be maintained for the primary user, simultaneously achieving a high channel capacity for secondary user requires robust spectrum sensing techniques. Transmissions in licensed bands are normally subjected to interference from adjacent bands, other secondary devices and ultra wideband devices etc. [12]. Additionally, the primary signal may be subjected to fading or shadowing [13] causing its SNR to drop below 0dB. Hence, reliable spectrum sensing at low SNR regimes becomes a necessity. In terms of hardware, this means that a substantial dynamic power detection range of the sensing device should be present to detect both low and high power primary users. There must be a continuous monitoring of the spectrum and fast adaptive capability. This requires wideband and high sampling rate (few Gbps) ADC/DAC's [14] and computationally fast DSP/FPGA's. Some of the commercially available hardware and software platforms for the cognitive radio are the GNU Radio [15], Universal Software Radio Peripheral (USRP) [16] and Shared Spectrum's XG Radio [17].

Transmit Power Control

The transmit power control problem for a multiuser scenario can be stated as [4]: *Given a limited number of spectrum holes, select the transmit power levels of n un-serviced users so as to jointly maximize their data-transmission rates, subject to the constraint that the interference-temperature limit is not violated.*

The solution to this problem is not as direct as it looks because increasing transmit powers of an un-serviced user increases the interference to all other users and may violate the interference temperature limit. The solution lies in a trade-off between data rates and residual

interference. Haykin in [4] models this situation as a non-cooperative game and applies the Nash Equilibrium and iterative water filling algorithm to derive a solution close to optimum.

Dynamic Spectrum Management

Dynamic spectrum management concerns the development of an effective strategy for efficient utilization of the RF spectrum. Its function is to build on the spectrum holes detected by the radio-scene analyzer and the output of transmit-power controller by selecting a modulation strategy that adapts to the time-varying conditions of the radio environment assuring reliable communication across the channel. Spectrum management is a holistic term that is sometimes defined so as to include a gamut of activities that enable the operation of a cognitive radio from spectrum sensing to spectrum decision and spectrum mobility. It involves characterizing each available spectrum hole using parameters like SNR, interference at the physical layer and link errors and RTT (Round Trip Time) etc. at higher layer. Because cognitive user is only a visitor to a licensed band, different layers of the cognitive radio must be able to adapt to what is called *spectrum handoff* [3]. Dynamic spectrum management also decides how cognitive radio nodes can communicate through ad-hoc channels or a cognitive radio network to share spectrum information.

Spectrum Sharing

Different spectrum sharing techniques have been proposed in literature based on four main principles viz. *architecture, spectrum allocation behaviour, spectrum access technique, and scope* [3]. Multiple-user spectrum access needs a co-ordinated mechanism to avoid collision and centralised spectrum sharing architecture has been proposed for this [18]. Distributed spectrum sharing has also been proposed wherein each sensing node takes an independent decision. For allocating a chunk of spectrum among multiple users, co-operative sharing techniques can be used where allocation and interference data is shared among independent nodes. On the other hand, in scenarios of non-cooperative and competitive users, game theory is being applied to model the intelligent behaviour of selfish users and find the self-forcing equilibrium point of operation. Depending on the spectrum access methodology, a cognitive radio may operate in the overlay or the underlay mode, both of which pose different challenges to spectrum sharing. Finally, available spectrum may be shared among cognitive users of a single network or across multiple networks [3].

1.2. Spectrum Sensing Techniques

Many techniques have been proposed in the literature to meet the challenging need of spectrum sensing namely energy detection, cyclostationary detection and matched filter detection etc. Energy detection [10][19][20] is one of the simplest technique due to its least computational complexity. An energy detector measures the RF energy present in a frequency band and compares it with the incumbent noise level in the band to give its sensing decision. As a result, it requires no prior knowledge of the primary signal's characteristics like modulation, carrier frequency etc. and it has been shown that energy detection is the optimal detection scheme for signals with no correlation structure when the false alarm rate must be limited [21]. But it suffers from many shortcomings, for e.g., the detection threshold for a CFAR (Constant False Alarm Rate) test is highly susceptible to changes in noise power. Subtle variations in the noise power or slight error in its estimation can make the energy detector highly non-robust [22]. Moreover an energy detector cannot differentiate between primary signal, noise and interference and at low SNR/SIR they can get easily confused leading to significant drop in detection rates. Also they do not work well for spread spectrum signals as the power spectrum of a spread spectrum signal is quite low [14].

The optimum detector for any signal is a matched filter (MF) but the complexity of implementing a matched filter receiver becomes prohibitively large given the fact that a cognitive receiver needs to implement a MF for each kind of primary signal, leading to a large implementation complexity [13][14]. Additionally, a MF must demodulate the received signal which requires perfect knowledge of the primary users signalling features such as bandwidth, operating frequency, modulation type and order, pulse shaping, and frame format. Co-operative spectrum sensing has also been proposed wherein multiple spatially separated sensing nodes can share their sensing decisions and overcome problems of shadowing and fading [13].

Cyclostationary spectrum sensing [11][13] exploits the periodic correlation in signals introduced during modulation onto binary pulses or carrier waves. Each class of modulated signals possesses second order wide sense cyclostationarity, meaning thereby, that their autocorrelation is periodic in time with certain period T [2] in contrast to wide sense stationary signals, whose mean and autocorrelation are independent of time. This periodicity can be translated into a distinct peak in the *Cyclic Autocorrelation Function* and *Spectral Correlation Density* of the signal at a *cyclic frequency* α directly related to period of

repetition T . This unique signature enables us to separate signals from stationary noise. Moreover, cyclostationary spectrum sensing can differentiate a desired signal, white noise and spectrally overlapping interference as they exhibit different cyclic frequencies and hence unlike energy detection, it can function robustly under high interference (low SINR) and fading scenarios. In practice, there are a limited number of licensed transmissions over a given spectral range having known bandwidth and carrier frequencies, for example, transmissions in TV bands. Thus, a prior knowledge of the signal periodicities can be assumed to be available. Some of the recent works on cyclostationary spectrum sensing are Poor et al. [12] where the authors use cyclostationarity based test statistic along with node collaboration to detect an OFDM signal. Authors in [23] use neural network based training with cyclic feature vectors for signal classification.

Though the advantage of modelling many signals as cyclostationary as an alternative to stationary signals was established in the late 1960's by L.E. Franks, it was not until the early 1990's that cyclostationary sensing received considerable attention when Gardner, Spooner and others discovered the application of cyclostationarity to the problems of detection, modulation recognition, DOA estimation and blind adaptive filtering [24]. Gardner in particular pioneered the non-stochastic or time series approach to analyse cyclostationary signals. Another major discovery by him was that linear time variant adaptive filtering could be used to optimally estimate a cyclostationary signal initiating a new field of filtering called Cyclic Wiener filtering [2]. He called these filters FRESH (FREquency SHift) filters and mathematically derived their governing equations and mean square error performance while estimating different cyclostationary signals [2].

1.3. FRESH Filters

FRESH (FREquency SHift) filters is a name given to linear time variant adaptive filters that can optimally detect a cyclostationary signal using its periodic correlation feature. As the name suggests these filters consist of a number of frequency shift branches followed by a LTI filter. For polyperiodic cyclostationary signals, each branch shifts the signal by a unique frequency and the outputs of all branches are summed up. Since cyclostationary signals are spectrally correlated, adding appropriately frequency shifted and filtered versions of a signal, improves the signal strength. Frequency shift filters can separate signals overlapping in time and frequency by using a non-overlapping part of the spectrum to cancel out a correlated part in the spectrum which is corrupted by interference. Thus by a series of operations of

frequency shifting and complex weighting a signal, two or more spectrally overlapping signals can be separated. It is also intuitive that adaptive implementations of these filters using LMS /RLS algorithms are possible. Gardner in [2] shows that trained FRESH filters can attain a low MSE in the presence of interference. The performance of a FRESH filter depends on the specific type of signal it is used to detect and the strength of cyclostationarity in the signal. It can be proved that a linear periodically time-variant filter that optimally estimates a cyclostationary signal is equivalent to a frequency shift filter [2]. The general form of FRESH filtering in time domain is given by

$$y(t) = \sum_{\eta} h_{\eta}(t) \otimes x_{\eta}(t) \quad (1.1)$$

where $h_{\eta}(t, u)$ is the Fourier coefficient of the periodic time varying impulse response $h(t, u)$ of the filter and $x_{\eta}(t)$ and $y(t)$ are the frequency shifted input $x_{\eta}(t) \triangleq x(t) \exp(i2\pi\eta t)$ and output signals respectively. This operation can be represented in the frequency domain as

$$Y(f) = \sum_{\eta} H(f) X_{\eta}(f) \quad (1.2)$$

Thus, the input is subjected to a number of frequency-shifting operations, each followed by a linear time invariant filtering operations and the results are added together. FRESH filters have till now been used for estimating signals such as BPSK and QPSK and separating multiple interfering signals with overlapping spectrum [2]. Authors in [25] use FRESH filters to detect a desired user in a multi user DS-CDMA scenario and show the observed SNR improvement at the output. Another work is [26], where the authors consider FRESH filters to detect BPSK signals with varying level of spectral interference. But till date to the best knowledge of the author, no work has been reported on the application of FRESH filtering for spectrum sensing of primary signals in cognitive radios. Cyclostationary spectrum sensing is much more robust at low SNR than energy detector under practical conditions and FRESH filters can potentially be used to reconstruct the primary signal.

1.4. Motivation and Problem Statement

Robust spectrum sensing at low SNR is a necessity that the computationally simple technique of energy detection cannot achieve, due to noise uncertainty and its inability to differentiate between desired and interference signals. As most practical signals being used, possess

cyclostationary features which can be potentially used to detect their presence, cyclostationary spectrum sensing can offer better detection of desired signal that will satisfy the strict performance constraints placed on cognitive devices. Since FRESH filters provide blind estimation of cyclostationary signals, therefore, it is intuitive to study their performance when applied to spectrum sensing. Additionally, an important aspect of this dissertation is to study spectrum sensing techniques for OFDM. This dissertation work aims to consider the following,

- A comparative analysis of different spectrum sensing techniques proposed in literature for cognitive radios and evaluation of their performance through simulation.
- Use cyclostationary features in signals for spectrum sensing, apply FRESH filters for signal detection and evaluate and compare its performance with the energy and cyclostationary techniques.
- Explore application of the aforementioned techniques to spectrum sensing in OFDM.

1.5. Organisation of the report

Chapter 2 provides a review of the two major spectrum sensing techniques proposed in literature viz. energy detection and cyclostationary spectrum sensing. It presents theoretical background on the development of both techniques and presents simulation results to show the corresponding average detection probabilities achieved at different SNR. The chapter also presents descriptive simulation examples verifying the presence of cyclic features in modulated signals and concludes by showing the advantage of cyclostationary spectrum sensing over energy detection in detecting signals at low SNR.

Chapter 3 discusses the theory of optimal frequency shift filtering of cyclostationary signals developed by Gardner [2] and presents the structure of FRESH filter and its adaptive implementations. It presents application of FRESH filters to detect a BPSK signal in the presence of noise/interference. Plots for average detection probability achieved at different SNR in AWGN and interference scenarios are presented, and conclusions on the selective advantages of using FRESH filters and the conditions necessary for them to work are given.

In chapter 4, we discuss the application of energy detection, cyclostationary detection and frequency shift filtering to OFDM. Specifically the effect of subcarrier orthogonality on cyclostationarity in OFDM is discussed and the need for cyclic prefix and Excess Bandwidth (EBW) for signal detection is presented. To enable robust spectrum sensing, we introduce

induced cyclostationarity in the cyclic OFDM signal and develop an optimal Neyman-Pearson detection algorithm for the induced features. Finally, the chapter presents simulation results to show that the proposed detector outperforms the energy detector and optimal time domain cyclostationary detector for cyclic prefixed OFDM signal.

Chapter 5 presents the conclusion of the thesis and areas of future work.

Chapter 2

Spectrum Sensing Techniques

Any cognitive radio must be able to reliably sense the presence of unused spectrum resource which could be opportunistically used for unlicensed transmission and concurrently also protect any incumbent licensed user from harmful interference. This necessitates that a cognitive user follow a listen-before-talk protocol. Such a protocol apart from setting up a definite framework for unlicensed access, would also lay down strict regulations on the QoS (Quality of Service) that must be met. The QoS in a cognitive radio's context depends on parameters like probability of detection promised to the primary user, rate of sensing to detect an upcoming in-band primary user (how often is sensing performed), the duration of sensing and the response time for *spectrum handoff* in case a primary user is detected, among others. The first global standard to legalise operation of cognitive devices IEEE 802.22 [27] in TV white spaces has specified strict constraints on all the above-mentioned parameters that all cognitive devices need to adhere to. It states that all such devices will provide $P_d > 0.9$ & $P_f < 0.1$. It also states that all DTV signals of RSS (Received Signal Strength) greater than -116dBm and all wireless microphone signals above -107dBm must be detected. While the maximum detection time for an upcoming in-band primary user is around 1 minute in case of DTV signals, for the low power wireless microphone signals that operate in the same frequency band, that threshold is set at 0.5-2 sec. Robust spectrum sensing at such low signal levels in a short time requires efficient spectrum sensing techniques. In the following sections, we consider energy detection technique, its mathematical model and its detection performance under low SNR regime. We also point out the failures of energy detector due to the phenomenon of SNR wall. Following this, sensing using cyclostationary detection is discussed and its mathematical background is presented along with simulation examples. It is shown that cyclostationary detection is more robust than energy detection.

2.1. Energy Detection

Energy detection is the simplest technique in terms of implementation complexity. It detects the presence of a signal by measuring the total incumbent energy in the band of interest and comparing it to a predefined threshold. This threshold must be decided in a manner, so as to limit the false alarm rate, and it can be set independent of the transmitted signal energy. Once the noise and signal variance are known, the problem of spectrum sensing can be formulated as a binary hypothesis testing problem. Using the complex baseband model of band-pass signal transmission, the received and transmitted signals are represented by their complex low-pass equivalents. The two hypotheses may be formulated as follows:

$$\begin{aligned} H_0 : y[n] &= w[n], \\ H_1 : y[n] &= s[n] + w[n]. \end{aligned} \quad (2.1)$$

where $y[n]$ is the received sample, $w[n]$ is an AWGN sample with variance σ_w^2 and $s[n]$ is the transmitted signal value. At the receiver the test statistic used is defined as the energy of N received samples.

$$\begin{aligned} \mathbb{E} &= \sum_{i=1}^N |y[i]|^2 \\ &= \sum_{i=1}^N |y_R[i]|^2 + |y_I[i]|^2 \end{aligned} \quad (2.2)$$

where N is the number of complex observation samples and $y_R[i]$ & $y_I[i]$ denote the real and imaginary parts of $y[i]$ each having a variance of $\sigma_w^2 / 2$. Under both the hypotheses, the test statistic \mathbb{E} is a sum of squares of $2N$ real Gaussian random variables with the equal variance. Hence the distribution of the random variable \mathbb{E} is the chi-square distribution with a non-centrality parameter=0 under H_0 and 2γ under H_1 .

$$\mathbb{E} = \begin{cases} \chi_{2N}^2 & , H_0 \\ \chi_{2N}^2(2\gamma) & , H_1 \end{cases} \quad (2.3)$$

where γ is the average SNR given by $\gamma = \frac{P}{\sigma_w^2}$ & $P = \frac{1}{N} \sum_{i=1}^N |s[i]|^2$. The probability of detection and false alarm are defined as,

$$\begin{aligned}
P_f &= \Pr\{\mathbb{E} > \lambda \mid H_0\} \\
P_d &= \Pr\{\mathbb{E} > \lambda \mid H_1\}
\end{aligned} \tag{2.4}$$

There are two ways of obtaining closed form expressions for these probabilities. The first, which is through direct integration of the chi-square distribution over the tail of the distribution function giving us the following results [28],

$$\begin{aligned}
P_f &= \frac{\Gamma(N, \frac{\lambda}{2})}{\Gamma(N, 0)}, \\
P_d &= Q_N(\sqrt{2\gamma}, \sqrt{\lambda}).
\end{aligned} \tag{2.5}$$

where $\Gamma(\cdot, \cdot)$ is the incomplete Gamma function given by $\Gamma(s, x) = \int_x^\infty t^{s-1} e^{-t} dt$ and $Q_M(\cdot, \cdot)$ is the generalized Marcum Q- function given by $Q_M(\alpha, \beta) = \frac{1}{\alpha^{M-1}} \int_\beta^\infty x^M e^{-(x^2 + \alpha^2)/2} I_{M-1}(\alpha x) dx$ where $I_n(x)$ is the modified Bessel function of the first kind [29]. Another way of computing the probabilities in (2.4) is through application of the Central Limit theorem assuming that the number of samples in question (N) is high, in which case the resultant distribution becomes normal and hence expressions for P_d and P_f can be obtained by finding the area under the Gaussian tail for which standard expression are available in terms of Q-function. We first find the probability values assuming that N real samples $y(n)$ are being used for energy detection. For the case of complex samples we will consider it as a special case of energy detection in real samples. Under this assumption, the mean of test statistic \mathbb{E} under the hypotheses H_0 and H_1 can be found mathematically by observing the equation (2.2) and (2.1). The mean values are given by $\mu_0 = N\sigma_w^2$ and $\mu_1 = N(\sigma_w^2 + P)$. To find the variance of \mathbb{E} under H_0 , we compute the following,

$$\begin{aligned}
E\{\mathbb{E}^2\} &= E\left\{\left(\sum_{i=1}^N |w(i)|^2\right)\left(\sum_{j=1}^N |w(j)|^2\right)\right\}, \\
&= \sum_{k=1}^N E\{|w(k)|^2 |w(k)|^2\} + E\left\{\sum_{i=1}^N \sum_{j=1}^{N-1} |w_i(n)|^2 |w_j(n)|^2\right\}, (i \neq j) (k \text{ is any integer}) \\
&= N \times E\{|w(n)|^4\} + N \times (N-1) E\{|w(i)|^2 |w(j)|^2\}, (i \neq j) \\
&= 3N\sigma_w^4 + N^2\sigma_w^4 - N\sigma_w^4, \\
&= 2N\sigma_w^4 + N^2\sigma_w^4. \\
\sigma_0^2 &= E\{\mathbb{E}^2\} - E\{\mathbb{E}\}^2, \\
&= 2N\sigma_w^4 + N^2\sigma_w^4 - N^2\sigma_w^4, \\
&= 2N\sigma_w^4.
\end{aligned} \tag{2.6}$$

Through a similar analysis assuming independence of the signal and noise samples, the variance of the test statistic under H_1 can be derived as $\sigma_1^2 = 2N(\sigma_w^2 + P)^2$. Using these expressions in the integral of Gaussian function from λ to infinity and using

$Q(x) = \frac{1}{\sqrt{2\pi}} \int_x^\infty e^{-x^2/2} dx$, we get the following,

$$\begin{aligned}
P_f &= \frac{1}{\sqrt{2\pi\sigma_0^2}} \int_\lambda^\infty e^{-\frac{(x-\mu_0)^2}{2\sigma_0^2}} dx \\
&= Q\left(\frac{\lambda - \mu_0}{\sqrt{\sigma_0^2}}\right) \\
&= Q\left(\frac{\lambda - N\sigma_w^2}{\sqrt{2N\sigma_w^4}}\right), \\
P_d &= \frac{1}{\sqrt{2\pi\sigma_1^2}} \int_\lambda^\infty e^{-\frac{(x-\mu_1)^2}{2\sigma_1^2}} dx \\
&= Q\left(\frac{\lambda - \mu_1}{\sqrt{\sigma_1^2}}\right) \\
&= Q\left(\frac{\lambda - N(\sigma_w^2 + P)}{\sqrt{2N(\sigma_w^2 + P)^2}}\right).
\end{aligned} \tag{2.7}$$

where λ is the threshold to be calculated. Now, when the incoming samples are complex, the sum of squares of N complex Gaussian random variables with variance σ_w^2 is equivalent to

the sum of squares of $2N$ real Gaussian random variables with variance $\sigma_w^2/2$. Hence the complex signal case becomes a special case of the real signal and the correct probabilities for the complex case are derived by replacing N by $2N$ and σ_w^2 by $\sigma_w^2/2$.

$$\begin{aligned} P_f &= Q\left(\frac{\lambda - N\sigma_w^2}{\sqrt{N\sigma_w^4}}\right), \\ P_d &= Q\left(\frac{\lambda - 2N(\sigma_w^2/2 + P)}{\sqrt{4N(\sigma_w^2/2 + P)^2}}\right). \end{aligned} \quad (2.8)$$

For a Constant False Alarm Rate (CFAR) test also known as the Neyman-Pearson test, we can select a desired maximum value for P_f , calculate the corresponding threshold λ and use this threshold to compute the resulting P_d . This gives us a mechanism to observe the probability of detection, also referred to here from as the detection performance, of energy detection for different values of the parameters P_f , N (number of complex samples being averaged), σ_w^2 (the noise variance) and P (the signal power). The two formulas in (2.8) can be solved together to eliminate λ and yield an expression for N in terms of P_f & P_d . Eliminating λ we get,

$$N = \frac{[Q^{-1}(P_f) - Q^{-1}(P_d)(1 + 2SNR)]^2 SNR^{-2}}{4} \quad (2.9)$$

The expression in [10] which holds for only real samples can be derived from this expression by doubling the value for N and replacing $\sigma_w^2/2$ by σ_w^2 . In this expression, for any arbitrary SNR, a corresponding N can be derived that satisfies the constraints of P_f & P_d . Hence ideally energy detector can robustly detect a signal at any signal to noise ratio given an appropriate number of samples. Figure 2.1 shows the P_{md} vs P_f plots for two different values of SNR and number of samples N also known as the Receiver Operating Curves (ROC) where P_{md} denotes probability of miss detection given as $P_{md} = 1 - P_d$. These curves have been obtained using equation (2.8) by calculating the detection probability corresponding to a range of values of the false alarm probability. As expected, with decreasing SNR, P_{md} also increases for the same P_f while increasing the limit of P_f causes P_{md} to decrease concurrently. Also

increasing the number of observation samples at the same SNR leads to an increase in the detection probability. It may be observed from figure 2.1 that for a given number of samples N , as the signal power decreases from -10dB to -15dB , the miss detection probability increases meaning thereby the detection probability has decreased. Similarly for a given SNR increasing the number of samples available for sensing improves the average detection probability. This represents the fundamental trade-off in a cognitive radio system. To counter the effect of a worse channel, a cognitive radio must either increase its sensing time, or be ready to accommodate a higher number of false alarms in order to maintain the same average probability of detection of the primary user. Alternatively, the cognitive radio may sacrifice some data rate to continue operation below the channel capacity. As a final recourse, the cognitive radio may look to opt for a more efficient sensing technique. It is the last choice that has been the motivation to design more efficient and robust spectrum sensing techniques.

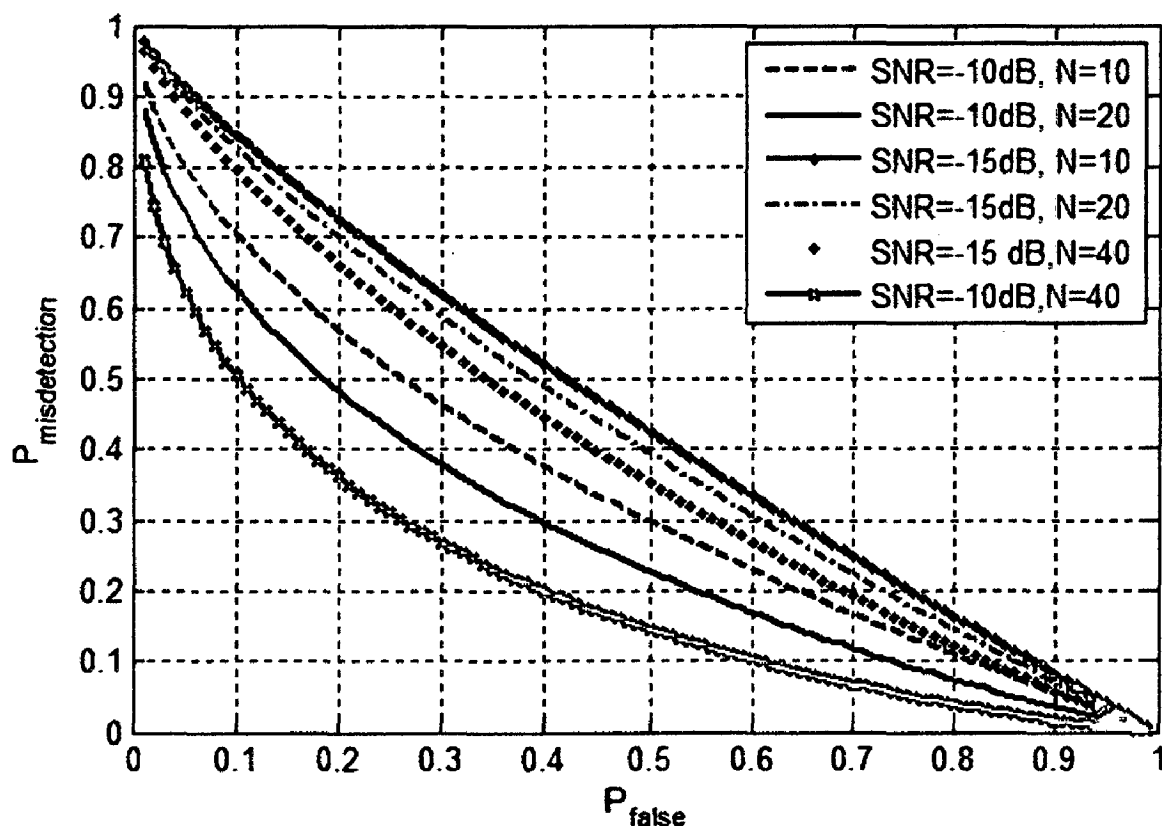


Figure 2.1: ROC curves for energy detector for different SNR and N (number of samples).

2.1.1. Effect of Uncertainty in Noise Variance

Though energy detection is a computationally inexpensive way to sense the spectrum, it involves an inherent trade-off that limits its ability to detect signals reliably in most practical scenarios. An energy detector assumes perfect knowledge of the ambient noise variance, in order to calculate the false alarm threshold λ . In practice, the noise power is measured during quiet periods of primary transmission [30] and this measurement can frequently be inaccurate due to co-channel interference from unsynchronised primary users or other legacy wireless devices. Further, any temperature change after the measurement, changes the ambient noise power, and non linearity of power devices also introduces noise uncertainty. A nominal value of noise power uncertainty is ± 1 dB [31]. This uncertainty leads to drastic drop in detection performance of the radiometer and renders it incapable of reliably detecting the signal below a SNR threshold called the SNR wall. Below the SNR wall, no matter how large the sensing time, the detection probability does not improve. This nature of energy detector can be characterized theoretically, as under noise uncertainty of x dB where $x = 10 \log_{10} \rho$ the detection and false alarm probabilities of equation (2.8) can be modified as follows [1]

$$\begin{aligned}
 P_f &= \max_{\sigma^2 \in [\frac{1}{\rho}\sigma_w^2, \rho\sigma_w^2]} Q\left(\frac{\lambda - N\sigma_w^2}{\sqrt{N\sigma_w^4}}\right) \\
 &= Q\left(\frac{\lambda - N\rho\sigma_w^2}{\sqrt{N\rho^2\sigma_w^4}}\right),
 \end{aligned} \tag{2.10}$$

$$\begin{aligned}
 P_d &= \min_{\sigma^2 \in [\frac{1}{\rho}\sigma_w^2, \rho\sigma_w^2]} Q\left(\frac{\lambda - 2N(\sigma^2/2 + P)}{\sqrt{4N(\sigma^2/2 + P)^2}}\right) \\
 &= Q\left(\frac{\lambda - 2N(\frac{\sigma_w^2}{2\rho} + P)}{\sqrt{4N(\frac{\sigma_w^2}{2\rho} + P)^2}}\right).
 \end{aligned} \tag{2.11}$$

Approximating $1 + \text{SNR} \approx 1$ and eliminating λ we get [1]

$$N \approx \frac{[Q^{-1}(P_f) - Q^{-1}(P_d)]^2}{[2\text{SNR} - (\rho - \frac{1}{\rho})]^2} \tag{2.12}$$

From the above equation it is clear that as $SNR \rightarrow \frac{1}{2}(\rho - \frac{1}{\rho})$, $N \rightarrow \infty$ and this is illustrated in figure 2.2 for $P_d = 0.9$ and $P_f = 0.1$. This phenomenon of the existence of a SNR threshold below which, the number of samples required to achieve a desired value of P_f & P_d approaches infinity is called SNR Wall. Thus for an uncertainty of $10\log_{10} \rho$ dB, the SNR wall is located at $10\log_{10}(\frac{\rho^2 - 1}{2\rho})$ dB.

Apart from the SNR wall, energy detector suffers from other shortcomings such as inability to differentiate interference from primary users and noise, and poor performance under low signal-to-noise ratio (SNR). An energy detector does not work efficiently for detecting spread spectrum signals since the power of the spread spectrum signals is highly spread out across a wide spectrum and the signal power in any given band is very low.

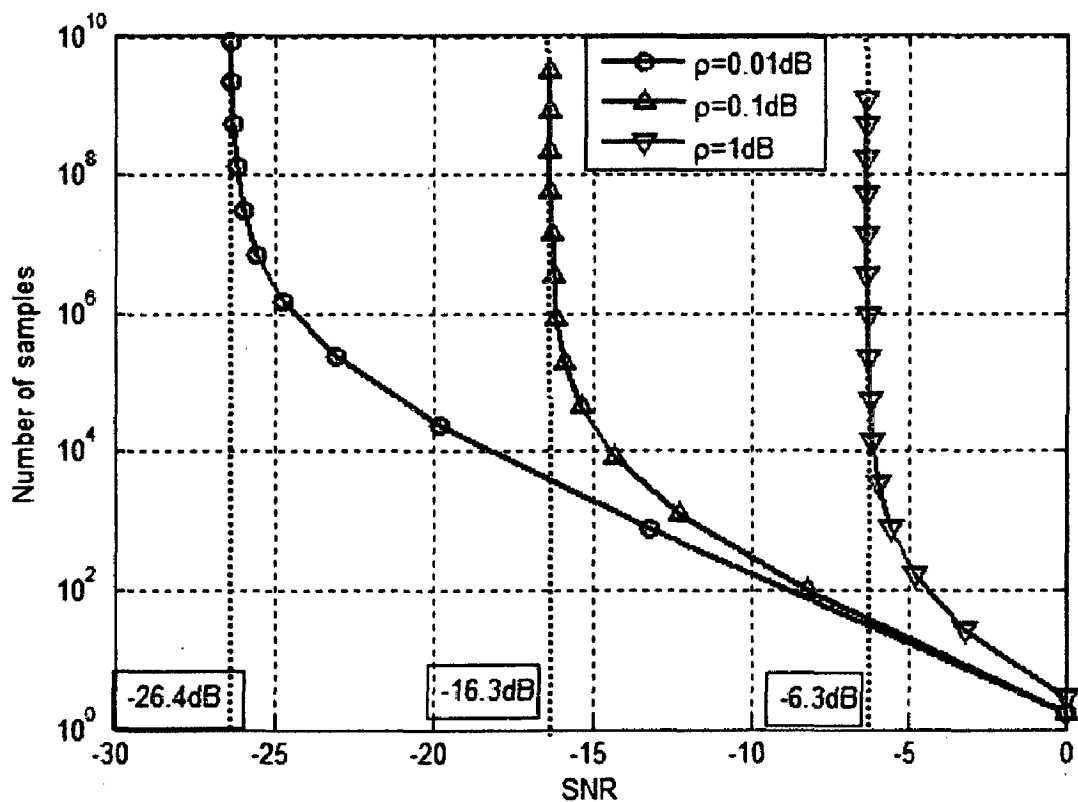


Figure 2.2: SNR walls in energy detection for noise uncertainty of 1 dB, 0.1 dB and 0.01 dB ($P_f=0.1$, $P_d=0.9$).

Narrowband interference or moderate noise levels can easily drown the signal energy causing an energy detector to fail. It must be noted that in spread spectrum signals, the received signal is convolved with the pseudo-random p-n sequence which serves to improve the SNR. But since a cognitive user does not possess any private information on the p-n sequence of the primary, it is impossible to reliably detect a primary user who uses a spread spectrum technique.

2.2. Cyclostationary Signal and its Properties

Cyclostationary signals can arise due to physical phenomenon like weather or certain man made operations like amplitude modulation, fractional sampling and multirate system filtering [32]. A discrete time signal x is called cyclostationary or cyclo-wide-sense-stationary with a period T (T being a positive integer) if its mean is periodic,

$$E\{x(t+IT)\} = E\{x(t)\}, \quad \forall t, l \in \mathbb{Z} \quad (2.13)$$

where \mathbb{Z} denotes the set of integers and/or its autocorrelation $R_{xx}(t, \tau) = E\{x(t+\tau/2)x^*(t-\tau/2)\}$ is periodic such that

$$R_{xx}(t+IT, \tau) = R_{xx}(t, \tau), \quad \forall t, \tau, l \in \mathbb{Z} \quad (2.14)$$

Since the autocorrelation function $R_{xx}(t, \tau)$ is periodic in the variable t , its discrete Fourier series coefficient can be expressed as

$$R_{xx}^\alpha(\tau) = \langle x(t+\tau/2)x^*(t-\tau/2)e^{-j2\pi\alpha t} \rangle \quad (2.15)$$

where the $\langle \cdot \rangle$ operation denotes time averaging as $\langle y \rangle = \lim_{Z \rightarrow \infty} \frac{1}{2Z} \sum_{l=-Z}^Z y(l)$. The Fourier series coefficient $R_{xx}^\alpha(\tau)$ is called the *Cyclic Autocorrelation Function (CAF)* and α is the cycle frequency [2]. In case of a discrete signal, the $R_{xx}^\alpha(\tau)$ can be written as

$$R_{xx}^\alpha(\tau) = \frac{1}{N} \sum_{l=\tau}^{N+\tau-1} x(l)x^*(l-\tau)e^{-i2\pi\alpha lT}, \quad (2.16)$$

Where T_s is the sampling time and N is the total number of samples of $x(n)$. This definition is a slight modification of equation (2.15) to support integral values of τ . Nevertheless, both

definitions give the same magnitude spectrum of the CAF. Using the definition in equation (2.15) we can write the periodic autocorrelation as the Fourier series,

$$R_{xx}(t, \tau) = \sum_{\alpha} R_{xx}^{\alpha}(\tau) e^{j2\pi\alpha t} \quad (2.17)$$

In a similar manner the conjugate cyclic autocorrelation function can also be defined as

$$R_{xx}^{\alpha*}(\tau) = \langle x(t + \tau/2)x(t - \tau/2)e^{-j2\pi\alpha t} \rangle, \quad (2.18)$$

and,

$$R_{xx}^{\alpha}(\tau) = \frac{1}{N} \sum_{l=\tau}^{N+\tau-1} x(l)x(l-\tau) e^{-i2\pi\alpha l T_s}. \quad (2.19)$$

As we know for stationary signals, the power spectral density (PSD) is defined as the Fourier transform of the autocorrelation function, similarly, for a cyclostationary signal its *Cyclic Spectral Density* (CSD) is defined as the Fourier transform of the cyclic autocorrelation function,

$$S_{xx}^{\alpha}(f) = \sum_{\tau=-\infty}^{\infty} R_{xx}^{\alpha}(\tau) e^{-j2\pi f \tau} \quad (2.20)$$

where f is the normalised frequency w.r.t. sampling frequency and lies between $[-\frac{1}{2}, \frac{1}{2}]$. The conjugate CSD, denoted by $S_{xx}^{\alpha*}(f)$, can be derived in a similar manner by taking the Fourier transform of the conjugate cyclic autocorrelation function. It can be proved that the cyclic spectral density of a signal $x(t)$ is equivalent to correlation of the Fourier transform coefficients of $x(t)$ at two distinct frequencies separated by the cyclic frequency α , and hence is also known as the *Spectral Correlation Density* (SCD) [24].

$$S_{xx}^{\alpha}(f) \triangleq \lim_{T \rightarrow \infty} T \langle X_T(t, f + \alpha/2) X_T^*(t, f - \alpha/2) \rangle \quad (2.21)$$

where $X_T(t, f)$ is the complex envelope of the spectral component of $x(t)$ with frequency f and approximate bandwidth $1/T$ given by $X_T(t, f) \triangleq \frac{1}{T} \int_{t-T/2}^{t+T/2} x(u) \exp(-i2\pi fu) du$ and $\langle \cdot \rangle$ denotes the time averaging. We can as well define a normalised value of the SCD called the *Spectral Correlation Function* (SCF) as [24]

$$\rho_{xx}^{\alpha} = \frac{S_{xx}^{\alpha}(f)}{[S_{xx}^0(f + \alpha/2)S_{xx}^0(f - \alpha/2)]^{\frac{1}{2}}} \quad (2.22)$$

For stationary signals, R_{xx}^{α} is non-zero only for $\alpha = 0$ while it is $0 \forall \alpha \neq 0$. On the other hand, for cyclostationary signals there exist distinct values of α other than 0 for which the CAF exhibits a peak, signifying the time-periodic nature of the signal. For the same cyclic frequencies α , the SCD shows a peak in the $\alpha - f$ domain. This means that if the signal exhibits cyclic frequency α then the power spectral density components of the signal at frequencies $f + \frac{\alpha}{2}$ and $f - \frac{\alpha}{2}$ are correlated. The importance of SCF is that it serves as an objective measure of cyclostationarity as for most signals like BPSK, QPSK, and AM the magnitude of SCF at their corresponding cyclic frequencies is equal to unity. Another useful parameter that can be defined from the SCD is the α -domain profile. It is defined mathematically as,

$$\text{profile}(\alpha) = \max_f S_{xx}^{\alpha}(f) \quad (2.23)$$

2.2.1. Cyclostationarity in Digital Modulated Signals

The cyclic frequencies α depend on various parameters of the transmitted signal such as its modulation type, pulse rate or baud rate, carrier frequency, bandwidth etc. If these parameters are known, we can find the cyclic frequency of the signal. In the following discussion, cycle frequencies for the general class of QAM signals are presented [2].

A real QAM signal can be written as

$$d(t) = c(t) \cos(\omega_0 t) + s(t) \sin(\omega_0 t) \quad (2.24)$$

If $c(t)$ and $s(t)$ are proportional then $d(t)$ is called an AM signal. Further, if the amplitude $c(t)$ which is proportional to $s(t)$ is a digital PAM signal,

$$c(t) = \sum_{r=-\infty}^{\infty} c_r p(t - rT_0 - t_0) \quad (2.25)$$

then $d(t)$ is called an amplitude-shift-keyed signal with a keying rate $1/T_0$. If the pulse $p(t)$ is a full duty cycle rectangular pulse and the digital variables c_r are binary valued with values of

± 1 , then this binary ASK signal is equivalent to a BPSK signal. If $s(t)$ is not proportional to $c(t)$ but is also a binary PAM signal with full duty cycle rectangular pulses, then $d(t)$ is a QPSK signal. In the most general case, when pulses in the QPSK signal are not restricted to be rectangular, and the total number of states of the pair of (c_r, s_r) is equal to M , the signal $d(t)$ is called an M -ary QAM signal.

For this general QAM signal, the spectral correlation density and the conjugate spectral correlation density can be derived as given in [2] by Gardner (refer to Appendix A). He obtains the following results for specific cyclic frequencies for each modulated signal. The important results are listed below.

$$\text{BPSK signal: } S_{dd}^{\alpha}(f) \neq 0 \text{ for } \alpha = k / T_0 \text{ \& } S_{dd}^{\alpha}(f) \neq 0 \text{ for } \alpha = \mp 2f_0 + k / T_0 \quad (2.26)$$

$$\text{AM signal: } S_{dd}^{\alpha}(f) \neq 0 \text{ for } \alpha = \mp 2f_0 \quad (2.27)$$

$$\text{QPSK signal: } S_{dd}^{\alpha}(f) \neq 0 \text{ for } \alpha = k / T_0 \quad (2.28)$$

where k takes all integral values. All the above mentioned signals exhibit discrete peaks in the conjugate/non-conjugate spectral correlation density at these frequency values. Further for all QAM signals whose amplitude/phase constellations exhibit quadrantal symmetry, the spectral correlation density functions are identical to that of the QPSK signal case with symmetric constellation, considered above. The presence of cyclostationarity can be verified through simulation of the above modulated signals. In the following section, present a simulation example that gives the plots of the cyclic autocorrelation function and the cyclic spectral density function of a BPSK modulated signal clearly showing cyclic peaks.

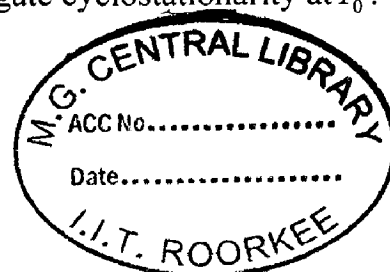
2.2.2. Simulation Example 1: Cyclostationarity in BPSK

Consider a complex BPSK signal $d(t) = c(t)e^{j2\pi f_c t}$ where $c(t) = \sum_{r=-\infty}^{\infty} c_r p(t - rT_0)$, $p(t)$ is a rectangular pulse of duration T_0 , f_c is the carrier frequency and $c(t)$ is a NRZ (Non-Return to Zero) encoded random binary wave with amplitudes of ± 1 . We sample the signal at a sufficiently high sampling frequency of $f_s = 10240\text{Hz}$ and choose the carrier frequency as $f_c = 0.25f_s = 25600\text{Hz}$. The pulse duration T_0 is so chosen that there are exactly 32 samples

per pulse. Hence the baud rate $1/T_0 = 102400/32 = 3200\text{Hz}$. For this BPSK signal, we compute the cyclic and conjugate autocorrelation function using equation (2.16), for the lag values $\tau = 1$ to 64 and $\alpha \in [-2f_c - \frac{2}{T_0}, 2f_c + \frac{2}{T_0}]$, in order to include all major cyclic peaks, and subsequently find the cyclic spectral density values for different α and f by reducing equation (2.20) to a finite number of lags τ . In order to keep the variance constant, we normalise the equation (2.20) by the square root of 64. The corresponding plots are shown in figure 2.3 and 2.4. A representative plot of the conjugate and non-conjugate cyclic autocorrelation function at lag=1 is given in figures 2.5 and 2.6. Lastly, we compute the alpha profile of the BPSK signal using equation (2.23). The resultant plot is shown in figures 2.7.

It is quite clear from figure 2.3 and figure 2.5 which plot the CSD and the CAF of the BPSK signal, that the signal possesses cyclostationarity at baud rate or $1/T_0$. This is especially evident in the CAF versus αT_0 graph wherein discrete peaks are visible at integral values of αT_0 . The graph of CSD shows small peaks for each integral value of αT_0 . The constant amplitude bar at $\alpha = 0$ accompanied by the central peak at a certain frequency f is due to the high DC value of autocorrelation among consecutive samples, similar to what a stationary signal would exhibit. A point to be noted here is that the magnitude of CAF peaks at the cyclic frequencies is much below unity which signifies that the strength of cyclostationarity that the BPSK signal exhibits at baud rate is weak.

On the other hand, figure 2.4 and figure 2.6 show the conjugate cyclostationarity present in the BPSK signal at a cyclic frequency of $2f_c = 51200\text{Hz}$. The plot of CAF in figure 2.6 clearly indicates the strong cyclic correlation among successive BPSK samples (τ is chosen to be 1) at twice the carrier frequency. Similarity, the CSD plot in figure 2.4 shows peaks of $S_{xx}^\alpha(f)$ at $\alpha = \pm 2f_0$. The magnitude of the conjugate CAF peak is very close to unity in contrast to the low peak value of CAF, meaning thereby that BPSK exhibits much stronger conjugate cyclostationarity at $2f_0$ than non-conjugate cyclostationarity at T_0 .



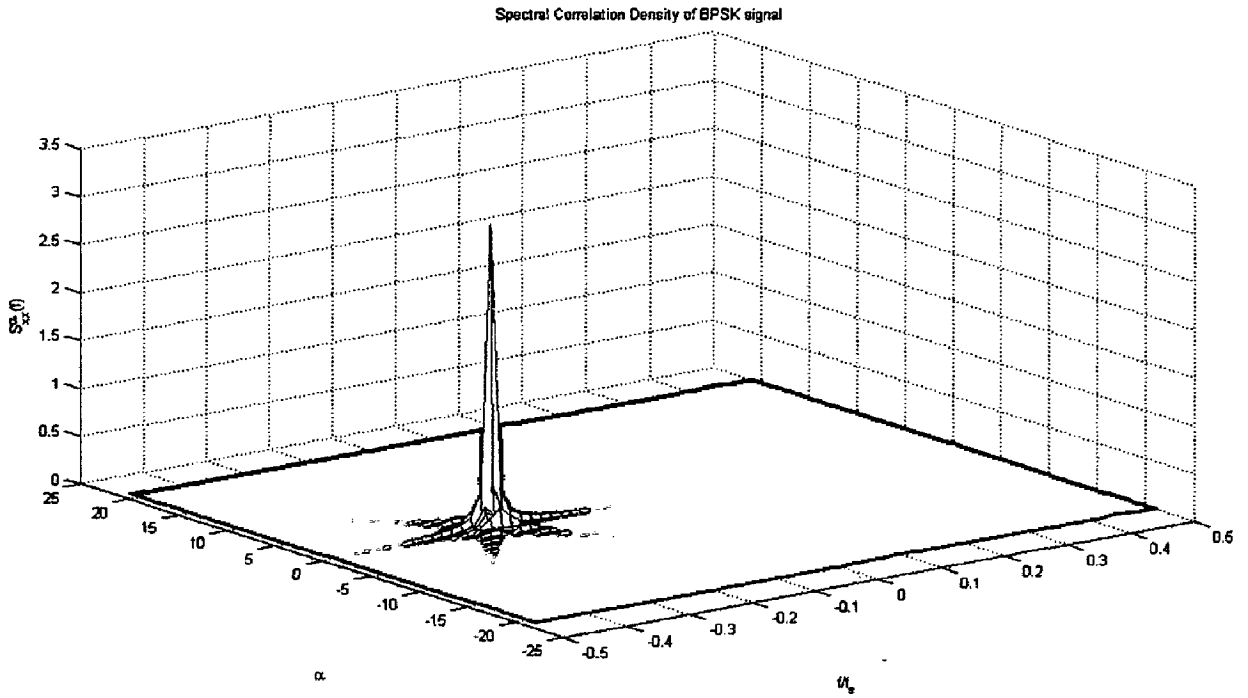


Figure 2.3: Plot of cyclic spectral density of BPSK signal versus α and f/f_s .

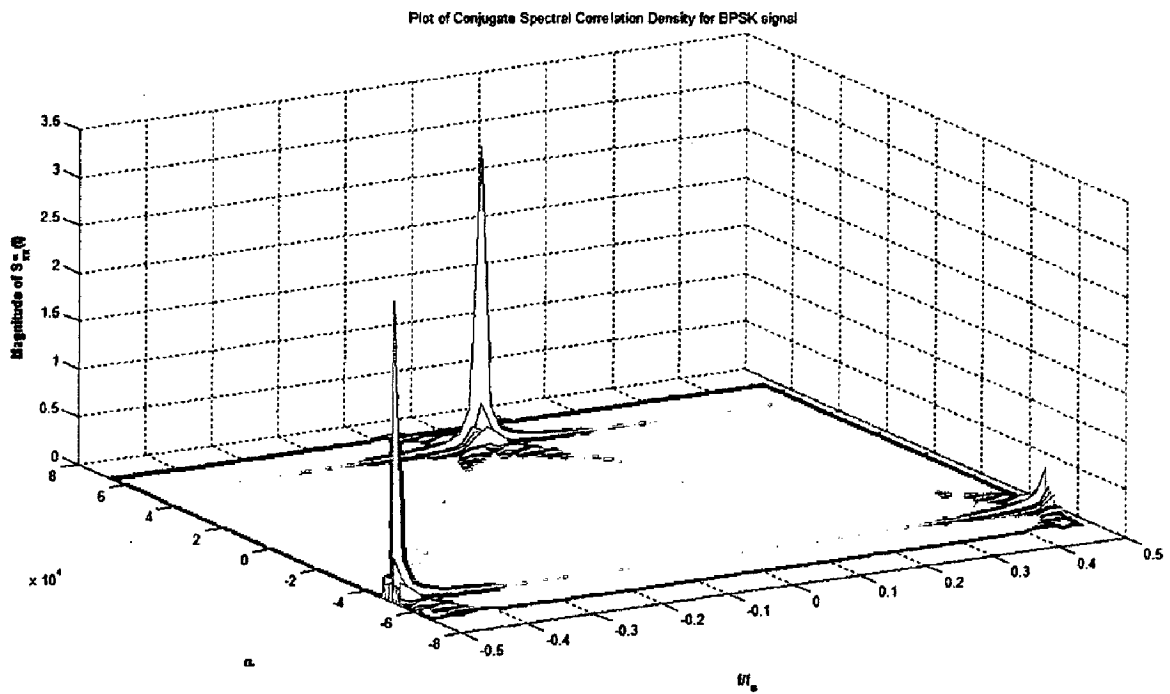


Figure 2.4: Plot of conjugate cyclic spectral density of BPSK signal versus α and f/f_s .

Cyclic Autocorrelation Function of a BPSK signal showing peaks at baud rate k/T_0

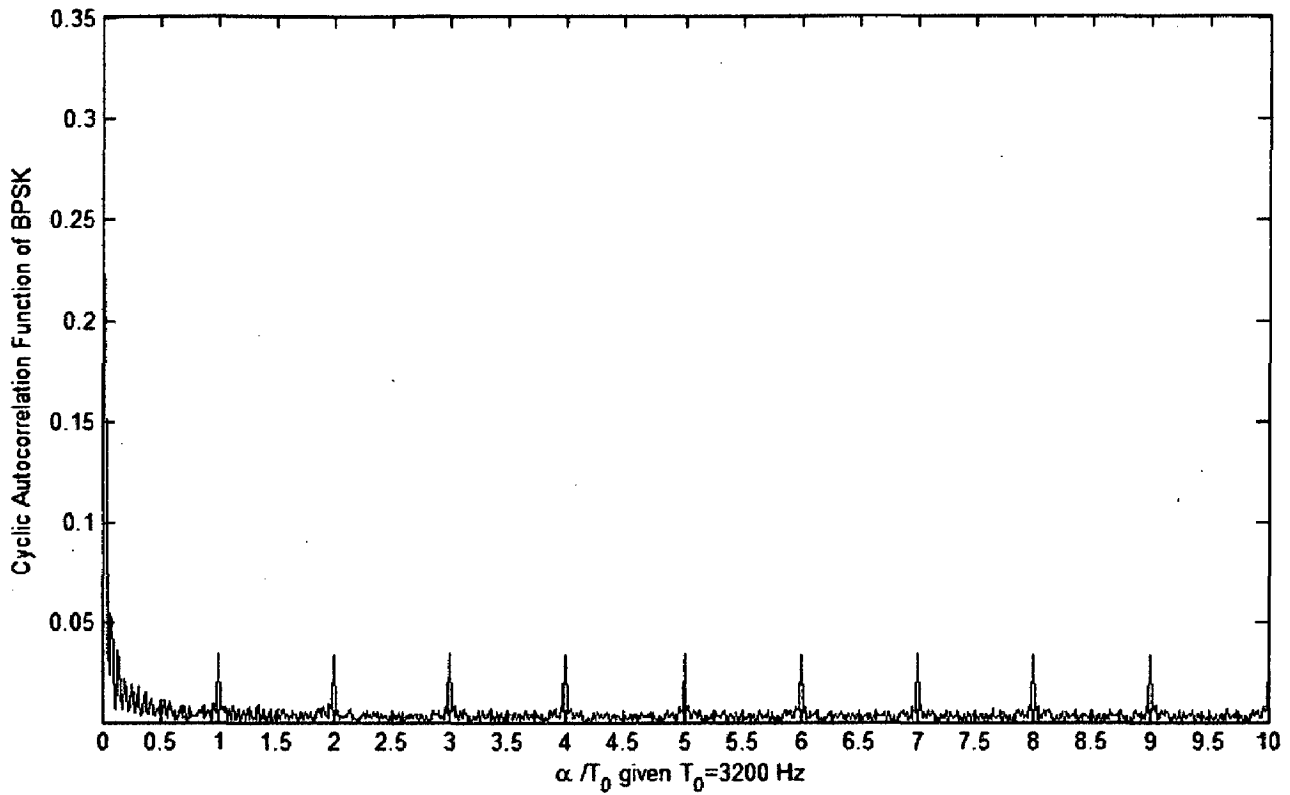


Figure 2.5: Cyclic autocorrelation function of BPSK signal.

Conjugate Cyclic Autocorrelation Function of a BPSK signal showing peaks at $2f_c$

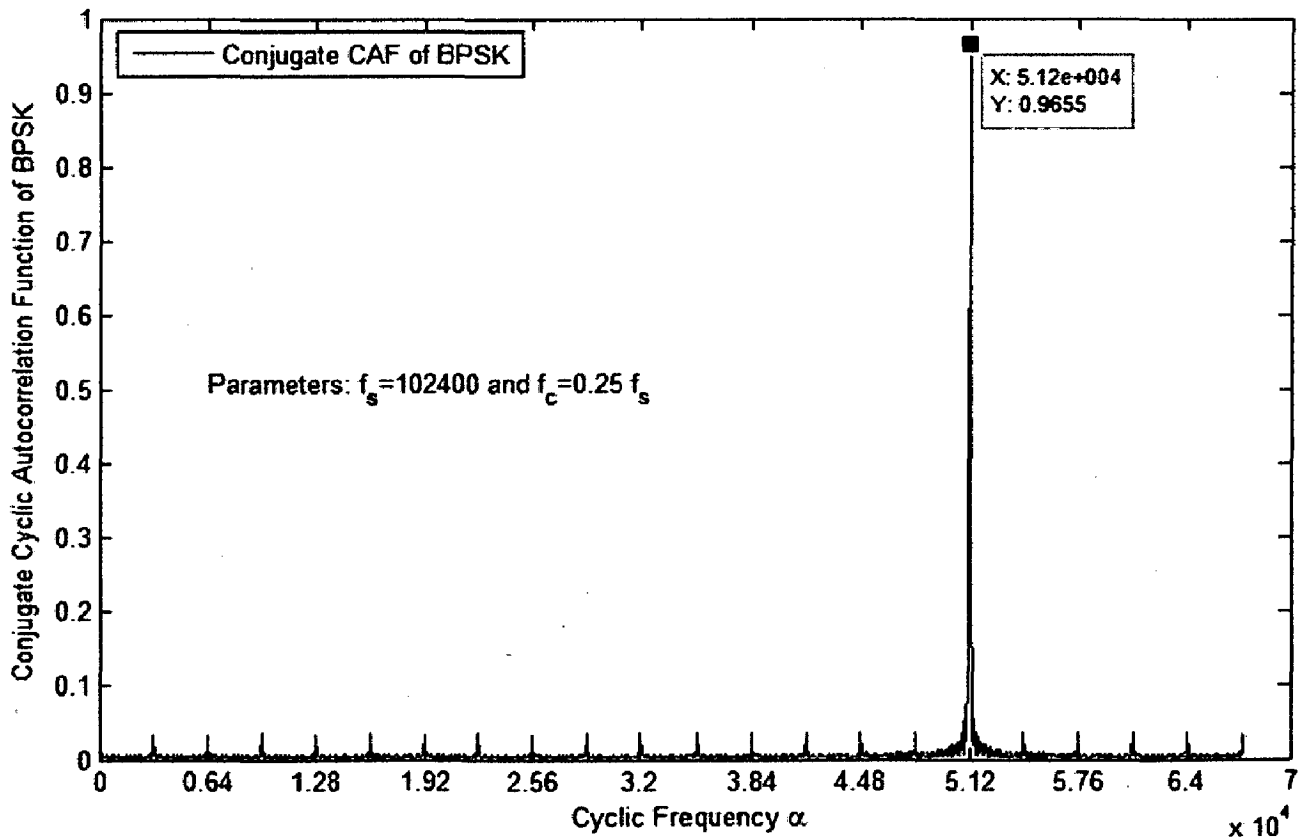


Figure 2.6: Conjugate cyclic autocorrelation function of BPSK signal.

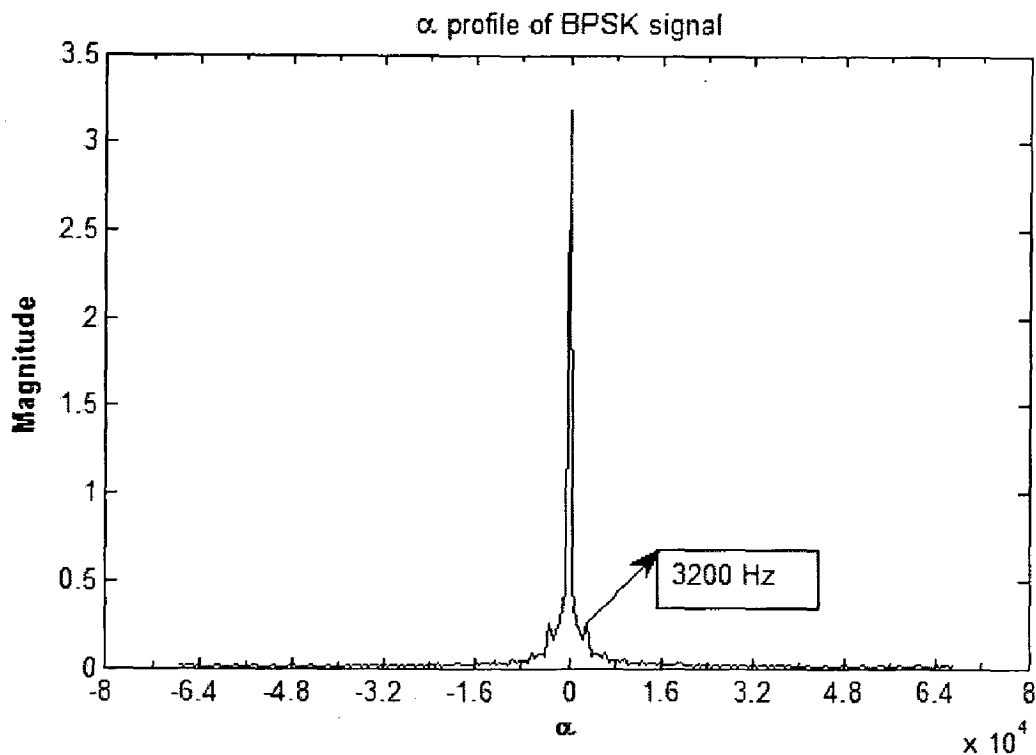


Figure 2.7: Alpha profile of BPSK signal.

Figure 2.7 shows the alpha profile of the BPSK signal, in which there is a central peak at $\alpha = 0$. The spectral correlation at $\alpha = 1/T_0$ is very low as compared to the DC value of alpha profile. This is due to the weak cyclostationarity at baud rate. The conjugate alpha profile of the signal (not shown here as it is obvious) shows distinct peaks at $\alpha = 2f_0, -2f_0$.

2.3. Cyclostationary Spectrum Sensing

When attempting to detect a BPSK signal, the strong cyclostationarity at twice the carrier frequency is a prominent signature that can be used for identification of the signal from a host of other interfering signals. Almost all kinds of digital QAM signals of the form as given in equation (2.24) exhibit cyclostationarity at either baud rate $1/T_0$ or twice the carrier frequency $2f_0$. This property can be used to isolate a desired signal from amongst other spectrally overlapping signals, if their symbol rates are distinct. An important application of cyclostationarity, thus, can be to detect whether a specific kind of signal is present in the RF band of interest. This could be useful to identify the presence of a specific user in a multi-user scenario wherein, say, simultaneously multiple transmissions from different users are happening in the ISM band, by identifying his unique cyclostationary features. In a cognitive radio scenario, cyclostationary feature detection can be used to ascertain whether a frequency

band is currently occupied by a primary user or not. This technique inherently is more robust than energy detection because it can differentiate between a primary user and multiple interfering secondary users with different cyclic frequencies allowing us to make independent policies for both scenarios while a radiometer would simply add up the energies of the primary and secondary transmissions, making the cognitive radio treat other secondary users as primary users and end up with a much worse spectral efficiency. Moreover, at low SNR it is comparatively easier to detect the cyclostationary features of signal than detecting its energy, which is a small addition to the already ample noise energy present in the band.

To enable cyclostationary detection in a manner similar to energy detection wherein the false alarm probability can be limited to a desired threshold and optimal detection performance be calibrated, we must develop a Neyman-Pearson test for cyclostationarity. Such an optimal test was first developed by Giannakis in [33] for a single cyclic frequency and multiple lags (τ) and it was extended to multiple cyclic frequencies recently by Poor et al. [12]. The observed CAF approximated over N samples is given by,

$$\begin{aligned}\hat{R}_{xx}^\alpha(\tau) &= \frac{1}{N} \sum_{t=1}^N x(t)x^*(t+\tau)e^{-j2\pi\alpha\tau} \\ &= R_{xx}^\alpha(\tau) + \epsilon_{xx}^{(T)}(\alpha, \tau)\end{aligned}\quad (2.29)$$

where $R_{xx}^\alpha(\tau)$ is the true value of the cyclic autocorrelation function and $\epsilon_{xx}^{(T)}(\alpha, \tau)$ denotes the error in estimation due to finite number of samples. Let $A = \{\alpha_n | n=1, \dots, P\}$ be the set of cyclic frequencies of interest and

$$\begin{aligned}\hat{\mathbf{r}}_{xx} &= \\ &[\text{Re}\{\hat{R}_{xx}(\alpha_1, \tau_{1,1}), \dots, \hat{R}_{xx}(\alpha_1, \tau_{1,N_1})\} \\ &\text{Im}\{\hat{R}_{xx}(\alpha_1, \tau_{1,1}), \dots, \hat{R}_{xx}(\alpha_1, \tau_{1,N_1})\} \\ &\dots \\ &\text{Re}\{\hat{R}_{xx}(\alpha_p, \tau_{p,1}), \dots, \hat{R}_{xx}(\alpha_p, \tau_{p,N_p})\} \\ &\text{Im}\{\hat{R}_{xx}(\alpha_p, \tau_{p,1}), \dots, \hat{R}_{xx}(\alpha_p, \tau_{p,N_p})\}]\end{aligned}\quad (2.30)$$

denotes a $1 \times 2N$ vector containing the real and imaginary parts of the estimated cyclic autocorrelation values at cyclic frequencies of interest stacked in a single vector. Here N is

given by $N = \sum_{n=1}^P N_n$. In order to test the presence of cyclostationarity, he defines the following hypotheses

$$\begin{aligned} H_0 : \hat{\mathbf{r}}_{\mathbf{xx}} &= \boldsymbol{\epsilon}_{\mathbf{xx}}, \\ H_1 : \hat{\mathbf{r}}_{\mathbf{xx}} &= \boldsymbol{\epsilon}_{\mathbf{xx}} + \mathbf{r}_{\mathbf{xx}} \end{aligned} \quad (2.31)$$

The vector $\boldsymbol{\epsilon}_{\mathbf{xx}}$ of the estimation errors, is asymptotically normally distributed, i.e., $\lim_{N \rightarrow \infty} \sqrt{N} \boldsymbol{\epsilon}_{\mathbf{xx}}$ is $\mathbf{N}(\mathbf{0}, \boldsymbol{\Sigma}_{\mathbf{xx}})$ [33. Appendix]. We construct a likelihood ratio test $\Lambda = \frac{f(\hat{\mathbf{r}}_{\mathbf{xx}} | H_1)}{f(\hat{\mathbf{r}}_{\mathbf{xx}} | H_0)}$ based on the distribution of $\hat{\mathbf{r}}_{\mathbf{xx}}$ under H_0 & H_1 and through simple mathematical manipulation, the final test statistic is chosen as $\mathbb{A} = 2 \ln \Lambda = M \hat{\mathbf{r}}_{\mathbf{xx}} \boldsymbol{\Sigma}_{\mathbf{xx}}^{-1} \hat{\mathbf{r}}_{\mathbf{xx}}^T$. The computation of each of the $2N \times 2N$ elements of the matrix $\boldsymbol{\Sigma}_{\mathbf{xx}}$ involves cumbersome calculation of cyclic periodogram values which can become computationally complex [33]. To make the process of detection, computationally tractable, we use only a select few cyclic frequencies and a single τ for detection. Instead of the above test statistic, we use a suboptimal but simpler time domain test statistic that uses the sum of cyclic autocorrelation function values at the desired cyclic frequencies to make a decision on the presence of the signal. Thus the new test statistic can be written as

$$\mathbb{A} = \sum_{n=1}^P \hat{R}_{\mathbf{xx}}^{\alpha_n} \quad (2.32)$$

Using this new test statistic, we set up a Neyman-Pearson test as follows:

Neyman-Pearson test for cyclostationarity with suboptimal sum test statistic:

1. Formulate the hypotheses $H_0 : \mathbb{A} = \xi_{\mathbf{xx}}$, where $\xi_{\mathbf{xx}}$ is the error in \mathbb{A} due to finite number of samples. $H_1 : \mathbb{A} = z + \xi_{\mathbf{xx}}$
2. Under hypothesis H_0 , set the false alarm probability to P_f and obtain from simulation, a threshold λ such that $\Pr(\mathbb{A} | H_0 > \lambda) = P_f$.
3. Under hypothesis H_1 , find the detection probability P_d by the formula $P_d = \Pr\{\mathbb{A} | H_1 > \lambda\}$.

In the following section, we illustrate the application of this cyclostationary test for spectrum sensing of the BPSK signal defined in simulation example 1 and evaluate the detection performance.

2.3.1. Simulation Example 2: Comparison of Cyclostationary & Energy Detection

Consider the BPSK signal of simulation example 1, defined in section 2.2.1, $d(t) = a(t)e^{j2\pi f_c t}$ where $a(t)$ is a NRZ rectangular pulse of duration T_0 . The carrier frequency f_c is set to be 25600 Hz, sampling frequency $f_s = 102400$ Hz and T_0 is 3200 Hz. We want to detect this BPSK signal with a maximum false alarm rate of 0.1. The SNR of the signal is varied from 0dB to -20dB. As shown in simulation example 1, BPSK exhibits strong cyclostationarity at frequencies $\alpha = 2f_c \pm k/T_0$. Hence we chose three cyclic frequencies for the purpose of detection and form the test statistic as below,

$$\mathbb{A} = \hat{R}_{xx}^{2f_c} + \hat{R}_{xx}^{2f_c + 1/T_0} + \hat{R}_{xx}^{2f_c - 1/T_0} \quad (2.33)$$

where \hat{R}_{xx}^α is found using equation (2.9). With no signal being transmitted, we conduct 1000 simulation runs to evaluate the test statistic and determine the threshold λ such that the rate of false alarm is limited to a maximum of 10 percent. Subsequently we conduct 1000 Monte Carlo runs at each SNR 0dB, -1dB, -2dB, ..., -20dB and observe the average probability of detection that this test statistic provides. The results of the simulation are plotted in figures 2.8 and 2.9.

The figures 2.8 and 2.9 present the probability of false alarm versus threshold λ and probability of detection versus SNR curves respectively. A total of 800 samples of the BPSK signal representing 25 complete pulse durations were used for detection.

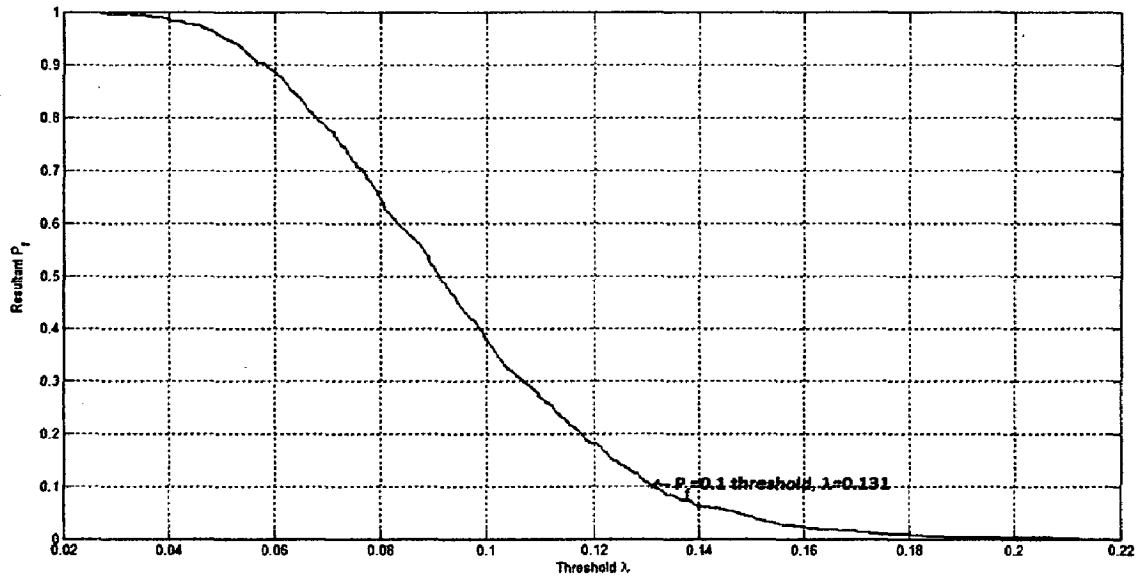


Figure 2.8: Variation of false alarm probability with threshold λ for cyclostationary detection.

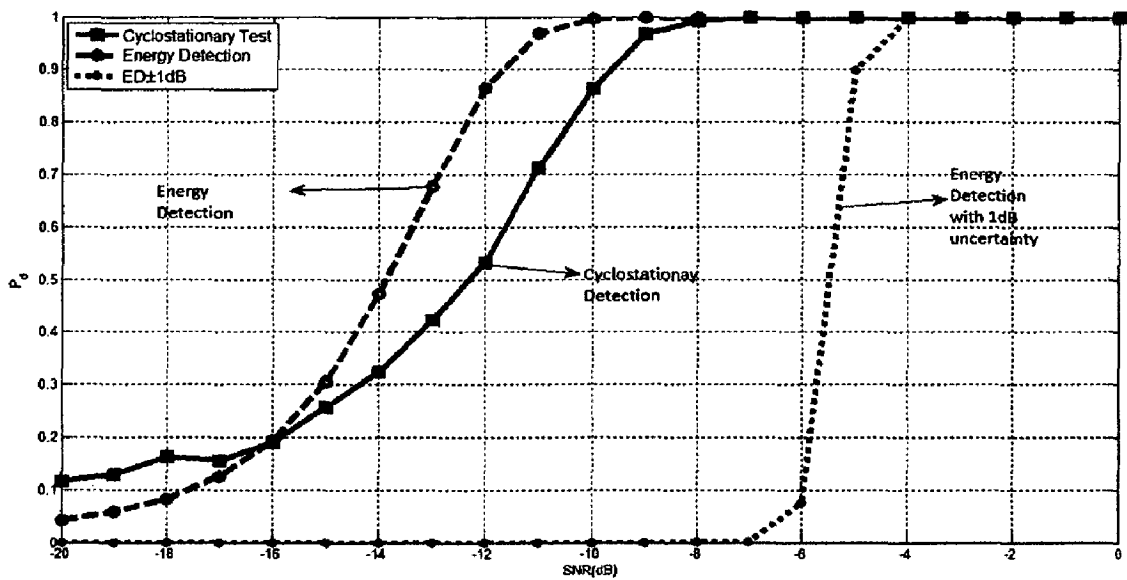


Fig. 2.9: Comparison of probability of detection curves of cyclostationary detection, energy detection, and energy detection with 1dB noise uncertainty for 800 received samples of BPSK signal.

Figure 2.8 shows the variation of average false alarm probability with λ by using the test statistic Λ . To satisfy $P_f = 0.1$, a threshold of $\lambda = 0.131$ was found to be appropriate. Figure 2.9 presents the detection probability measured according to aforementioned Neyman-Pearson test. It clearly shows that cyclostationary detection, represented by the continuous line plot with square marker, has a 1 dB SNR loss as compared to an energy detector using the same number of samples, for a detection probability of 0.9. Energy detector outperforms the cyclostationary detector at SNR's above -16 dB.

This is along expected lines as energy detector is a near optimal detector for signals at high SNR in the absence of any correlation structure in the signal and when the noise variance is perfectly known [21]. But at low SNR below -16 dB, cyclostationary detection gives better results because of the non-robustness of energy detector. In most practical cases, noise variance uncertainty of the order of 1dB or more (meaning thereby the instantaneous noise power can exceed or fall below the calibrated power by not more than 1dB) is quite common and the rightmost dot-dash line shows the severely degraded performance of energy detection under 1dB of noise uncertainty. Hence cyclostationary detection is a much more robust technique of detection than energy detection. Though, it should be kept in mind that optimal cyclostationary detection is a computationally intensive task and hence most spectrum sensing systems developed to date either use energy detection based sensing with adaptive noise variance estimation or a two layer sensing architecture recently proposed for devices implementing IEEE 802.16 that includes coarse sensing with radiometers followed by fine sensing with techniques like cyclostationary detection if necessary. But suboptimal techniques like those discussed above can be used to make cyclostationary detection computationally feasible with a marginal loss in detection performance.

Till now we have explored cyclostationary spectrum sensing from the perspective of detection theory, applying Neyman-Pearson test for constructing an optimal test for detecting a signal such that its false alarm rate is limited below a threshold. Gardner [2], [24] developed a new approach to *optimally*¹ detect cyclostationary signals in the presence of noise/interference by using an adaptive filtering approach. He developed the structure and theory of FRESH (Frequency SHift) filters which can optimally estimate a cyclostationary signal by minimizing the mean square error between the input and output using Linear

¹Optimal here means MMSE. It should not be confused with earlier definitions of optimum that were used for a Neyman-Pearson optimum test.

Conjugate Linear (LCL) filtering. These filters exploit spectral correlation in the signal, in a manner similar to the spatial correlation based Wiener filters proposed by Wiener for estimating stationary signals [34], but due to the cyclostationary nature of the signal, they are periodically time varying in nature.

Using a FRESH filter for the detection of primary signals in a cognitive radio scenario would give us an alternate way of exploiting cyclostationarity of signals and may offer a potentially better spectrum sensing technique. With this background in mind, we discuss the theoretical development of FRESH (FREquency SHift) filters and their application to spectrum sensing.

Chapter 3

FRESH (Frequency Shift) Filters For Spectrum Sensing

Frequency shift (FRESH) filters were proposed by Gardner in his work [2] and the first development of the optimum MMSE (Minimum Mean Square Error) estimating filters for cyclostationary signals was given by Gardner in his 1972 PhD thesis [35] which was later extended to complex signals by W.A. Brown while showing that FRESH filters are able to separate spectrally overlapping signals as a function of the receiver complexity. Gardner developed a time-averaged theory wherein the performance of a filter is characterized in terms of time averaged mean square error instead of the using stochastic approach of ensemble averaging. Using this theory he developed time averaged definitions for cyclic autocorrelation function and spectral correlation density of cyclostationary signals. This time averaged approach was used to develop the statistical theory behind frequency shift filters, called *cyclic Wiener filtering* [2]. Quoting from the paper by Gardner [2], "*This theory generalizes Wiener's theory of optimum time-invariant filtering of stationary time-series to optimum polyperiodic (multiply periodic) time variant filtering of cyclostationary time series*". Due to their time varying nature, FRESH filters are also known as LAPTIV (Linear Almost Periodic Time Varying) filters [36]. The structure of a frequency shift filter consists of a number of frequency shifting branches each followed by a linear time invariant (LTI) filter. The reason is that a FRESH filter works by cancelling out the portion of signal spectrum aliased by the interference, using the frequency subband which is un-aliased. Since in a cyclostationary signal, spectral correlation exists between bands separated by the cyclic frequency, the frequency shift filter consists of a number of branches that successively exploit this correlation.

Frequency shift filters have been applied for removal of co-channel interference and detection of signals under fading [37]. Adaptive implementations of FRESH filters using LMS algorithm have been proposed by Zhang et al. in [38]. The same authors also propose a novel blind adaptive FRESH (BA-FRESH) filter structure in [39] and show that the mean square error of the proposed BA-FRESH filter converges to that of the trained LMS FRESH filter in a few hundred samples, a critique of which is given by Adlard in [26]. Whitehead et al. in

[25] discuss BA-FRESH filtering based multiuser detection for interference suppression in DS-CDMA. The same authors in [40] develop LCCMA (Linearly Constrained Constant Modulus Algorithm) blind adaptive FRESH filters with low complexity for the same purpose. Other significant works in FRESH filtering have been the PhD thesis of Adlard [26] in which he discusses the optimal detection of cyclostationary signals using FRESH filtering and the various challenges associate with the design of blind adaptive FRESH filters. More recently, Ojeda and Grajal in [41] have tried to detect an interference corrupted signal by constructing a FRESH filter to reject the interference using its cyclostationary properties, followed by an atomic detector proposed earlier by the same authors. In [36], the same authors prove theoretically that FRESH filters can work robustly even under frequency offset, given that their rate of convergence is sufficiently high.

Although the theoretical foundation frequency shift filtering of periodically correlated time signals was laid long back, their application to spectrum sensing in cognitive radios offers new challenges and possibilities that may be utilized to yield a better spectrum sensing technique. This chapter looks at FRESH filters from the traditional perspective of mean square error performance of FRESH filters to detect cyclostationary signals. It presents the theoretical background and simulation results for various adaptive implementations of FRESH filters. Instead of basing its sensing decision on the received signal, the sensing device performs a suboptimal but simple test on the frequency shift filtered received signal. Simulation results are presented which show that under a constraint of maximum false alarm rate, the FRESH filter based spectrum sensing technique offers better detection performance than energy detection and cyclostationary detection.

3.1. Cyclic Wiener Filtering

The output $y(t)$ of a linear time variant filter for an input $x(t)$ can be written as follows,

$$y(t) = \int_{-\infty}^{\infty} h(t,u)x(u)du \quad (3.1)$$

where $h(t,u)$ is the time varying impulse response of the filter. When this $h(t,u)$ is periodic in time with more than one period, the resultant filter becomes a polyperiodic filter or a LAPTIV filter. The impulse response $h(t,u)$ can be expanded as a Fourier series over integer multiples of its fundamental frequency $1/T_0$ where T_0 is the period of the filter response.

$$h(t, u) = \sum_{\eta} h_{\eta}(t - u) \exp(i2\pi\eta u) \quad (3.2)$$

In this series, the Fourier coefficients $h_{\eta}(\tau)$ for each value of τ are given by

$$h_{\eta}(\tau) = \langle h(t + \tau, t) \exp(-i2\pi\eta t) \rangle \quad (3.3)$$

where $\langle \cdot \rangle$ is the average over all time t . Substituting (3.2) into (3.1) we get

$$y(t) = \sum_{\eta} h_{\eta}(t) \otimes x_{\eta}(t) \quad (3.4)$$

where \otimes denotes the convolution operation and $x_{\eta}(t) \triangleq x(t) \exp(i2\pi\eta t)$ is a frequency shifted version of $x(t)$. Thus for finite energy, Fourier transformable signals, we can write

$$Y(f) = \sum_{\eta} H_{\eta}(f) X_{\eta}(f - \eta) \quad (3.5)$$

The above equation means that in a polyperiodic filter, the input is subjected to a number of frequency-shifting operations, each followed by a linear time invariant filtering block and the results from all branches are added together. This analysis establishes the fact that polyperiodic filtering is same as FREquency SHift filtering. The next step is then to prove that such a filter structure is indeed the optimum structure for estimating cyclostationary signals.

In equation (3.4), for complex signals $x(t)$ (bandpass or complex lowpass equivalents), apart from the signal itself, the conjugate of the signal must also be filtered. Such a method of filtering is referred to as *Linear Conjugate Linear (LCL) filtering*. The general form of LCL-FRESH filtering is

$$\hat{d}(t) = \sum_{m=1}^M a_m(t) \otimes x_{\alpha_m}(t) + \sum_{n=1}^N b_n(t) \otimes x_{-\beta_n}^*(t) \quad (3.6)$$

where M is the number of linear branches and N is the number of conjugate linear branches of FRESH filter with weights denoted by a_m and b_n . $x_{\alpha_m}(t)$ and $x_{-\beta_n}^*(t)$ are the frequency shifted inputs defined as $x_{\alpha_m}(t) \triangleq x(t) \exp(i2\pi\alpha_m t)$ and $x_{-\beta_n}^*(t) \triangleq x^*(t) \exp(-i2\pi\beta_n t)$. Using vector concatenation we define the following composite weight vector,

$$\mathbf{h}(t) = [a_1(t), \dots, a_M(t), b_1(t), \dots, b_N(t)]' \quad (3.7)$$

$$\mathbf{z}(t) = [x_{\alpha_1}(t), \dots, x_{\alpha_M}(t), x_{-\beta_1}^*(t), \dots, x_{-\beta_N}^*(t)]' \quad (3.8)$$

The equation (3.6) can be thus re-expressed as $\hat{d}(t) = \mathbf{h}'(t) \otimes \mathbf{z}(t)$. This gives us $M+N$ simultaneous Wiener equations that can be solved to give an optimum set of weights.

$$\mathbf{S}'_{zz}(f) \mathbf{H}(f) = \mathbf{S}_{dz}(f) \quad (3.9)$$

Here $d(t)$ denotes the desired signal which in a cognitive radio terminology is also called the SOI (Signal of Interest). $\mathbf{S}_{dz}(f)$ is the cross-correlation vector of $d(t)$ & $\mathbf{z}(t)$. Similarly $\mathbf{S}_{zz}(f)$ is the auto-correlation matrix of $\mathbf{z}(t)$. The matrix $\mathbf{S}_{zz}(f)$ and the vector $\mathbf{S}_{dz}(f)$ are obtained by Fourier transforming the following correlations

$$\begin{aligned} R_{zz}(\tau) &= \langle \mathbf{z}(t+\tau/2) \mathbf{z}^\dagger(t-\tau/2) \rangle \\ R_{dz}(\tau) &= \langle d(t+\tau/2) \mathbf{z}^\dagger(t-\tau/2) \rangle \end{aligned} \quad (3.10)$$

Substituting the definitions of $\mathbf{z}(t)$ in terms of $x(t)$ into (3.9) yields the optimum LCL-FRESH filtering equations: [2]

$$\begin{aligned} \sum_{m=1}^M S_x^{\alpha_k - \alpha_m} \left(f - \frac{\alpha_m + \alpha_k}{2} \right) A_m(f) + \sum_{n=1}^N S_{xx}^{\beta_n - \alpha_k} \left(f - \frac{\beta_n + \alpha_k}{2} \right) B_n(f) \\ = S_{dx}^{\alpha_k} \left(f - \frac{\alpha_k}{2} \right), k = 1, 2, \dots, M, \end{aligned} \quad (3.11)$$

$$\begin{aligned} \sum_{m=1}^M S_{xx}^{\beta_k - \alpha_m} \left(f - \frac{\alpha_m + \beta_k}{2} \right) A_m(f) + \sum_{n=1}^N S_{xx}^{\beta_k - \beta_n} \left(-f + \frac{\beta_n + \beta_k}{2} \right) B_n(f) \\ = S_{dx}^{\beta_k} \left(f - \frac{\beta_k}{2} \right), k = 1, 2, \dots, N, \end{aligned} \quad (3.12)$$

Where $A_m(f)$ and $B_n(f)$ are the Fourier transforms of the weight vectors $a_m(t)$ and $b_n(t)$ respectively. The spectrum of the error $e(t) \triangleq \hat{d}(t) - d(t)$ whose mean squared value is minimized by the multivariate Wiener filter, is given by

$$S_e(f) = S_d(f) - \mathbf{S}_{dz}^\dagger(f) \mathbf{H}(f), \quad (3.13)$$

where $S_{dz}^\dagger(f)$ is the hermitian operation. The equation (3.13) can be expressed more explicitly using (3.11) and (3.12) as

$$S_{ee}(f) = S_{dd}(f) - \sum_{m=1}^M S_{dx}^{\alpha_m} \left(f - \frac{\alpha_m}{2} \right)^* A_m(f) - \sum_{n=1}^N S_{dx}^{\beta_n} \left(f - \frac{\beta_n}{2} \right)^* B_n(f). \quad (3.14)$$

For purely stationary signals we can apply the following special conditions.

$$S_{xx}^\alpha(f) \equiv S_{xx}^{\alpha^*}(f) \equiv S_{dx}^\alpha(f) \equiv S_{dx}^{\alpha^*}(f) \equiv 0 \quad (3.15)$$

for all $\alpha \neq 0$ and for $\alpha = 0$ we also have (for complex envelopes $x(t)$)

$$S_{xx}^0(f) \equiv S_{dx}^0(f) \equiv 0 \quad (3.16)$$

Consequently for $M=1$, $N=0$ and $\alpha_1=0$ in the optimum FRESH filter in (3.6) reduces to a single convolution $\hat{d}(t) = a_0(t) \otimes x_0(t)$ and the equation (3.11) and (3.12) reduce to

$$S_{xx}^0(f) A_0(f) = S_{dx}^0(f) \quad (3.17)$$

which yields the transfer function $A_0(f)$ for the conventional Wiener filter. Generalizing this terminology for cyclostationary signals, the optimum FRESH filter specified by (3.11) and (3.12) with M, N , $\{\alpha_m\}$ and $\{\beta_n\}$ optimally chosen is called a cyclic Wiener filter. When N or M or $\{\alpha_m\}$ and $\{\beta_n\}$ is constrained in any way, the resultant minimum-time-averaged-squared error filter given by equations (3.11) and (3.12), is a *constrained* optimum FRESH filter.

It is evident from the derivation of the FRESH filter using an approach similar to the Wiener filter that adaptive implementations of FRESH filter using standard weight update algorithms like LMS and RLS is possible. This gives us the flexibility to operate FRESH filter either in the training mode or decision directed mode in an environment where the characteristics of the primary signal like SNR may be unknown and varying.

The set of $\alpha_1 \cdots \alpha_M$ and $\beta_1 \cdots \beta_N$ called the cyclic frequencies, has to be chosen judiciously according to the SOI (Signal of Interest). For many signals such as QAM, QPSK, BPSK, PAM etc. the cyclic frequencies can be calculated a-priori as described in Chapter 2 section 2.2.1. In the following Fig. 3.1, the LCL filter structure for a QAM signal has been shown.

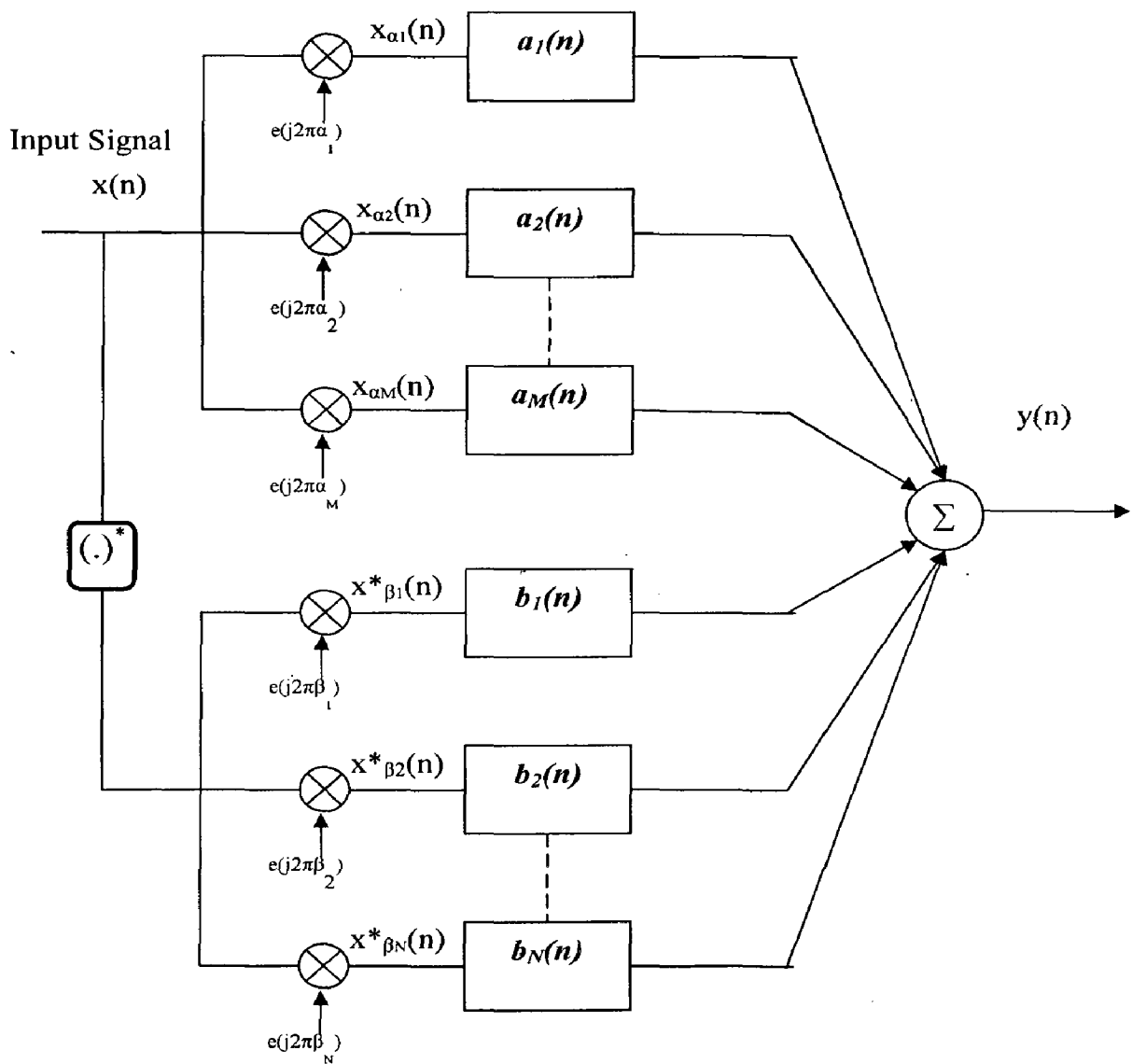


Figure 3.1: Structure of a LCL-FRESH filter.

In the above figure, the CL (Conjugate Linear part) is absent and hence contains no frequency shift while the L (linear) part has frequency shifts of $\alpha = \left\{ \frac{\pm 1}{T_0}, \frac{\pm 1}{T_0}, \dots, \frac{\pm K}{T_0} \right\}$, signifying $M=K$ and $N=0$ in the equation (3.11) and (3.12). Each of the frequency shifts is followed by a Time Invariant filter (TI) and the final output is added.

The weights of the TI filter are unknown in reality and it is not possible to beforehand predict the weights owing to the changing primary scenario. Hence, adaptive implementation of FRESH filters is necessary wherein the weights can converge to the optimum value.

3.2. Adaptive Fresh Filters

3.2.1. LMS Adaptive FRESH Filter

If a training signal is known then, a LMS (Least Mean Squares) adaptive FRESH filter can be constructed in a similar way as a LMS adaptive Wiener filter. The structure of such a filter using only linear non-conjugate filtering is shown in Fig. 3.2. The structure has M (or N) FIR filters for the L (or CL) signal part that are fed with frequency shifted versions of the signal. The output of the filters is summed and compared with a desired signal. The instantaneous error signal is used to adjust the filter weights in a Least Mean Squares manner. After a sufficient number of iterations, the output converges to the desired signal.

The output of the LMS adaptive filter is given by $\hat{y}(n) = \sum_{i=1}^M \mathbf{h}'_i \mathbf{x}_i(n)$ where the weights are $\mathbf{h}'_i = [h_i(1), h_i(2) \dots h_i(L-1)]'$ and $h_i(k)$ is the k -th filter coefficient of the i -th FIR filter, L is the filter length and $\mathbf{x}_i(n)$ is the frequency shifted version input signal $\mathbf{x}(n)$ in the i -th branch. The summation is made over both the linear and conjugate linear branches; a representative number 1 to M is taken here. Making a single vector equation for \mathbf{h} and for $\tilde{\mathbf{x}}(n)$.

$$\mathbf{h}' = [\mathbf{h}'_1, \mathbf{h}'_2, \dots, \mathbf{h}'_M]' \quad (3.18)$$

$$\tilde{\mathbf{x}}(n) = [\mathbf{x}'_1(n), \mathbf{x}'_2(n), \dots, \mathbf{x}'_M(n)]' \quad (3.19)$$

where $()'$ denotes transpose operation. We can now write the output of the filter as

$$\hat{y}(n) = \mathbf{h}'\tilde{\mathbf{x}}(n) \quad (3.20)$$

The LMS filter coefficient update equation can be written as

$$\mathbf{h}(n+1) = \mathbf{h}(n) + \mu e^*(n)\tilde{\mathbf{x}}(n) \quad (3.21)$$

where $e(n) = d(n) - \hat{y}(n)$ and $d(n)$ is the desired signal assuming that a training signal is available. Such a filter can be used in a training mode of a receiver wherein the transmitted signal is known to the receiver. It is fast converging as compared to the blind adaptive filter.

3.2. Blind Adaptive FRESH Filter

When a training signal is not available we cannot use the above LMS-adaptive filter because we do not know the desired signal. We must blindly adapt the weight vectors according to the received signal. This is a particularly challenging problem as highlighted in [26], as the presence of interference signal can badly condition the desired signal. Most of the earlier works such as [2], [37] use training signals with which filter weights can be tuned. However in a cognitive radio scenario, such a training signal is not available since, there exists no collaboration between the primary and secondary user. Hence, for such a context, blind adaptive filters become a basic need. Zhang in [38] has proposed a structure that tries to maximise the correlation between filter outputs. But Adlard in [26] points out theoretical fallacies in the structure and presents simulation results to expose the inability of such a structure to blindly reject interference. The general structure of a BA-FRESH filter is shown in figure 3.3.

The input signal is reused as the desired signal. The idea behind this operation is that the spectrum of the SOI embedded in the received signal and the spectrum of the frequency shifted versions of the received signals exhibit high correlation as the frequency shifts used are the cyclic frequencies of the SOI. Hence the FRESH filter tries to maximise this correlation and adapts the weights accordingly. On the other hand, neither the white noise samples, nor the interference signal possess spectral correlation at these frequencies. Thus when their corresponding spectrum is frequency shifted by the FRESH filter and added to the original received signal, the spectral peaks do not overlap resulting in a low correlation and hence cancellation of the interference signal and noise can be achieved.

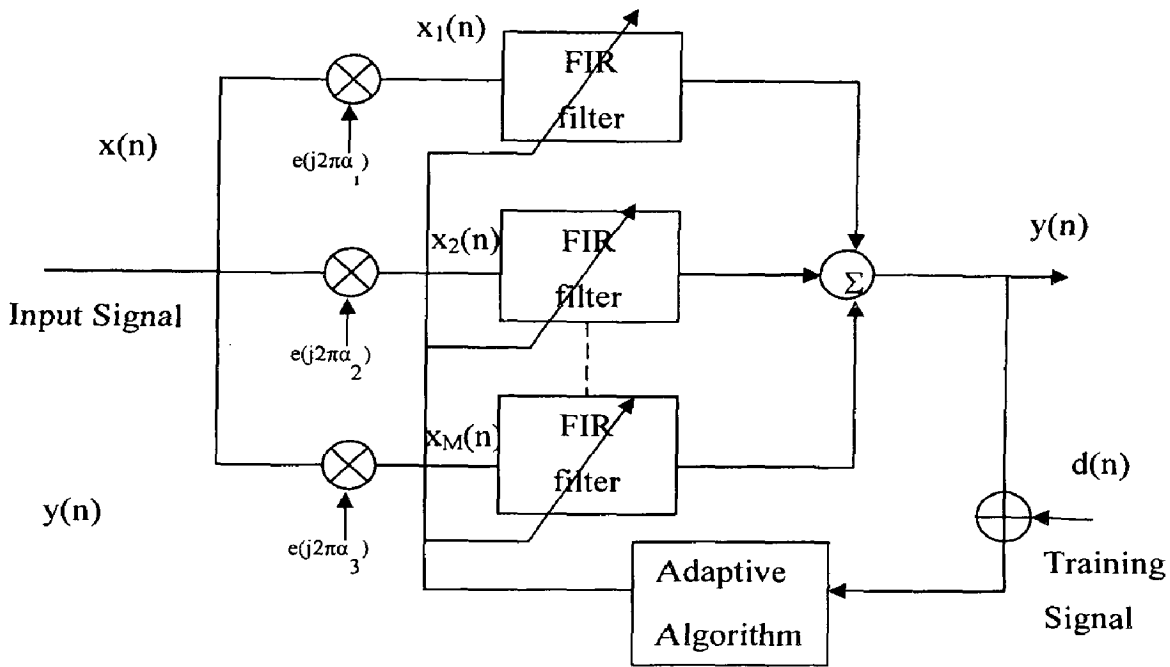


Fig.3.2: Structure of an adaptive FRESH filter using LMS algorithm.

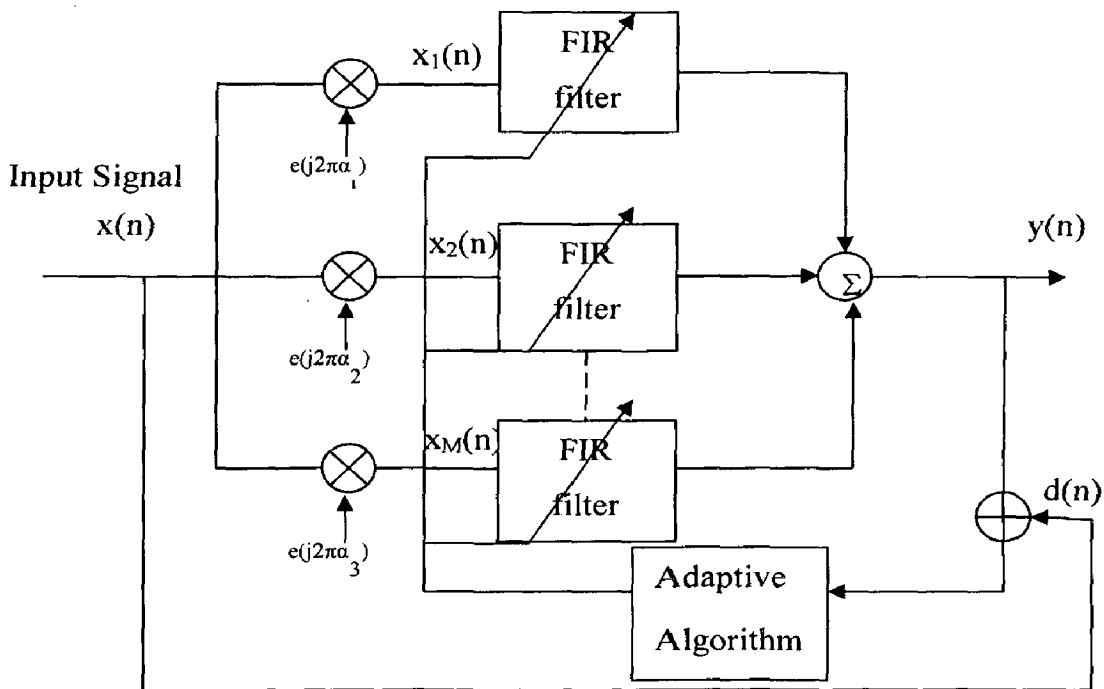


Fig. 3.3: Structure of a blind adaptive FRESH filter.

3.3. FRESH filter based Spectrum Sensing

Using the structure and theory of FRESH filtering discussed in the previous sections, this section considers the application of FRESH filters to signal detection for spectrum sensing [42]. The passband transmitted signal is assumed to be a complex BPSK signal of the form $x(t) = s(t) \exp(j2\pi f_c t)$ corrupted by AWGN with variance $\sigma_u^2 = 1$. $s(t)$ is NRZ encoded rectangular waveform with baud rate T_0 and random amplitudes of ± 1 , the carrier frequency $f_c = 307200 \text{ Hz}$. The received signal $r(t) = x(t) + u(t)$ can have a SNR from 0dB upto -20 dB. Our first task is to detect the BPSK signal at these SNR using FRESH filtering operation.

3.3.1 Signal Detection

As we know that BPSK has two cyclic frequencies namely a strong conjugate cyclostationarity at $2f_c \pm \frac{k}{T_0}$ and a weak non-conjugate cyclic correlation at multiples of $\frac{1}{T_0}$

Following the construction delineated in section 3.1, the simplest blind adaptive FRESH filter structure has only 2 branches one each corresponding to each cyclic frequency. The filter length $L = 64$ and the FIR filter weights are chosen to be zero initially. The weights are adapted in a blind manner using the LMS algorithm. This two branch FRESH structure is shown in figure 3.4. At the receiver, the signal $r(t)$ is first sampled at a sufficiently high rate to avoid aliasing at cyclic frequencies upto and beyond $2f_c$. The sampling rate is chosen to be $f_s = \frac{1}{T_s} = 102400 \text{ Hz}$. The pulse duration T_0 is set in a manner so as to obtain 32 samples

per pulse. Thus the baud rate $\frac{1}{T_0} = \frac{f_s}{32} = 3200 \text{ Hz}$. After sampling, the received signal is

$$r(n) = x(n) + u(n) \quad (3.22)$$

where $r(n) = r(nT_s)$. As the samples $r(n)$ become available, the weights of the FRESH filter are adapted through the Least Mean Square (LMS) algorithm in a blind manner. $y(n)$ denotes the output of the FRESH filter which is the sum of the outputs of all the branches and $r(n)$ serves as the desired signal. Hence the estimation error at the filter output can be given as

$$e(n) = r(n) - y(n) \quad (3.23)$$

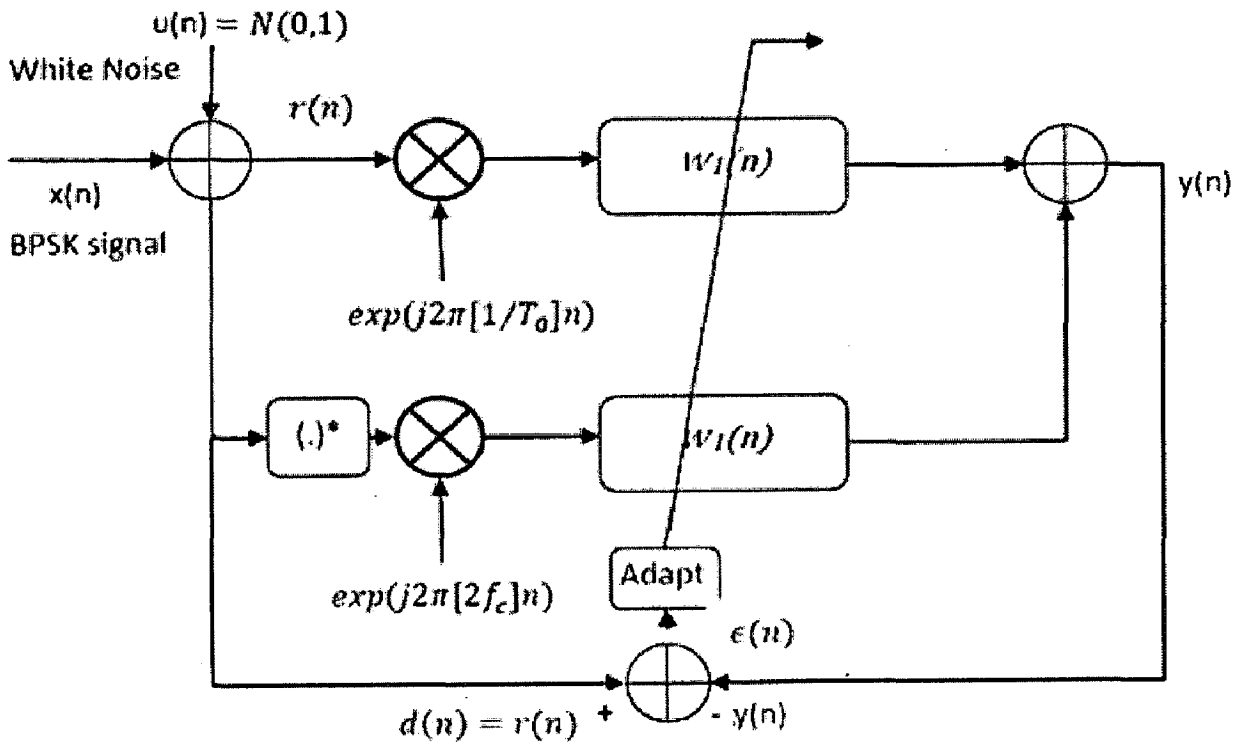


Figure 3.4: Two branch blind adaptive FRESH filter .

In order to minimize the mean square error (MSE) given by $E\{\|e(n)\|^2\}$ the LMS weight update equation is applied,

$$\mathbf{w}(n+1) = \mathbf{w}(n) + \mu \tilde{\mathbf{r}}(n) e^*(n) \quad (3.24)$$

Here $\tilde{\mathbf{r}}(n)$ denotes length L vector formed by concatenating the frequency shifted values of the received signal $r(n)$. Also, n denotes the time index and μ is the step size. The weights are updated until reasonable convergence in the mean square error is seen to occur. It should be noted that since the desired signal is a noisy version of the input, hence once the filter converges, ideally the value of MSE would be equal to the variance of AWGN and the output variance should match with the transmitted signal variance. But due to misadjustment error introduced by the weight update algorithm and finite number of iterations being used, the resultant mean square error will be in excess of the noise variance. This excess MSE depends on the value of the step size μ . The value of μ has to be chosen empirically in order to minimize this excess MSE and also maintain a suitable rate of convergence for the FRESH filter. Hence, the first step is to observe the convergence of the FRESH filter in mean square error as shown in figure 3.5.

Figure 3.5 shows MSE of the FRESH filter for $\mu = 5 * 10^{-5}$ and SNR 0dB. The mean square error has been obtained simulating the two branch FRESH filter shown in figure 3.4 for detecting the BPSK signal at 0dB, and by averaging the mean square of 100 independent Monte Carlo runs. It can be observed that the frequency shift filter converges to a MSE of around 1.2 around 6000 samples. The filter gives an excess MSE of 0.2 over the noise variance because with only 2 branches, the filter is not able to completely exploit the cyclostationary features of the BPSK signal. In order to explore the variation in excess MSE with the number of frequency shifts, we improve the design of the 2 branch filter and include 4 more cyclic shifts. We now use three cyclic frequencies of the BPSK signal $x(t)$ namely, $\alpha_1 = \frac{1}{T_0}$, $\alpha_2 = 2f_c$ and $\alpha_3 = 2f_c + \frac{1}{T_0}$. A BA-FRESH (Blind Adaptive FRESH) filter is constructed as shown in figure 3.6. The filter has two branches for linear filtering and four branches for conjugate linear filtering. These six branches have the frequency shifts of $\alpha = \{\pm\alpha_1, \pm\alpha_2, \pm\alpha_3\}$ respectively.

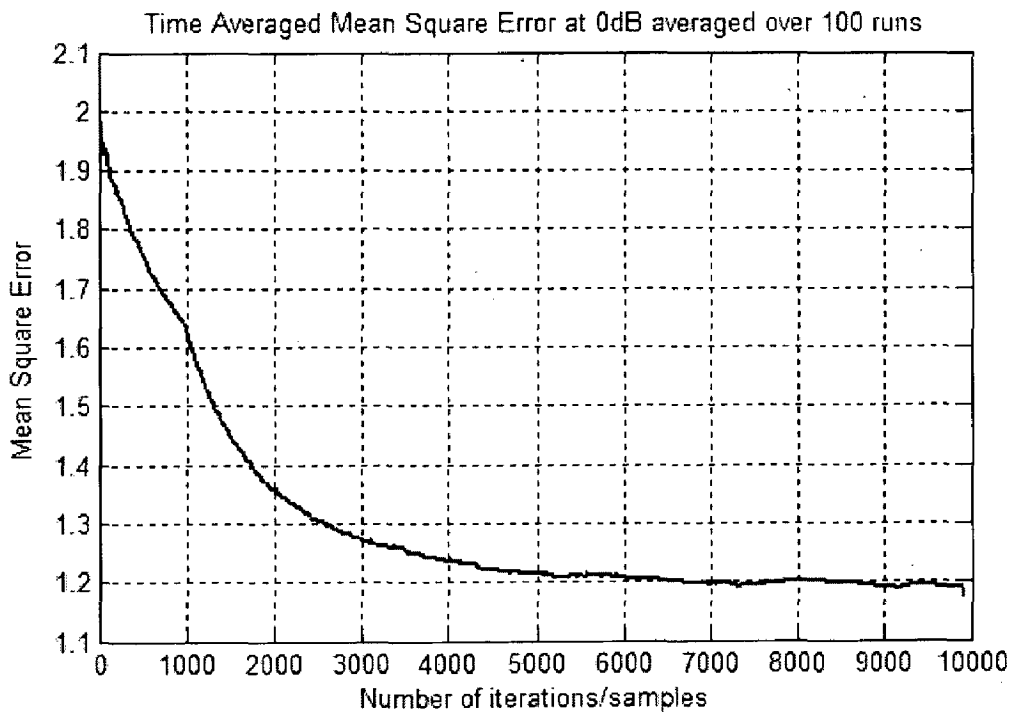


Figure 3.5: Time averaged MSE of the two branch LMS blind adaptive FRESH filter.

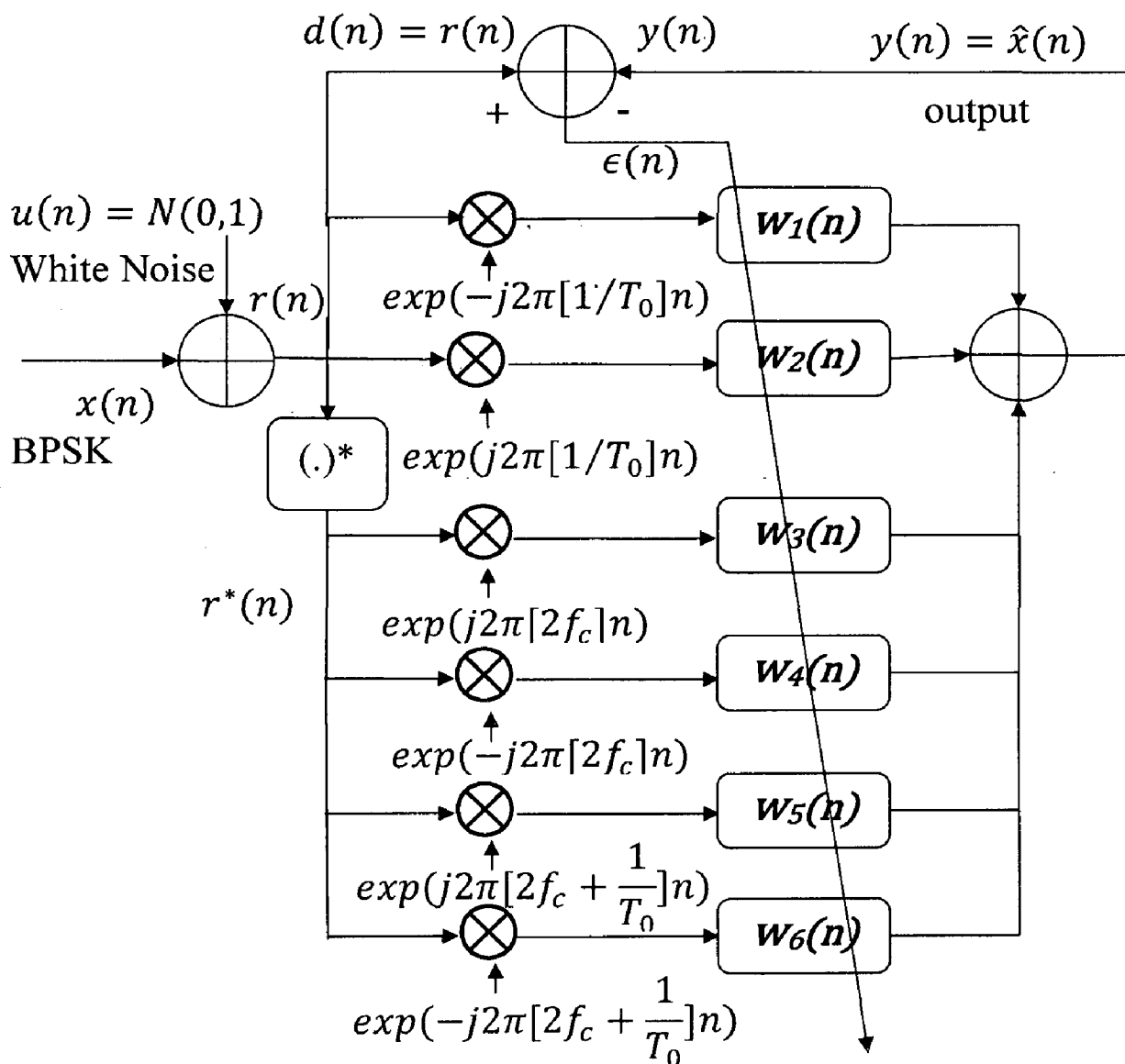


Figure 3.6: Six branch blind adaptive FRESH filter.

In the above figure 3.6, w_i denotes the length L weight vectors of each FIR filter, for $i=1$ to 6. This FRESH filter has the ability to exploit both conjugate and non-conjugate cyclostationarity of BPSK over a larger set of cyclic frequencies. Figure 3.7 plots the mean square error curves for this filter for different step-size values. As a reference we also include the MSE curves for the 2-branch FRESH filter. It is clear that increasing the number of frequency shifts decreases the excess MSE. Based on the plots, the optimum value of μ is found to be 5×10^{-5} . It is true that after a certain limit, increasing the number of frequency shifts does not lead to substantial improvement in the excess MSE as it is fundamentally limited by the misadjustment due to the weight update algorithm like LMS/RLS. Hence, we stick to the 6 branch FRESH filter for the purpose of detecting a BPSK signal.

In order to compare the performance of the weight adaption algorithm, we also develop an RLS-FRESH. Since RLS is faster converging than LMS and has lesser misadjustment errors, hence it is expected to yield better results in signal estimation by FRESH filters. The RLS algorithm used is briefly stated below.

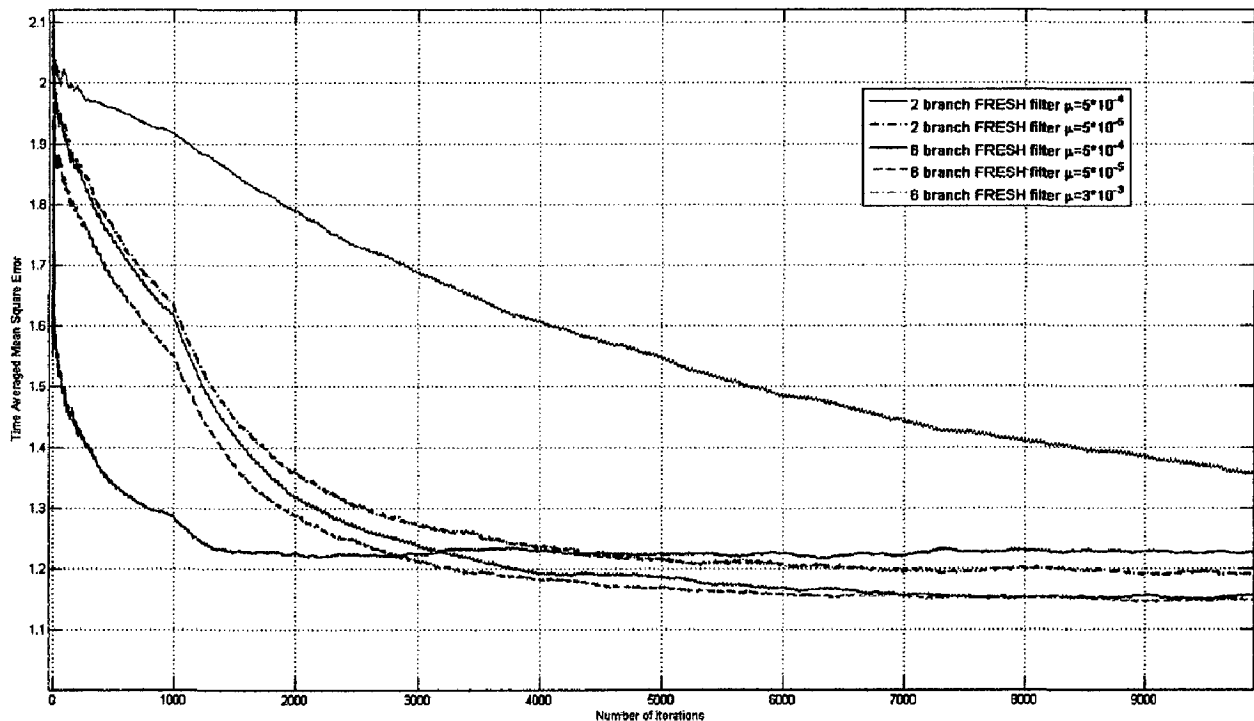


Figure 3.7: Comparison of time averaged mean square error for the six branch and two branch LMS blind adaptive FRESH filter for three values of step size μ .

RLS Algorithm [34]

Parameters:

λ =forgetting factor (assumed unity).

δ =initializing value for $\mathbf{P}(0)$.

L =length of filter.

Initialization:

$\mathbf{w}_i = \mathbf{0}$, $i=1,2,\dots,L$

$\mathbf{P}(0) = \delta^{-1}I$ where I is an identity matrix of rank L

$x(k)=0$, $k=-L,\dots,-1$

Computation: For $n=0,1,2,\dots$

$$\mathbf{x}(n) = \begin{bmatrix} x(n) \\ x(n-1) \\ \vdots \\ x(n-L) \end{bmatrix}$$

$$\alpha(n) = d(n) - \mathbf{w}^H(n-1)\mathbf{x}(n)$$

$$\mathbf{g}(n) = \frac{\mathbf{P}(n-1)\mathbf{x}(n)}{\lambda + \mathbf{x}^H(n)\mathbf{P}(n-1)\mathbf{x}(n)} \quad (3.25)$$

$$\mathbf{P}(n) = \lambda^{-1}\mathbf{P}(n-1) - \lambda^{-1}\mathbf{g}(n)\mathbf{x}^H(n)\mathbf{P}(n-1)$$

$$\mathbf{w}(n) = \mathbf{w}(n-1) + \alpha^*(n)\mathbf{g}(n).$$

3.3.2 Spectrum Sensing

The cognitive radio must make a spectrum sensing decision on the frequency shift filtered received signal. Since by filtering the signal, we have suppressed any noise and interference present in the received signal, the SNR of the signal has improved. To make a decision on the presence of the signal, the cognitive radio formulates a statistical test on the output $y(n)$ of the FRESH filters. This statistical test checks for the presence of the desired cyclic frequencies in

the filtered signal. If a primary signal such as BPSK is present, then the filtered signal would possess discrete peaks at the cyclic frequencies of baud rate and twice the carrier frequency. Hence, purpose to use the suboptimal sum test developed in section 2.3 that uses the sum of the cyclic autocorrelation values of the signal at its cyclic frequencies as the test statistic. The test is restated here.

The test statistic \mathbb{A} is given by

$$\mathbb{A} = \sum_{n=1}^P \hat{R}_{zz}^{\alpha_n} \quad (3.26)$$

where P denotes the set of desired cyclic frequencies which in our case is $P = \left\{ 2f_c, 2f_c - \frac{1}{T_0}, 2f_c + \frac{1}{T_0} \right\}$, $z(n)$ is the output of the filter and $\hat{R}_{zz}^{\alpha_n}$ is the conjugate cyclic autocorrelation of z calculated at cyclic frequency α_n with the cap denoting the use of N samples for calculation as given by equation (2.17) reproduced here for clarity,

$$R_{xx}^{\alpha}(\tau) = \frac{1}{N} \sum_{l=\tau}^{N+\tau-1} x(l)x(l-\tau)e^{-i2\pi\alpha l/T_s} \quad (3.27)$$

Using this new test statistic, we set up a Neyman-Pearson test as follows:

Neyman-Pearson test for Signal Detection:

1. Formulate the hypotheses $H_0 : \mathbb{A} = \chi_{zz}$, where χ_{zz} is the error in \mathbb{A} due to excess mean square error, finite $H_1 : \mathbb{A} = r_{sum} + \chi_{zz}$ number of samples and periodic time varying transformation of noise samples by FRESH filter and r_{sum} is the true value of the test statistic under no noise scenario.
2. Under hypothesis H_0 , set the false alarm probability to P_f and obtain from simulation, a threshold λ such that $\Pr(\mathbb{A} | H_0 > \lambda) = P_f$.
3. Under hypothesis H_1 , find the detection probability P_d by the formula $P_d = \Pr\{\mathbb{A} | H_1 > \lambda\}$.

An interesting phenomenon to be observed here is that although AWGN samples possess no cyclostationarity and when this suboptimal sum test is used in the context of cyclostationary

spectrum sensing, there should be no contribution to the test statistic from a possible cyclic correlation term from noise samples. It is only due to using a finite number of samples that the test statistic does not converge to the true value. However, in the present context, when no signal is present, the noise samples after passing through a LAPTV (Linear Almost Periodic Time Varying) filter become cyclostationary and exhibit discrete peaks at the cyclic shifts that are used in the FRESH filter [32]. This acts as an additional constraint along with the fact that we must detect the signal using a finite number of samples.

To evaluate the performance of the proposed test, we simulate the BA-FRESH filter in figure 3.6 using the LMS and RLS algorithms. We conduct 1000 simulation runs to evaluate the test statistic A when no signal is transmitted. Using the distribution of test statistic A we determine the threshold λ such that the rate of false alarm is limited to a maximum of 10 percent. Subsequently we conduct 1000 Monte Carlo runs at each SNR 0dB, -1dB, ..., -20dB and observe the average probability of detection that the test statistic provides.

Figures 3.8-3.11 show the results of the simulation obtained using $N=400, 800, 1600$ and 3200 respectively. The plots include a comparison between the corresponding detection curves obtained by using the BA-FRESH filter with LMS and RLS adaptive algorithms, energy detection (equation 2.8), energy detection with 1dB noise uncertainty (equation 2.10, 2.11) and the suboptimal sum test used for cyclostationary detection (Simulation Example 2, equation 2.31).

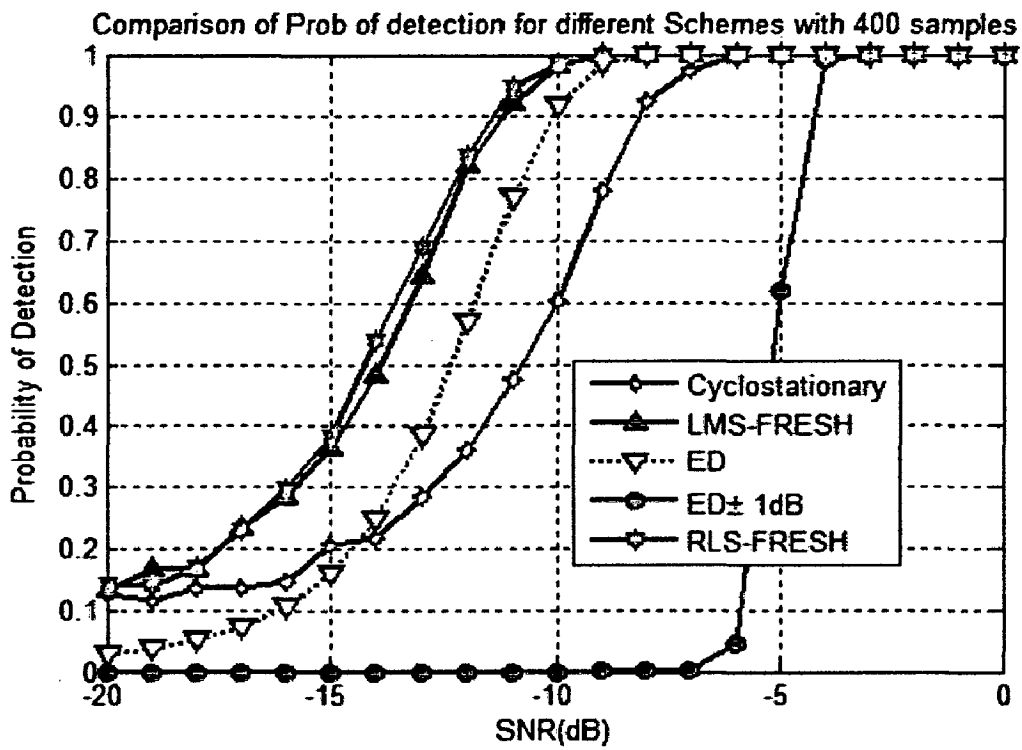


Figure 3.8: Comparison of probability of detection curves for different techniques with $N=400$ samples.

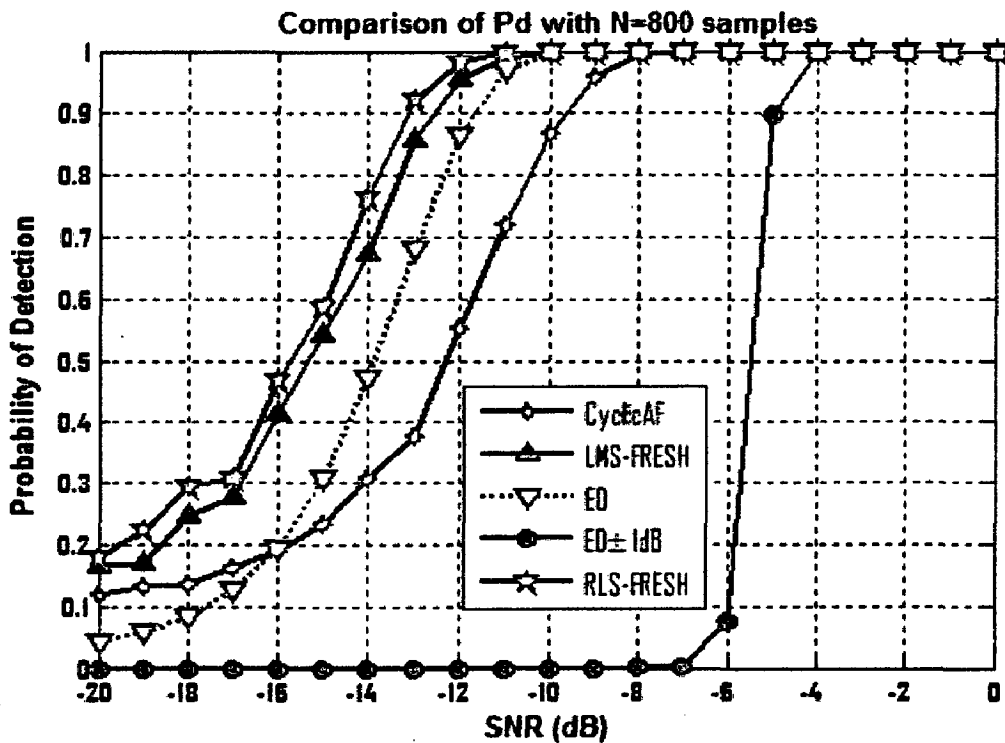


Figure 3.9: Comparison of probability of detection curves for different techniques with $N=800$ samples.

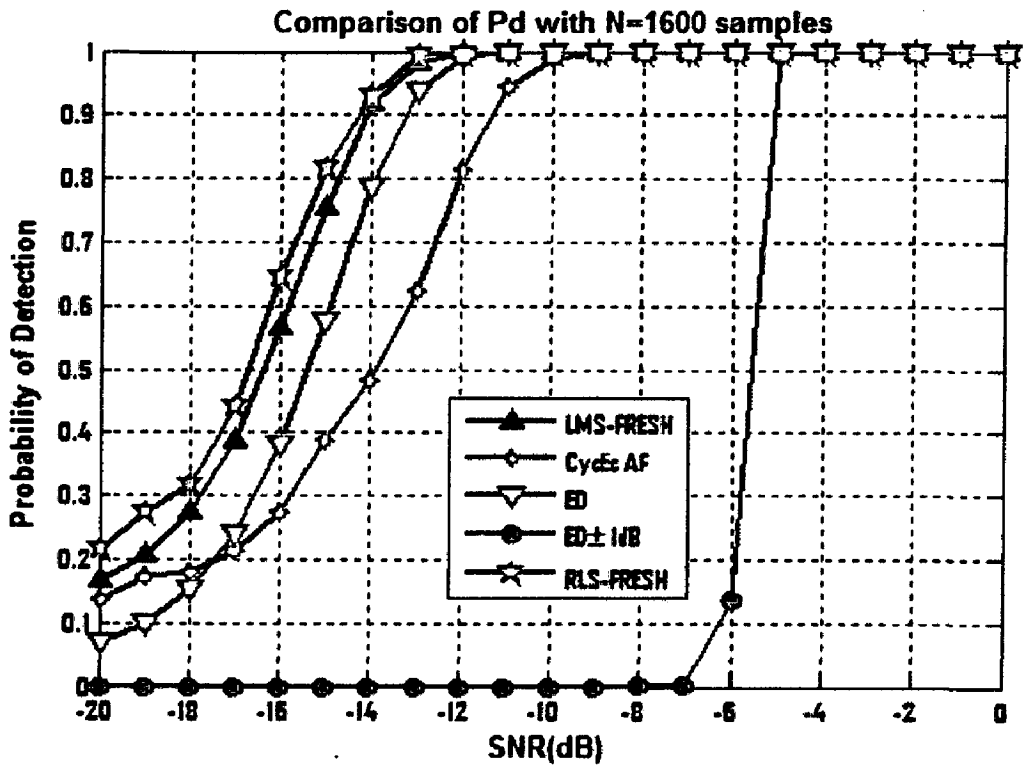


Figure 3.10: Comparison of probability of detection curves for different techniques with N=1600 samples.

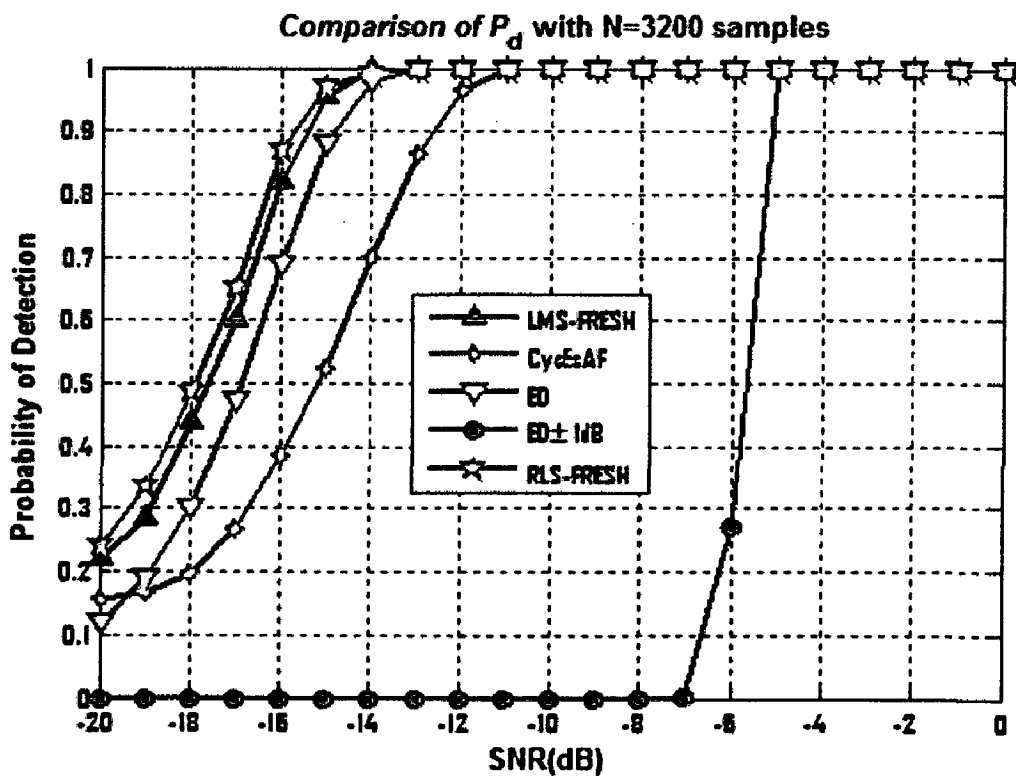


Figure 3.11: Comparison of probability of detection curves for different techniques with N=3200 samples.

As we can see from figures 3.8-3.11, FRESH filtering followed by the proposed sum test yields better average probability of detection curves than all other techniques. In the low SNR regime (below 0dB), where it difficult to reliably detect the signal, FRESH filter based detection outperforms energy detection and cyclostationary detection. Also the RLS-FRESH filter gives better detection performance than the LMS-FRESH counterpart and it has also been observed that it shows a faster rate of convergence. It is important to note from the four plots that the probability of detection for a given SNR increases as we employ a higher number of samples for sensing. For all the stated schemes viz. FRESH filtering, energy detection (assuming no noise distribution uncertainty) and cyclostationary detection, the difference in detection performance is only visible at low SNR values (below -5dB) and this difference decreases progressively as number of samples N increases. It is worth noting that for lower values of N (400 and 800) cyclostationary detection performs better than energy detection below -16 dB SNR. This indicates that relying on cyclostationary features for spectrum sensing is a better option at such low SNR.

3.3.3 Signal Detection with Interference Signal Present

For the same BPSK signal, an interference signal of frequency $f_{\text{inter}}=0.1f_s$ and INR (Interference to Noise Ratio) of 0dB was introduced. The blind adaptive FRESH filter is trained with the interference corrupted received signal and performance of signal detection was observed. It is observed that for low number of samples (around thousand), the FRESH filter's output differs from the transmitted signal and the MSE value is large enough to indicate a lack of convergence. On observing the cyclic autocorrelation function of the output signal, it is found that, the CAF shows a similar magnitude peak at the cyclic frequency of the interferer as compared to the signal cyclic frequency. As a result, the sum test statistic does not perform well enough to give a suitable probability of detection performance and it is observed that cyclostationary detection outperforms frequency shift filtering using the sum hypothesis test as shown in figure 3.12.

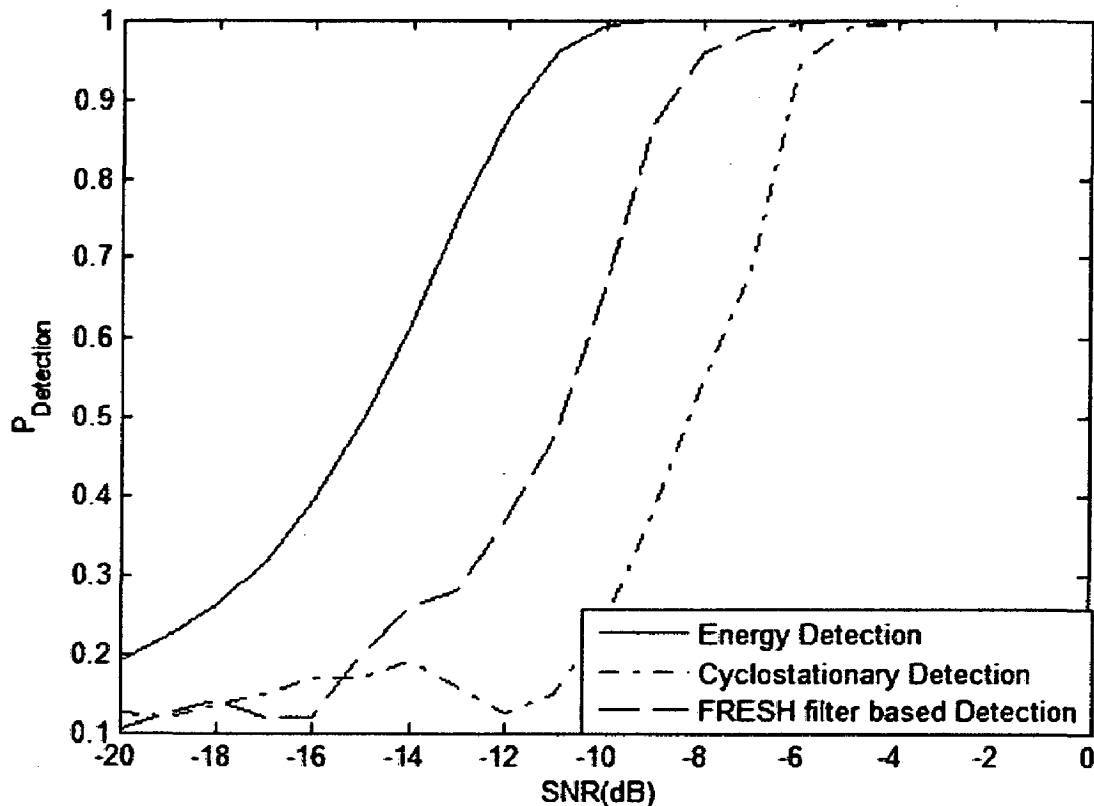


Figure 3.12: Comparison of probability of detection curves for different techniques with 0dB interference.

The reason for this failure is assumed to be the fact that with low number of samples available for sensing, a blind adaptive FRESH filter is unable to converge to the optimum set of weights as the desired signal is corrupted by a high level of AWGN and spurious signals. Similar problem was identified by Adlard [26]. But FRESH filters can still work under interference, given that increased number of samples are used for sensing. In this experiment, we increase the number of samples from 800 to 30800 and observe the detection performance of FRESH filter. It is seen that with 0dBm interference, the average detection probability achieved by using the sum hypothesis test is just below the detection performance of FRESH filter based detection using 800 samples when no interference is present. Figure 3.13 presents the detection curves for both the cases. This proves that unlike an energy detector, FRESH filters can reject interference and work robustly although with more number of samples.

Another strategy may be to use a locally generated desired signal using an independent BPSK source and use it to as a training signal for the FRESH filter. Further study is required to fully explore the performance of FRESH filters under interference and to develop robust BA-FRESH filters in the presence of interference.

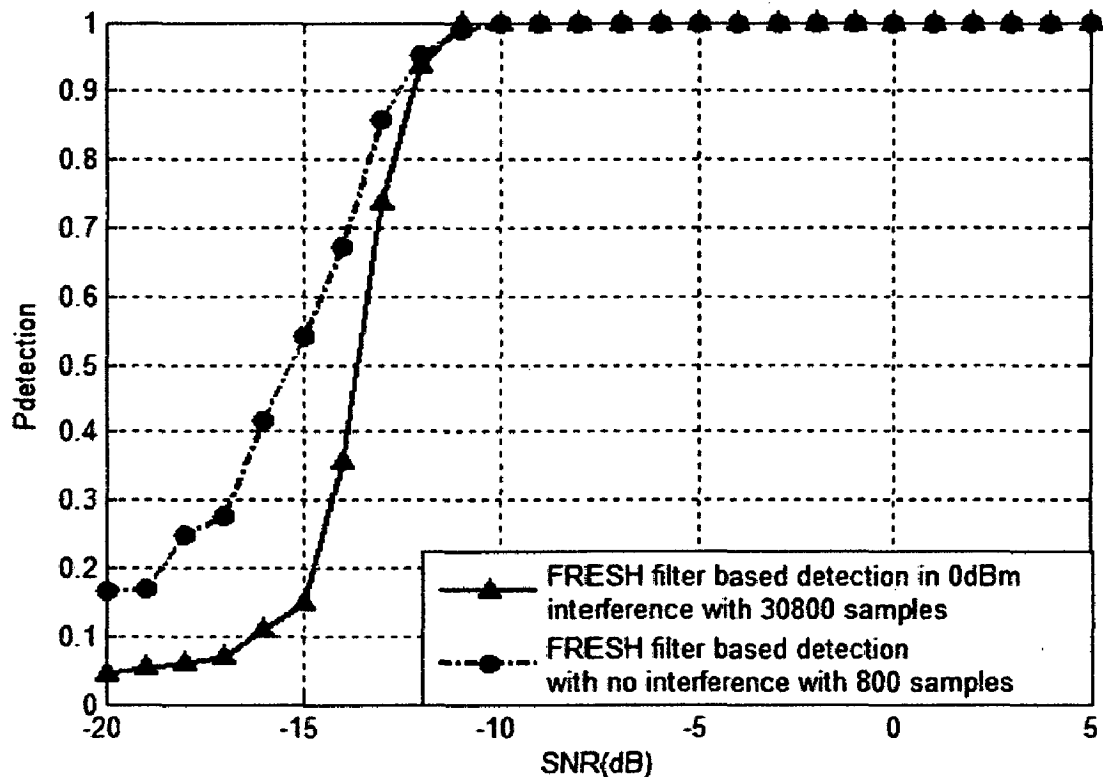


Figure 3.13: Comparison of probability of detection curves for FRESH filter based detection in AWGN with 800 samples and with BPSK interference at 0dB INR with 30800 samples.

Based on the study and simulations of FRESH filters, it can be suggested that by optimally exploiting the cyclostationary features of signals, FRESH filters can be suitable to meet the stringent requirements for spectrum sensing in the upcoming cognitive radio standards like IEEE 802.22, in terms of probability of detection and minimum sensitivity in SNR. While FRESH filters perform better than energy detection and cyclostationary detection, for spectrum sensing in the presence of AWGN, presence of interference deteriorates their performance, and more number of samples are required to maintain the same level of detection performance. Another limiting factor for the practical implementation of FRESH filters is the computational complexity involved in designing filters and ensuring a fast enough rate of convergence. But, as more and more powerful DAC/ADC's are being produced and highly complex circuitry can be realised on FPGA, it is reasonable to assume that FRESH filters can be used as part of standalone sensing devices. Moreover for an ADC sampling at 2Gps, sampling 3200 values would take about five-hundredth of a millisecond, a fairly short time in which sensing decisions can be taken.

Chapter 4

Spectrum Sensing for OFDM signals

We have seen in the previous chapters, the use of energy detection, cyclostationary detection and FRESH filter based detection for spectrum sensing in a single-carrier environment like BPSK. The complete class of digital QAM signals with quadrantal symmetry defined by equation (2.22) exhibits cyclic frequencies at either baud rate or twice the carrier frequency or both. Most of the literature, till quite recently, discusses the application of spectrum sensing techniques for such single carrier systems based on the assumption that the legacy transmissions of primary users adopt these transmission techniques. But, over last few years a tremendous need for substantial increase in data rates and spectral efficiency has been felt. Thus the interest of the community has shifted from single carrier to multi-carrier techniques which provide us the capability to increase data rates and simplify the receiver hardware while pinning down harmful effects like ISI.

One of the most popular multicarrier techniques is OFDM (Orthogonal Frequency Division Multiplexing). Many of the current and future technologies for wireless communication such as WiFi, LTE and DVB-T, use OFDM signalling [21]. Therefore it is reasonable to assume that cognitive radios must be able to detect OFDM signals. In order to combat Inter-Symbol Interference (ISI) every OFDM symbol carries a cyclic prefix (CP) whose length is equal to or greater than the channel length. While this helps mitigate ISI, it also introduces certain correlation structure in the OFDM symbol which can be used for its detection. This section presents a brief discussion of OFDM and explains why the task of spectrum sensing in this orthogonal multicarrier scheme is more challenging than the single carrier counterparts. It presents simulation results to present the inability of FRESH filters to detect OFDM and explores the reasons behind. It presents theoretical derivations for the detection performance of energy detection and cyclostationary detection in cyclic prefixed OFDM using an optimal Neyman-Pearson detector. Finally it proposes the application of induced cyclostationary signatures in OFDM and develops an optimal detector for the same.

4.1 Orthogonal Frequency Division Multiplexing (OFDM)

OFDM is a multicarrier transmission technique in which the incoming data is modulated onto orthogonal subcarriers. As opposed to FDM (Frequency Domain Multiplexing) where the complete frequency band is split into non-overlapping chunks of spectrum, each allotted to an independent user, subcarrier spectrum in OFDM overlap hence leading to better spectral efficiency. In order to maintain the orthogonality between individual subcarriers, the total bandwidth W is split into N_c subcarriers. The incoming serial stream of data is converted to a parallel stream with N_c samples in one symbol. These N_c symbols are modulated onto the N_c subcarriers using a rectangular pulse shaping. The mathematical representation of baseband OFDM is given by the following equation [43]:

$$x(t) = \sum_{n=0}^{N_c-1} \sum_{l=-\infty}^{\infty} d_{n,l} g(t - lT_s) e^{j(2\pi/N_c)nt} \quad (4.1)$$

where N_c is the number of subcarriers, $1/T_s$ is the symbol rate of OFDM and also of each subcarrier, $g(t)$ is the rectangular pulse of length T_s , and $d_{n,l}$ are the data symbols obtained from a symbol mapper such as 16-QAM or QPSK. In practical systems, this operation can be easily implemented by using an IFFT (Inverse Fast Fourier Transform) block which is commercially available in ASIC (Application Specific Integrated Circuit) form. The advantage of OFDM is that it increases the symbol duration N_c times i.e. $T_s = N_c T_0$ where T_0 is the duration of a data symbol. This helps reduce ISI as the OFDM symbol duration becomes N_c times the initial duration T_0 hence channels with few multi-paths, the delay spread of the channel becomes insignificant compared to the symbol length. Also the bandwidth of each subcarrier becomes lesser than the coherence bandwidth of the channel thus preventing any frequency selective distortion in the symbols. By this phenomenon, OFDM can convert a frequency selective fading channel into a flat fading channel, thus helping greatly reduce the complexity of equalization at the receiver. In order to mitigate any resultant ISI, OFDM uses a cyclic prefix (CP), which is a copy of the portion of the OFDM symbol from its end appended to its beginning. At the receiver this CP is chopped off and the useful OFDM symbol is retrieved. Usually CP lengths of $T_s/4$ are chosen though sometimes $T_s/2$ & T_s length CP may also be used depending on the channel length. A complete block diagram of an OFDM system is shown in figure 4.1.

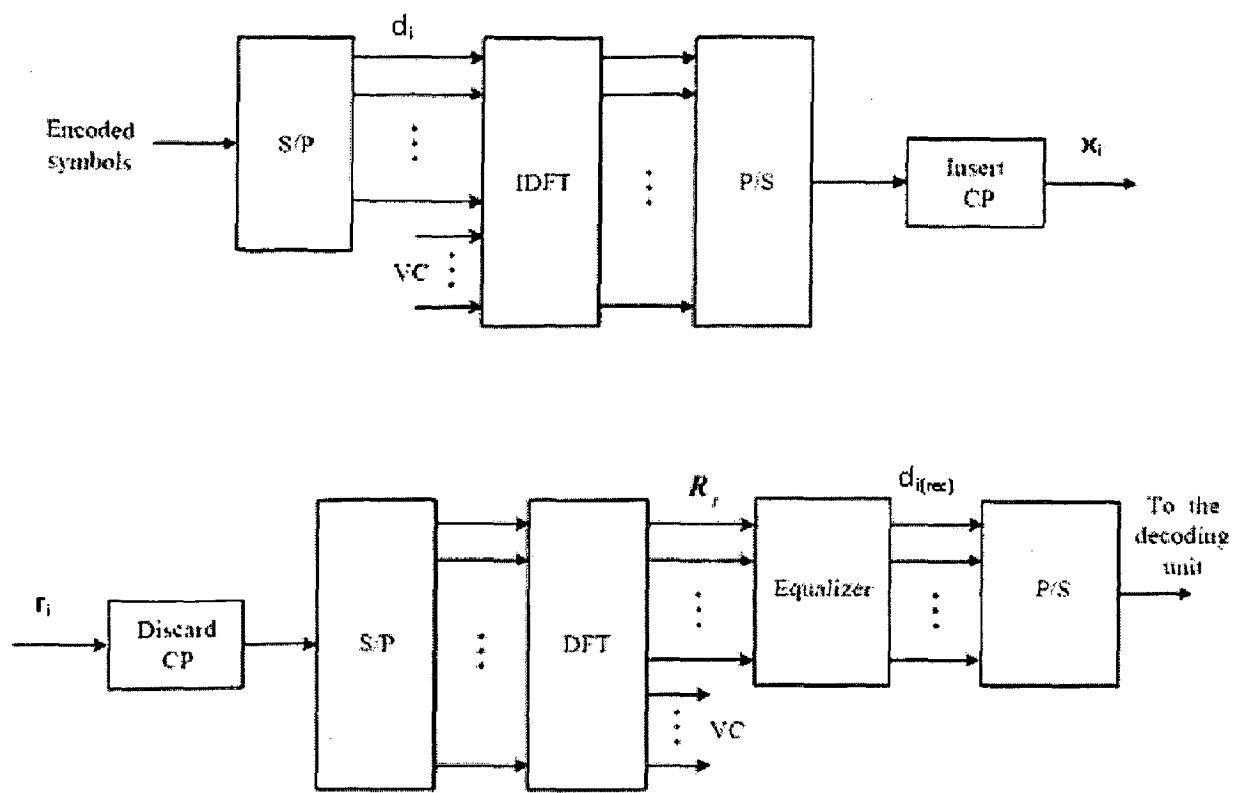


Figure 4.1: OFDM transmitter and receiver block diagram.

4.2 Energy Detection

Spectrum sensing in OFDM can be performed by any of the earlier discussed methodologies. The simplest technique among them is energy detection. In OFDM frequently guard bands at the ends of the OFDM spectrum are left out in order to avoid out-of-band interference to the adjacent bands. OFDM offers cognitive radio, the capability to insert null/virtual sub-carriers in the spectrum to leave any primary users operating in the band undisturbed. Additionally a single subcarrier is left unoccupied on both sides of the primary band to give extra protection from interference. These guard subcarriers and guard bands can be efficaciously used by the cognitive transmitter and receiver to make independent measurements of the noise power. Also noise power can be estimated during quiet periods of cognitive radios that are synchronized across a geographic region [30]. Once the noise power estimate is available the interference temperature limit for that band can be calculated and the receiver and transmitter can jointly decide on the operating characteristics namely detection probability, false alarm rate, sensing duration, transmitted signal power, frequency of operation etc. For example, if the interference temperature in a band rises suddenly due an upcoming nearby primary signal,

the cognitive radio must decide either to increase its sensing duration to maintain the desired probability of detection or may settle to increase its false alarm rate resulting in opportunity losses. Thus the task of noise power measurement is integral to spectrum sensing in OFDM.

At the cognitive receiver the passband OFDM signal is first down converted to baseband and passed through a band pass filter whose bandwidth is equal to the bandwidth over which the spectrum sensing device can operate. This baseband signal is now sampled at a rate greater than at least twice this bandwidth to yield samples $r(n)$. Two hypotheses can be formulated on these samples as stated below,

$$\begin{aligned} H_0 : r(n) &= w(n), \\ H_1 : r(n) &= x(n) + w(n). \end{aligned} \tag{4.2}$$

where $w(n)$ denotes the AWGN in the channel with power σ_w^2 and $x(n)$ is the OFDM signal with power σ_x^2 . Using the samples $r(n)$, energy of the signal is calculated using the test statistic

$$\mathbb{E} = \sum_{i=1}^N |r(i)|^2 \tag{4.3}$$

Since the signal and noise samples are independent, the test statistic \mathbb{E} follows the chi-square distribution under H_1 and H_0 as derived in section 2.1. The results are restated here for clarity.

$$\mathbb{E} = \begin{cases} \chi_{2N}^2 & , H_0 \\ \chi_{2N}^2(2\gamma) & , H_1 \end{cases} \tag{4.4}$$

where γ is the average SNR given by $\gamma = \frac{\sigma_x^2}{\sigma_w^2}$.

The probability of false alarm and the probability of detection can be found by using equation (2.8) as

$$P_f = \frac{\Gamma(N, \frac{\lambda}{2})}{\Gamma(N, 0)}, \quad (4.5)$$

$$P_d = Q_M(\sqrt{2\gamma}, \sqrt{\lambda}).$$

where $\Gamma(\cdot, \cdot)$ is the incomplete Gamma function given by $\Gamma(s, x) = \int_x^\infty t^{s-1} e^{-t} dt$ and $Q_M(\cdot, \cdot)$ is the generalized Marcum Q- function given by $Q_M(\alpha, \beta) = \frac{1}{\alpha^{M-1}} \int_\beta^\infty x^M e^{-(x^2 + \alpha^2)/2} I_{M-1}(\alpha x) dx$ where $I_n(x)$ is the modified Bessel function of the first kind [29]. The plot of detection probability for signal with SNR from 0dB to -20 dB with a false alarm probability of 0.05 is shown in figure 4.2.

The blue curve shows the theoretical detection performance of energy detection using 400 samples generated using equation (4.5) with $N=400$ samples, while the red curve shows the theoretical probability of detection curve obtained using noise uncertainty assumption of 1dB, generated using equations (2.10) and (2.11). It can be seen that when distributional uncertainty of the order of 1dB is present in the noise variance, there is a SNR loss of around 5dB for maintaining the probability of detection at 0.9. It must be asserted that an energy detector is blind to the modulation technique, hence its performance at any given SNR for a specific number of samples remains same for all kinds of digital modulated signals. This detection performance of energy detector is the maximum achievable probability of detection at any given SNR for signals which are i.i.d. (independent and identically distributed) corrupted by AWGN. This results from the fact that under the above two assumptions, an optimal maximum likelihood ratio test for the presence of a signal, simplifies to a test statistic that involves calculating the energy of the received samples.

But for signals where a correlation structure is present, better detection probability can be achieved by using a spectrum sensing scheme that exploits the correlation between samples.

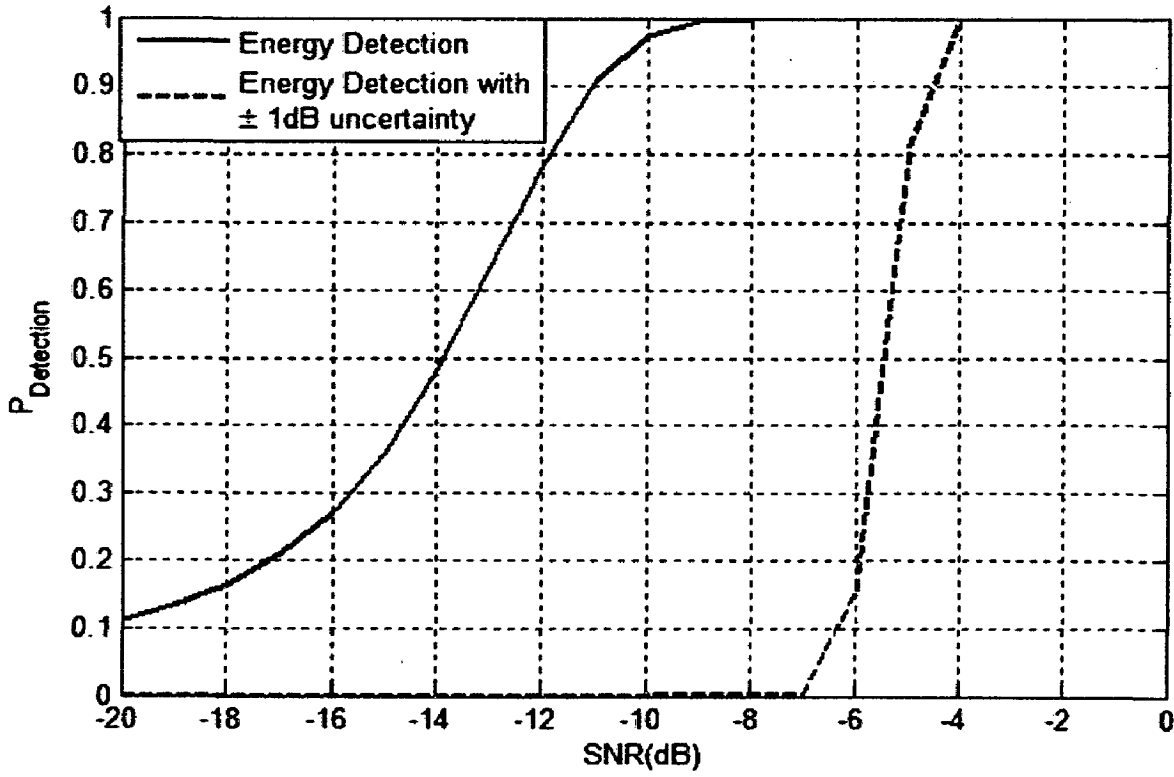


Figure 4.2: Theoretical probability of detection curves for energy detection with $N=400$ samples.

4.3 Cyclostationary Detection

As outlined in section 2.2.1, each QAM modulated subcarrier in OFDM will independently exhibit cyclostationarity at symbol rate which can be exploited to detect the specific subcarrier signal. By analogy, an OFDM signal with symbol rate $1/T_s = 1/N_c T_0$, should possess cyclic correlation at its symbol rate T_s . But, due to orthogonality between the subcarriers, the cumulative OFDM signal does not possess any cyclostationarity [44]. To avoid the loss of cyclostationarity, a cyclic prefix is inserted before each OFDM symbol which destroys the subcarrier orthogonality. For the baseband OFDM using a CP of length

T_{cp} , the transmitted signal in the time domain is given by
$$x(t) = \sum_{n=0}^{N_c-1} \sum_{l=-\infty}^{\infty} d_{n,l} g(t-lT) e^{j(2\pi/N_c)nt}$$

where T is the total OFDM symbol duration after the addition of CP given by $T = T_s + T_{cp}$.

The signal $x(t)$ can be written as $x(t) = \sum_{n=1}^N x_n(t)$ where $x_n(t) = e^{j2\pi/T_s nt} v(t)$ where the complex

envelope of QAM signal denoted by $v(t)$ is given as $v(t) = \sum_k d_k g(t - kT)$. The cyclic autocorrelation of the signal $x(t)$ can now be written as[44]

$$R_{xx}^\alpha = R_{vv}^\alpha(t, \tau) \cdot \frac{\sin\left(\frac{N_c \pi \tau}{T_s}\right)}{\sin\left(\frac{\pi \tau}{T_s}\right)} \cdot e^{j\frac{\pi}{T_s}(N_c - 1)\tau} \quad (4.6)$$

When the signal is sampled at $t = nT_0 = \frac{nT_s}{N_c}$, then for delays $\tau = 0, \pm T_s$, the value of the central sinc function and $R_{vv}^\alpha(t, \tau)$ is non-zero for $T \neq T_s$, but when $T = T_s$, which means the CP length is zero, $R_{vv}^\alpha(t, \tau)$ becomes zero for lags $\tau = \pm T_s$, thus destroying the cyclostationarity at symbol rate in OFDM.

This means that baud rate cyclostationarity in OFDM cannot be exploited for detection. Even the cyclic peaks due to cyclic prefix are small in magnitude. The result is that using cyclostationary based techniques for detection of OFDM would yield poor results than expected.

To substantiate the above fact, we simulate an OFDM signal without any cyclic prefix and with input symbol rate $1/T_0 = 6400 \text{ Hz}$ and $N_c = 64$. The subcarrier symbol rate is $1/T_s = 1/N_c T_0 = 6400/64 = 100 \text{ Hz}$. The cyclic autocorrelation function of this OFDM signal is shown in figure 4.3. It is evident that no cyclic peaks are present in the signal as predicted earlier. Now, a CP of length $T_s/4 = 8$ samples is inserted at the beginning and OFDM symbol duration increases to 80 samples. Due to cyclic prefix, the signal shows cyclostationarity at multiples of the frequency $1/T = 4/5T_s = 80 \text{ Hz}$. The plot in figure 4.4 shows the cyclic autocorrelation function the cyclic prefixed OFDM signal at lag 64. The presence of discrete peaks at multiples of 80 Hz confirms the presence of cyclostationarity in cyclic prefixed OFDM.

Even though cyclic prefix introduces correlation in OFDM, with such low magnitude of cyclostationarity in the OFDM signal, it is not possible to apply cyclostationary detection for spectrum sensing of OFDM signal. Hence we introduce the concept of Excess Bandwidth.

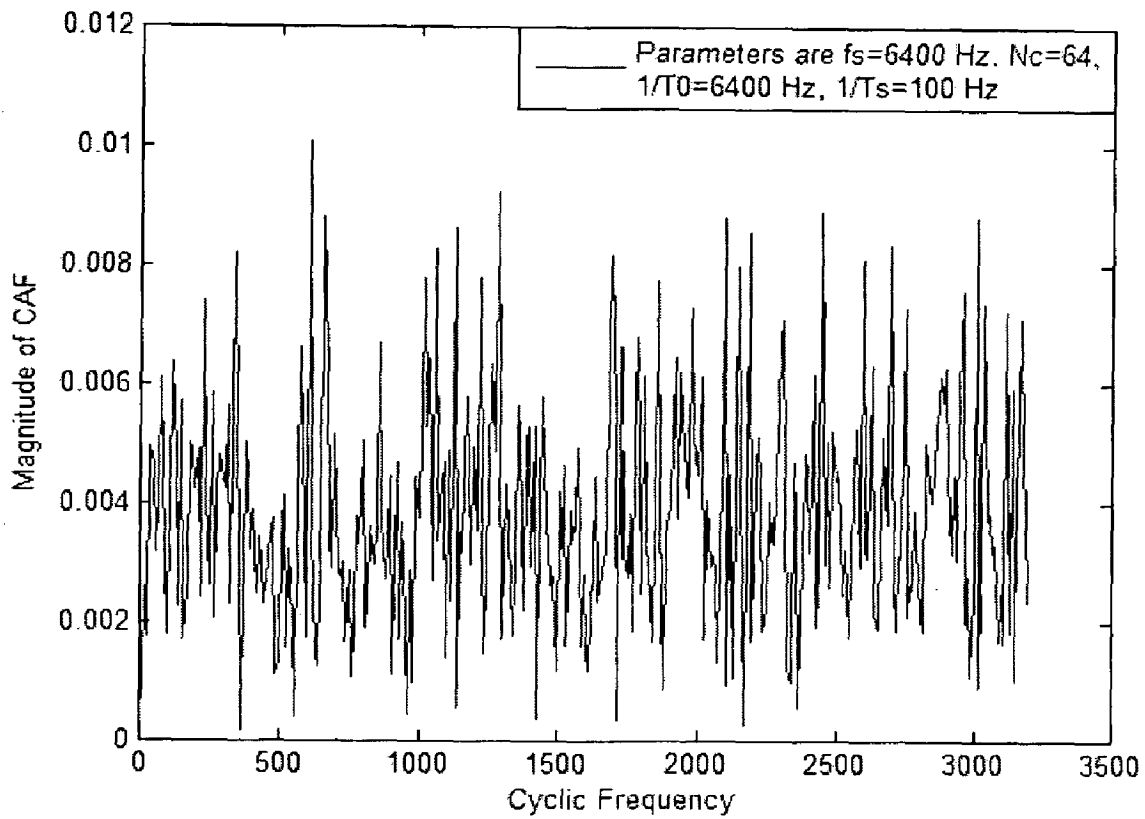


Figure 4.3: Normalised CAF of an OFDM signal at lag 1.

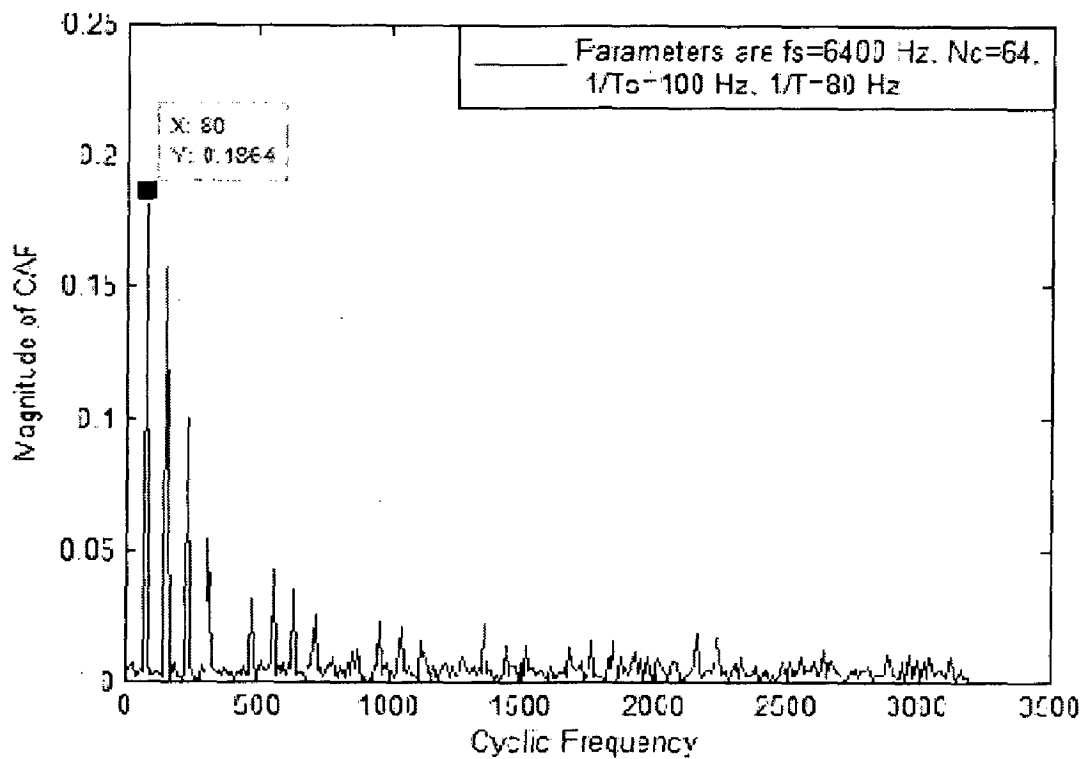


Figure 4.4: Normalised CAF of a CP-OFDM signal at lag 64.

4.3.1. Excess Bandwidth

Since the peaks in cyclic autocorrelation function of OFDM even after insertion of cyclic prefix are quite low, we introduce some excess bandwidth in the signal. In the previous simulation, the sampling frequency is equal to the subcarrier baud rate hence no extra bandwidth is present over which spectral correlation may be exploited. In this section, we try to introduce excess bandwidth using pulse shaping in the frequency domain, which means before the IFFT operation of OFDM. The primary aim is to provide redundancy in the frequency domain spectrum of OFDM, which will introduce spectral correlation in the signal without affecting the orthogonality of the subcarriers, such that the resultant cyclostationarity can be used to detect the signal [45]. It is expected that such an OFDM signal would possess stronger cyclostationarity. There are two methods to introduce correlation in the signal.

A. Time domain rectangular pulses

When rectangular pulses are used to modulate data onto subcarriers, then a redundancy is introduced in the time domain which provides for cyclostationary features. For example,

using $g(t) = \begin{cases} T & (t < T_0 / K) \\ 0 & (\text{otherwise}) \end{cases}$ where K denotes the up-sampling factor, the signal is sampled

at K times the original rate. As the data sample is repeated K times, a spectral peak is generated at a frequency of f_{su} / K where f_{su} is the new sampling frequency. But the induced peaks at f_{su} / K are very low in magnitude and they offer no special leverage over the earlier case. Rather, it increases the hardware cost drastically as higher sampling rate ADC/DACs are required. The cyclic autocorrelation function of an OFDM signal using time domain rectangular pulses is shown in figure 4.5. The value of K is chosen as 32 and $f_{su} = 102400 \text{ Hz}$. The resultant peaks at $f_{su} / K = 3200 \text{ Hz}$ are observed to have low magnitude peaks in the cyclic autocorrelation function. Similar OFDM signal when simulated with a $T_s/4$ cyclic prefix also shows no substantial improvement in the cyclic peaks at the OFDM symbol rate.

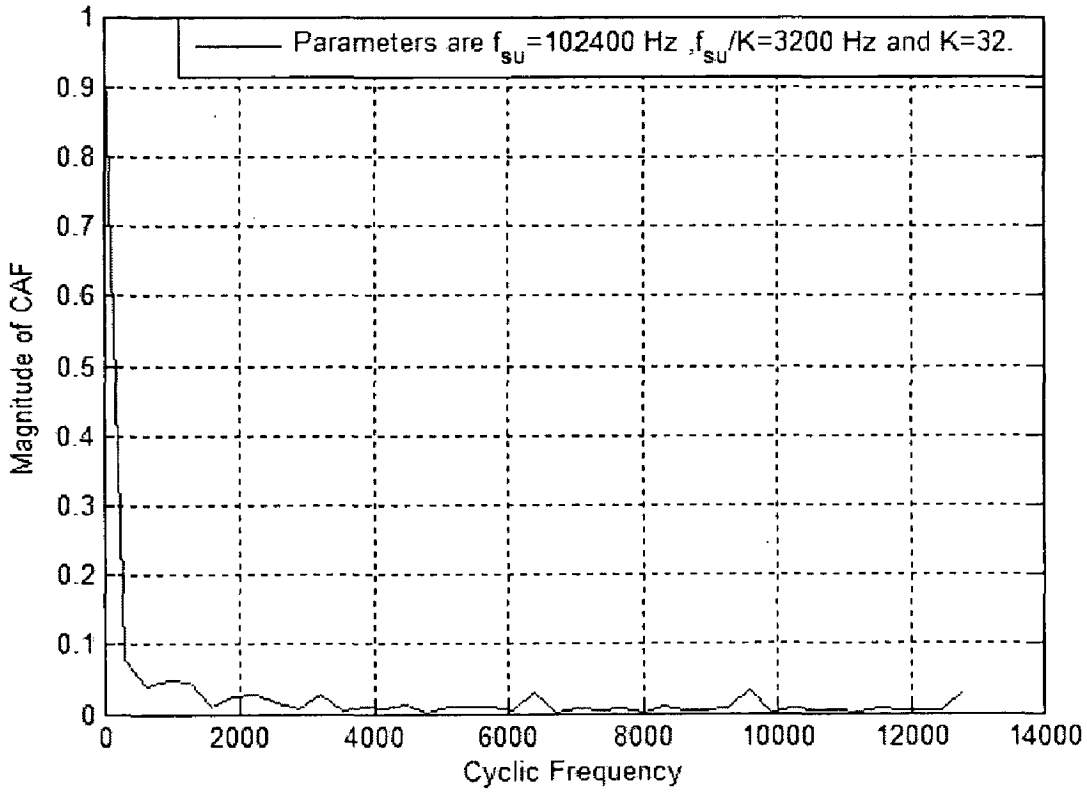


Figure 4.5: Normalised CAF of an OFDM signal using time domain rectangular pulses.

B. Raised Cosine Pulse Shaping

Another method of introducing redundancy is by using raised cosine (RC) pulses. Raised cosine pulses offer the flexibility of introducing variable excess bandwidths (EBW) in the signal through the roll off parameter. Also, it is much less wasteful and requires an increase in the overall bandwidth by the excess bandwidth of each subcarrier on either side. Additionally, it maintains orthogonality between subcarriers and hence sustains the basic properties of OFDM signal. The raised cosine pulse spectrum is given as follows [46],

$$G_{rc}(f) = \begin{cases} T_s & \left(0 \leq |f| \leq \frac{1-\beta}{2T_s} \right) \\ \frac{T_s}{2} \left\{ 1 + \cos \left[\frac{\pi T_s}{\beta} \left(|f| - \frac{1-\beta}{2T_s} \right) \right] \right\} & \left(\frac{1-\beta}{2T_s} \leq |f| \leq \frac{1+\beta}{2T_s} \right) \\ 0 & \left(|f| \leq \frac{1+\beta}{2T_s} \right) \end{cases} \quad (4.7)$$

where β is the roll off factor that can be adjusted between 0 and 1 corresponding to excess bandwidths of 0% and 100% and $1/2T_s$ is the single sided bandwidth of OFDM subcarrier.

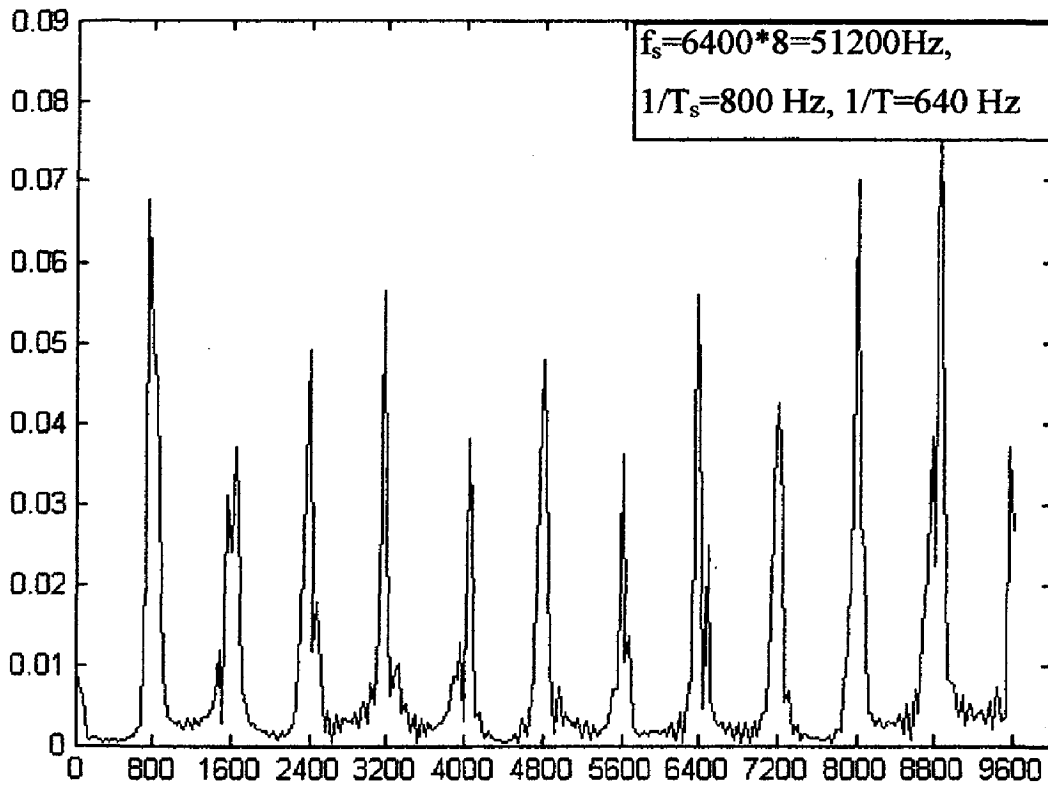


Figure 4.6: Normalised CAF of an OFDM signal at lag 1 using RC shaping with 100% excess bandwidth.

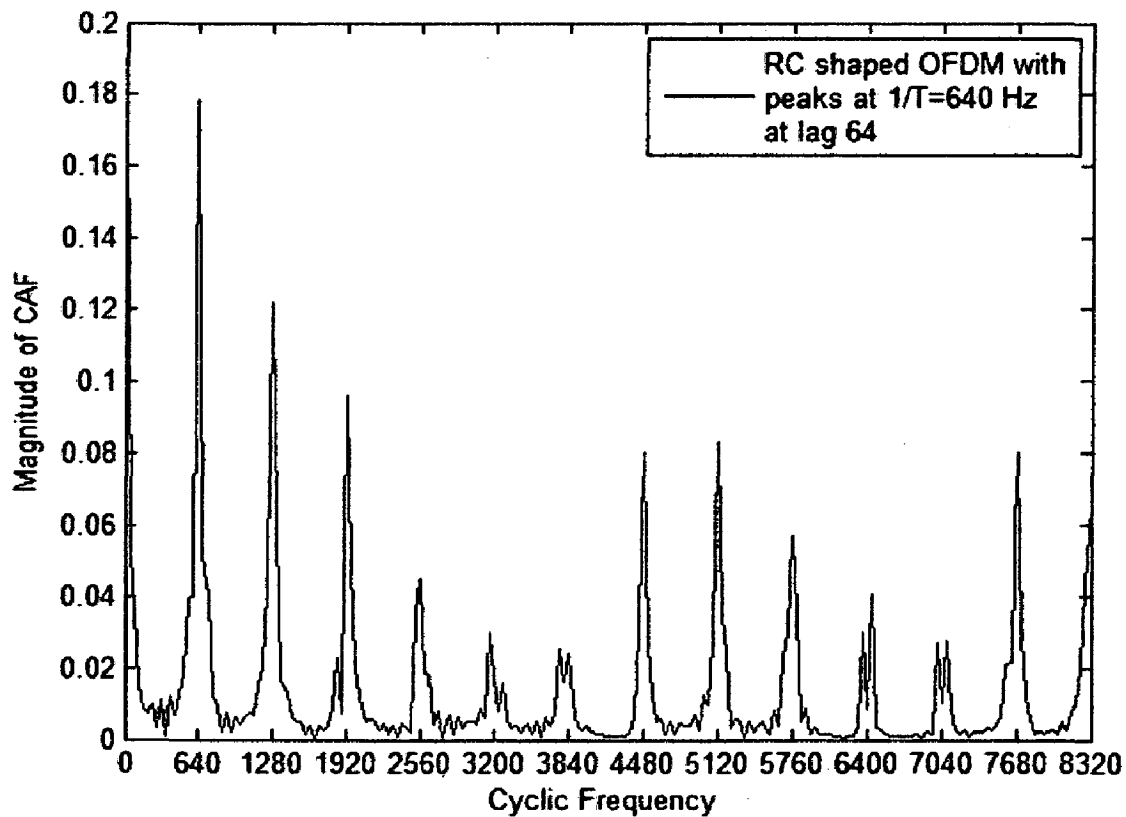


Figure 4.7: Normalised CAF of a CP-OFDM signal at lag 64 using RC pulse shaping with 100% excess bandwidth.

The cyclic autocorrelation function of an OFDM signal using $\beta=1$ raised cosine shaping with $N_c=64$, $\text{lag}=1$ and $K=8$ is shown in figure 4.6. The parameters of the OFDM signal are $f_s=6400*8=51200$ Hz, $1/T_s=800$ Hz, $1/T=640$ Hz. Figure 4.7 shows the CAF of the CP-OFDM signal at lag 64 which clearly show the peaks at multiples of $1/T=640$ Hz. From figure 4.6-4.7, it can be observed that using raised cosine pulse shaping accentuates the cyclic peaks of OFDM signal. The reasonably strong cyclostationarity exhibited by the raised cosine shaped OFDM can be used to detect the OFDM signal.

4.4 FRESH Filter based Detection

As outlined in the section 3.3, to detect a cyclostationary signal, a frequency shift filter can be constructed wherein the values of frequency shifts in each branch is equal to a unique cyclic frequency of the signal. For a baseband OFDM signal the inclusion of cyclic prefix is necessary to preserve its cyclostationarity at the OFDM symbol rate. Moreover, the cyclic peaks can be made more prominent by using a raised cosine filter to shape the signal prior to modulation onto the orthogonal subcarriers. Hence, we consider an OFDM signal with input pulse rate of $1/T_0=6400$ Hz. The symbols are obtained from a 4-QAM constellation mapper with variable amplitudes. In order to introduce excess bandwidth, the signal is sampled at a rate of $8*6400$ Hz with 8 as the up-sampling factor and the samples are passed through a raised cosine filter with roll off factor $\beta=1$, resulting in a 100% excess bandwidth. The number of subcarriers is 64 and CP length is $T_s/4$. OFDM signal has cyclic frequencies of 640 Hz, 1280 Hz, 1920 Hz etc. and smaller magnitude correlation at 800 Hz, 1600 Hz, 2400 Hz and so on.

For this purpose a FRESH filter is constructed as shown in figure 4.8. Four frequency shifts are used corresponding to the first four multiples of $1/T$. For the purpose of spectrum sensing, the sum test of section 2.3 is used. The number of samples available for sensing is fixed to $N=3200$. Initially, 1000 Monte Carlo runs are performed without any signal to ascertain empirically the distribution of the test statistic under the null hypothesis. A false alarm limit of 0.1 is used to calculate a suitable threshold λ for the test statistic. Subsequently, at each SNR from 0dB to -20 dB, the probability of detection is calculated by averaging over 1000 runs. To compare the detection performance, the same test statistic is used on received signal directly without frequency shift filtering. Similar methodology is used to derive results for P_d versus SNR curves. The experiment is repeated for $N=6400$ and 9600 samples. The combined simulation results are shown in figures 4.9-4.11.

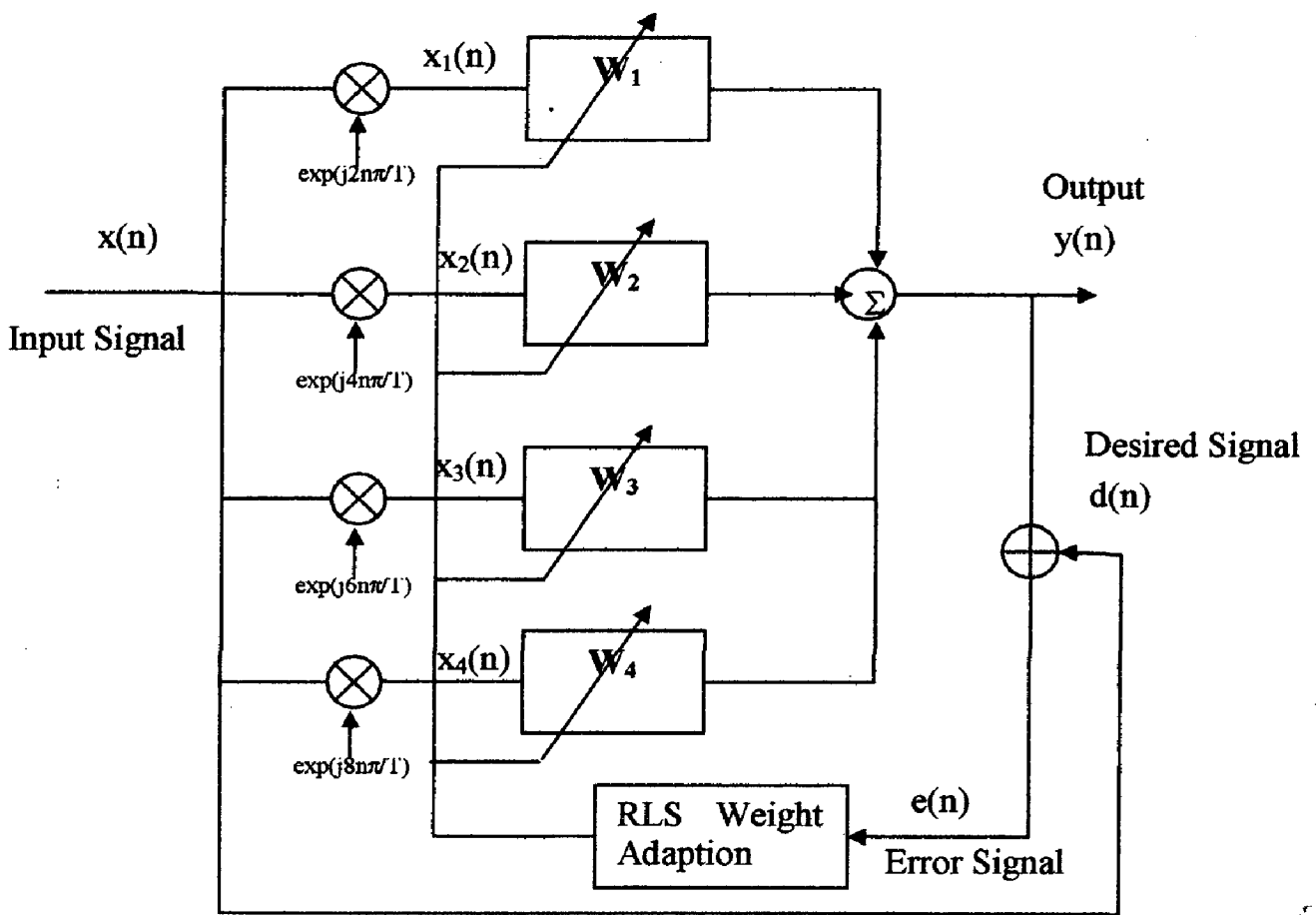


Figure 4.8: FRESH filter to detect an RC shaped CP-OFDM signal with $1/T=640$ Hz.

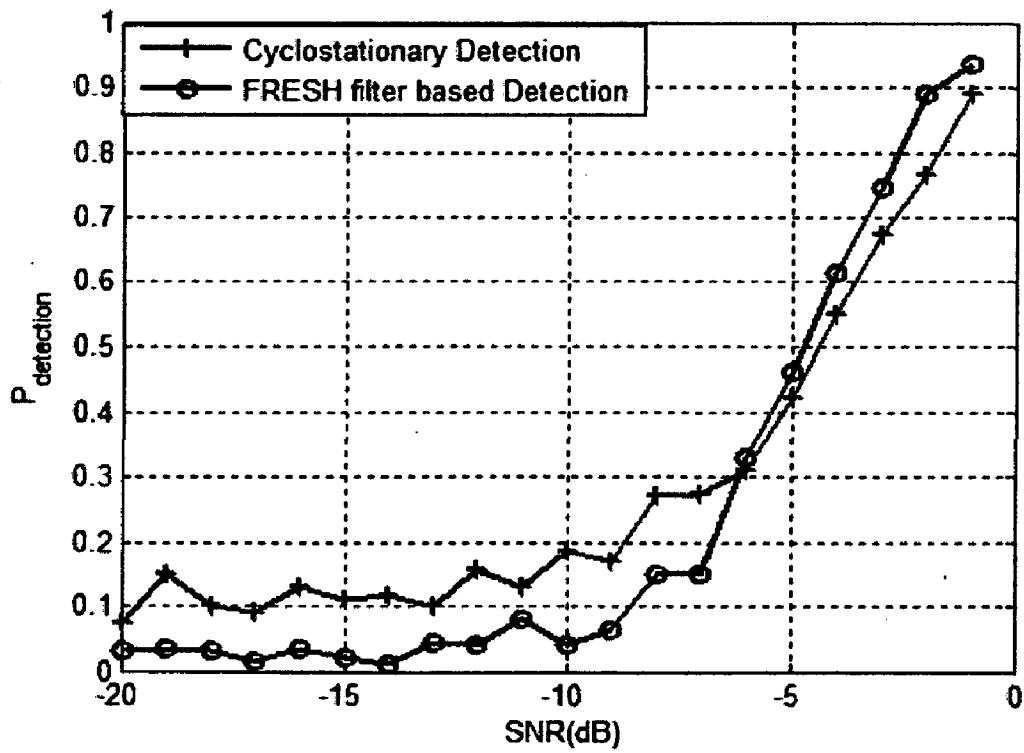


Figure 4.9: Comparison of probability of detection curves for cyclostationary detection and FRESH filter based detection for $N=3200$ samples.

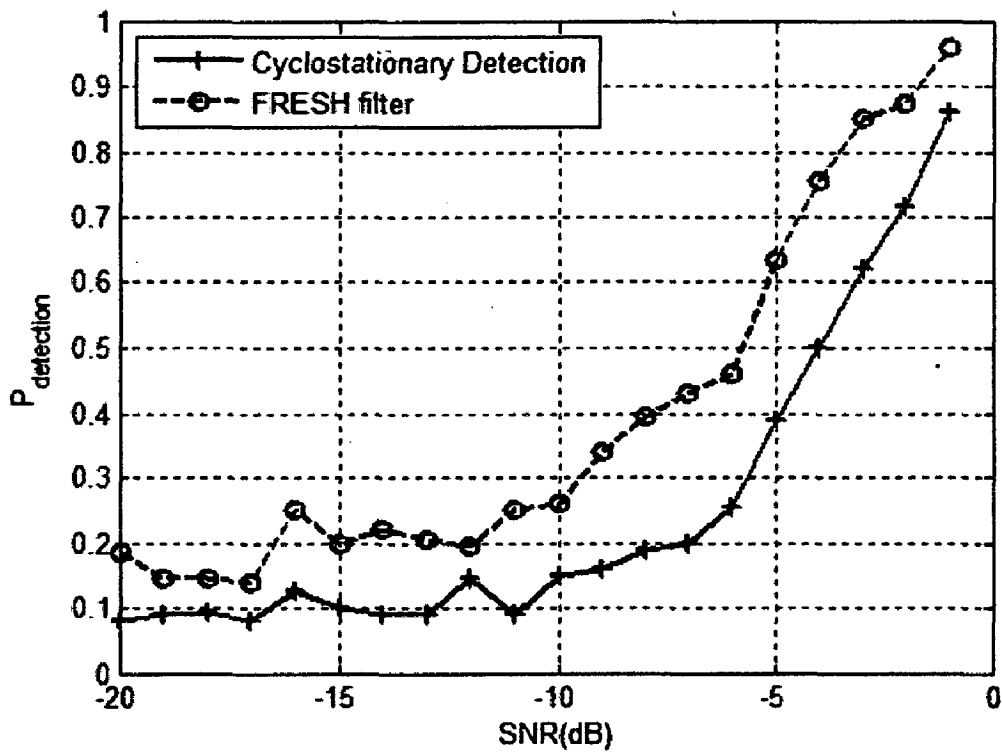


Figure 4.10: Comparison of probability of detection curves for cyclostationary detection and FRESH filter based detection for $N=6400$ samples.

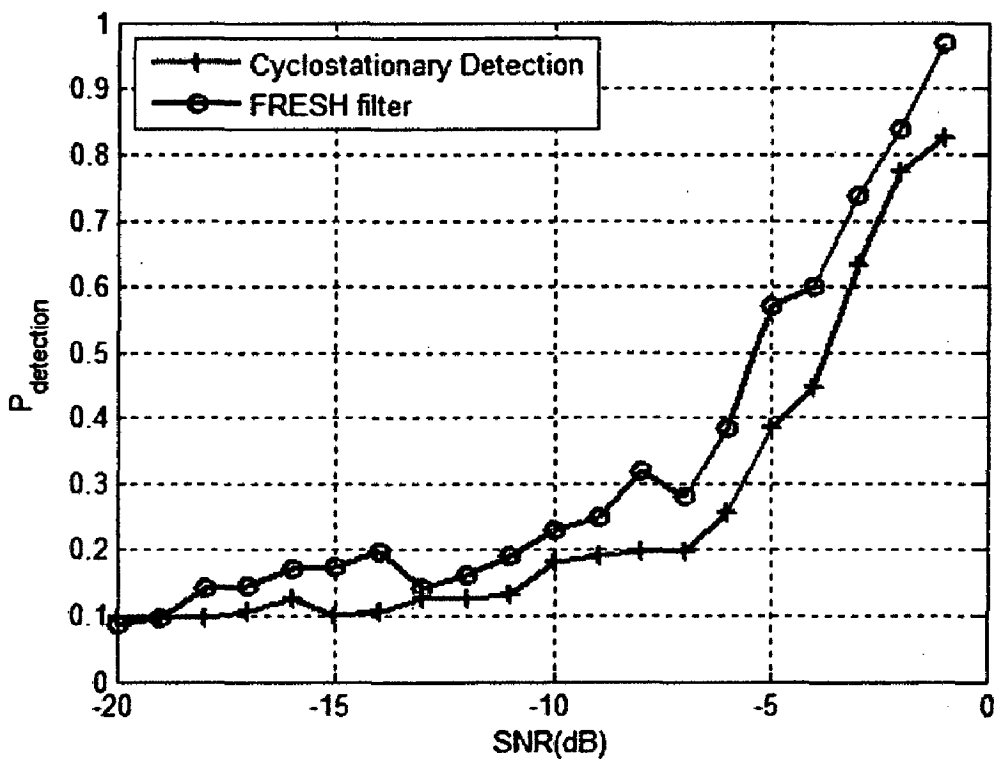


Figure 4.11 Comparison of probability of detection curves for cyclostationary detection and FRESH filter based detection for $N=9600$ samples.

It can be seen from figures 4.9-4.11 that frequency shift filtering using the sum hypothesis test gives better performance of detection in OFDM over simple cyclostationary detection. Although the improvement in detection with 3200 samples is not substantial, with more number of samples, the detection performance increases. But in comparison to the detection performance of energy detection in figure 4.2 the probability of detection offered by FRESH filters is similar to the worst case performance of an energy detector but with a magnitude of 10 increase in the number of samples (from 400 to 6400). Also as a comparison to the probability of detection plots obtained for BPSK in section 2.3.1, the corresponding detection rates at any given SNR are much less for OFDM. Nevertheless, FRESH filters are robust in the sense that their performance will improve with more number of samples, but a worse case energy detector cannot achieve a desired probability of detection if it has already reached the SNR wall. Thus FRESH filter based detection may be used in scenarios where the noise uncertainty is large or sensing at SNR below the SNR wall is required.

This section brings up two major issues. One is that it is much more challenging to detect OFDM using its inherent cyclostationarity, owing to the limited low magnitude of cyclic autocorrelation peaks. Secondly, a sub-optimal test statistic to exploit cyclostationarity is no more sufficient in OFDM, and an optimum test must be designed which can fully exploit the correlation structure in OFDM. This prompts us to instead use a time-domain test for cyclostationarity in OFDM which optimally detects the cyclic prefix. To solve the problem of weak correlation, we introduce induced cyclostationarity in the OFDM signal.

4.5 Induced Cyclostationary Detection

Induced Cyclostationarity is a feature that can be intentionally embedded in the physical properties of a signal which may be easily detected and generated [47]. Such features can be introduced in an OFDM signal, giving rise to additional cyclostationary signatures that can aid signal acquisition and detection reliably. These are more useful than inherent cyclostationary features such as cyclic prefix in OFDM because they can be introduced at any desired cyclic frequency and easily manipulated to distinguish the SOI from other interfering users, as opposed to inherent features, which would entail significant altering of a standard waveform, if they are desired to be modified. Cyclostationary signatures for OFDM were introduced by Sutton et al. in their recent paper [47] in which they develop a low complexity technique for embedding cyclostationary signatures in OFDM based waveforms and present a method to detect them.

Though induced cyclostationarity offers immense practical advantage, an optimal method for its detection has not been discussed by the authors in [47]. Optimal detection of such intentionally introduced features requires an ab-initio analysis of the OFDM waveform and development of a maximum likelihood based test statistic that can optimally exploit the correlation introduced in the OFDM signal according to a Neyman-Pearson test. Optimal detection in OFDM has been studied by Axell and Larsson in [21] in which the authors set up a vector matrix model for OFDM and derive the optimal Neyman-Pearson detector for CP-OFDM (Cyclic Prefix OFDM). They compare the optimal detector to the energy detector and show that in the absence of any cyclic prefix, energy detector is the optimum sensing technique.

This section presents the vector matrix model introduced by authors in [21] for CP-OFDM. It further augments the model by introducing induced cyclostationarity. Simulation results are shown to verify the cyclostationarity features induced. Finally, we develop an optimal Neyman-Pearson detector for an OFDM signal with induced cyclic features. The performance of this detector is tested through simulation and it is observed that the detector is able to achieve better probability of detection than the optimal detector for cyclic prefixed OFDM and energy detector developed in [21].

4.5.1. Induced Cyclostationarity

Orthogonal frequency division multiplexing (OFDM) signals may be represented in the baseband as a composite of N statistically independent subchannel quadrature amplitude modulated (QAM) signals [43]

$$x(t) = \sum_{n=0}^{N_c-1} \sum_{l=-\infty}^{\infty} d_{n,l} g(t-lT) e^{j(2\pi/T_s)nl} \quad (4.8)$$

where $x(t)$ is the complex envelope of the OFDM signal with a cyclic prefix, $d_{n,l}$ is an independent and identically distributed message symbol sequence, N_c is the number of subcarriers and $g(t)$ is the square shaping pulse of duration $T=T_s+T_{cp}$, where T_s is the source symbol length and T_{cp} is the length of cyclic prefix. $g(t)$ has the form of $g(t) = \begin{cases} 1 & |t| < T_s/2 \\ 0 & |t| > T_s/2 \end{cases}$

Each subcarrier carries independent streams of data which are orthogonal to each other. If instead of modulating some of the subcarriers with independent data streams, we send the

same sequence of symbols on more than one subcarrier, thus creating a redundancy in the OFDM. This operation can be mathematically represented by [47]

$$d_{n,l} = d_{n+p,l}, \quad n \in M \quad (4.9)$$

where M denotes the subset of subcarriers that is mapped onto another subset of subcarriers which is at a distance of p subcarriers from the original subset M . This introduction of statistical dependence between certain subcarriers of an OFDM signal results in the spectral correlation as given in equation (4.10), where M is the set of mapped subcarriers and $G(f)$ denotes the Fourier transform of rectangular shaping pulse $g(t)$ [44]. Figure 4.12 shows the generation of cyclostationary signature by introducing correlation between subcarriers. Figure 4.13 shows the cyclic autocorrelation function of an OFDM signal with the parameters $N_c=256$, $f_s=25600$ Hz, $1/T_s=100$ Hz, $M=13$ and $p=243$. The induced cyclostationary peak occurs at p/T_s which equals 24300 Hz in our case. The signal uses rectangular time domain pulses to modulate data onto subcarriers.

$$S_{xx}^{\alpha}(f) = \begin{cases} \frac{\sigma_d^2}{T} \sum_{n=0}^{N_c-1} G\left(f - \frac{n}{T_s} + \frac{\alpha}{2}\right), & \alpha = \frac{k}{T} \\ G^*\left(f - \frac{n}{T_s} - \frac{\alpha}{2}\right), & \\ \frac{\sigma_d^2}{T} \sum_{n=0}^{N_c-1} G\left(f - \frac{n}{T_s} + \frac{\alpha}{2}\right), & \alpha = \frac{p}{T_s} \pm \frac{k}{T}, n \in M \\ G^*\left(f - \frac{n+p}{T_s} - \frac{\alpha}{2}\right), & \\ 0 & \alpha \neq \frac{k}{T}, \frac{p}{T_s} \pm \frac{k}{T} \end{cases} \quad (4.10)$$

where σ_d^2 is the variance of QAM symbols $d_{n,l}$, T_s is the source symbol duration and T is the OFDM symbol duration given by $T=T_s+T_{cp}$. Induced cyclostationary peaks occur at $\alpha = p/T_s \pm k/T$.

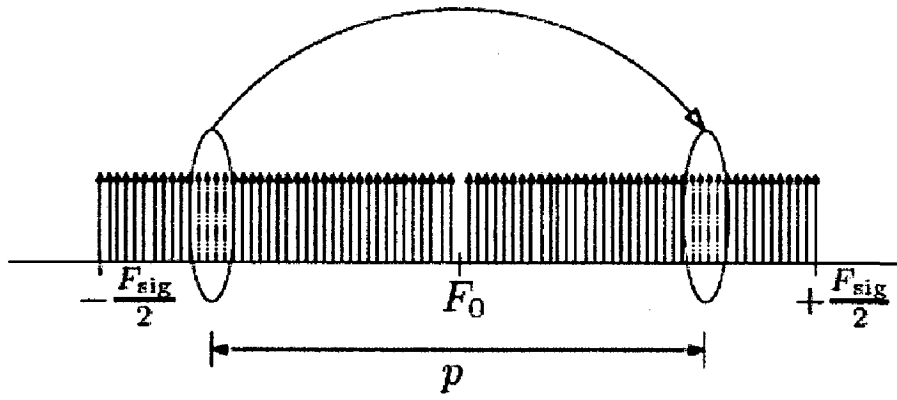


Figure 4.12: Generation of induced cyclostationarity in OFDM by mapping of subcarriers.

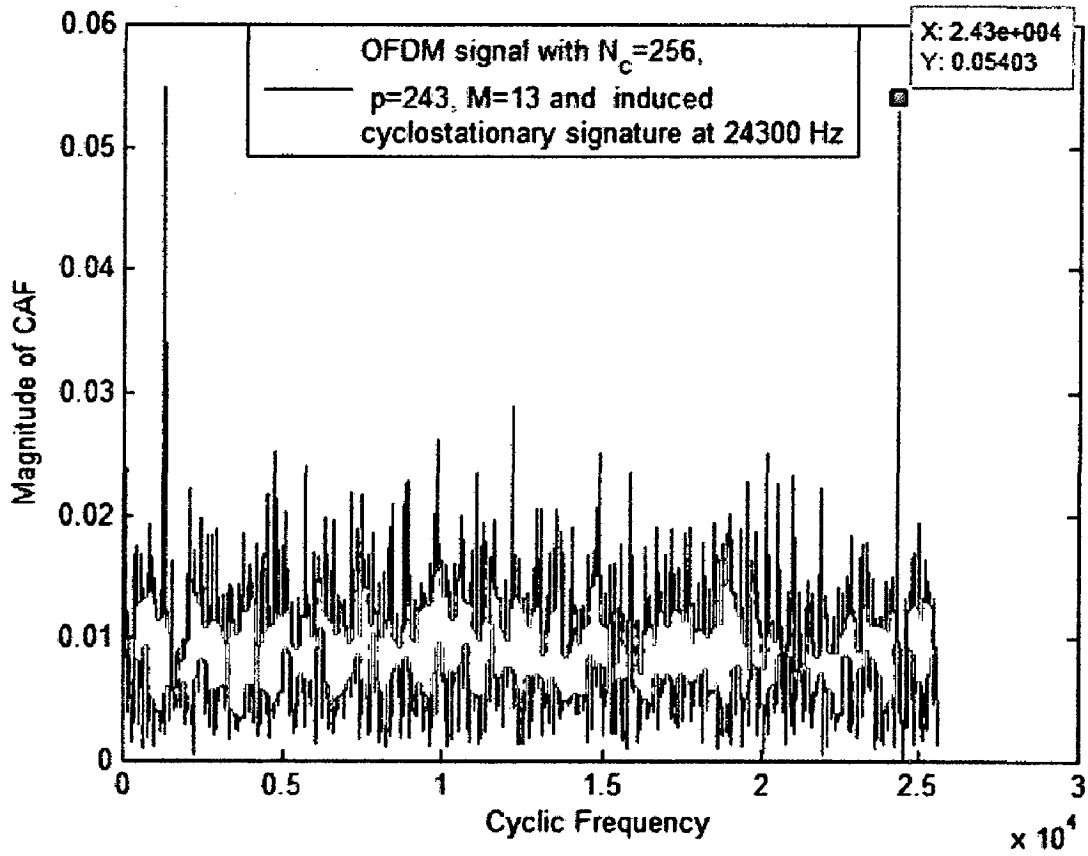


Figure 4.13: Normalised CAF for OFDM signal with induced cyclostationarity at $p/T_s = 24300$ Hz.

4.5.2. Optimal Detector for Induced Cyclostationarity in OFDM

At the receiver the cyclic prefixed OFDM signal $x(t)$ is corrupted by AWGN $w(t)$. After down-converting the received waveform the signal is sampled at a rate $f_s=k/T_0$, where T_0 is the baud rate of each subcarrier which is N_c times the baud rate of the OFDM symbol. The digital CP-OFDM samples are given by [43]

$$x(k) = \sum_{k=-N_{cp}}^{k=N_c-1-N_{cp}} \sum_{n=0}^{N_c-1} d_{n,k} g(k) e^{j2\pi \frac{n}{N_c} k} \quad (4.11)$$

A vector of received samples \mathbf{r} is formed, consisting of $K(N_c+N_{cp})$ samples where K denotes the number of OFDM symbols received and $N=(N_c+N_{cp})$ denotes the number of samples in one OFDM symbol assuming N_c is the number of subcarriers used and N_{cp} is the number of cyclic prefixed symbols. Consider the length N vector of sampled values of the received signal \mathbf{r} that consists of the OFDM signal and noise, i.e.,

$$\mathbf{r} = \mathbf{s} + \mathbf{w} \quad (4.12)$$

where \mathbf{s} is the vector of N samples of the transmitted OFDM signal given as $\mathbf{s} = \{x(0), x(T_s), \dots, x(NT_s)\}'$ and \mathbf{w} is the vector of noise samples of the same length N . To detect an OFDM signal optimally, a Neyman-Pearson test must be constructed in which the two hypotheses to be discriminated are

$$\begin{aligned} H_0 : \mathbf{r} &= \mathbf{w} \\ H_1 : \mathbf{r} &= \mathbf{s} + \mathbf{w} \end{aligned} \quad (4.13)$$

Assuming that N is quite large, and noise samples are independent, the distribution of complex vector \mathbf{r} under H_0 is [21]

$$p(\mathbf{r} | H_0) = \frac{1}{\pi^N \sigma_w^{2N}} \exp\left(-\frac{\|\mathbf{r}\|^2}{\sigma_w^2}\right), \quad (4.14)$$

where N is the length of the vector \mathbf{r} . Under the hypothesis H_1 , the distribution of the vector \mathbf{r} must be ascertained. Since the signal samples \mathbf{s} are formed by taking an IFFT operation, assuming that the length of the IFFT (N_c) is sufficiently large and the mean of the signal is zero, the distribution of \mathbf{s} under H_1 can be assumed as $CN(\mathbf{0}, \Sigma_s)$ where Σ_s is the co-variance

matrix of the vector \mathbf{s} of OFDM signal samples of length N . Our task is to derive this co-variance matrix Σ_s based on the correlation structure in the OFDM signal.

First, the derivation of co-variance matrix for a CP-OFDM signal is presented which presents a framework for further deriving the co-variance matrix for a CP-OFDM signal containing induced cyclostationarity. Let \mathbf{q}_i denote the length N_c -vector of data associated with the i -th OFDM symbol. A CP-OFDM symbol \mathbf{s}_i is then obtained by repeating the last N_c elements of \mathbf{q}_i at the beginning of the symbol. This can be written as [21]

$$\mathbf{s}_i = \mathbf{U}\mathbf{q}_i, \quad (4.15)$$

where,

$$\mathbf{U} = \begin{bmatrix} \mathbf{0}_{N_{cp} \times N_c - N_{cp}} & \mathbf{I}_{N_{cp}} \\ & \mathbf{I}_{N_c} \end{bmatrix}, \in \mathbb{R}^{(N_{cp} + N_c) \times N_c}$$

For example, for an representative OFDM system with $N_{cp}=1$ and $N_c=4$, the matrix \mathbf{U} would be

$$\mathbf{U} = \begin{bmatrix} 0 & 0 & 0 & 1 \\ 1 & 0 & 0 & 0 \\ 0 & 1 & 0 & 0 \\ 0 & 0 & 1 & 0 \\ 0 & 0 & 0 & 1 \end{bmatrix}$$

When we consider a block of K OFDM symbols for detection, the total signal vector can be defined as

$$\mathbf{s} = \mathbf{T}\mathbf{q} \quad (4.16)$$

where the $(N_{cp}+N_c) \times (N_c)$ matrix \mathbf{T} is defined as [21]

$$\mathbf{T} = \begin{bmatrix} \mathbf{U} & \mathbf{0} & \cdots & \mathbf{0} \\ \mathbf{0} & \mathbf{U} & & \mathbf{0} \\ \vdots & & \ddots & \vdots \\ \mathbf{0} & \mathbf{0} & \cdots & \mathbf{U} \end{bmatrix}, \in \mathbb{R}^{K(N_{cp} + N_c) \times KN_c}$$

and the vector \mathbf{q} is given by the $\mathbf{q} = [\mathbf{q}_1, \mathbf{q}_2 \cdots \mathbf{q}_K]'$ where the operation (') denotes transpose.

Now the co-variance matrix of the transmitted signal \mathbf{s} can be written as

$$\Sigma_s = E\{\mathbf{s}\mathbf{s}^H\} = E\{\mathbf{T}\mathbf{q}(\mathbf{T}\mathbf{q})^H\} = \mathbf{T}E\{\mathbf{q}\mathbf{q}^H\}\mathbf{T}^H \quad (4.17)$$

where \mathbf{T}^H denotes the Hermitian of matrix \mathbf{T} .

Case 1: No Induced Cyclostationarity Present in the OFDM signal

When no correlation structure has been introduced in the input of the IFFT block in OFDM, i.e. when no intentional cyclostationarity has been induced in the OFDM signal, the elements of vector \mathbf{q} are independent and identically distributed with a variance of σ_x^2 . Hence, the covariance matrix becomes $\sigma_x^2 \mathbf{I}$. Here x is the baseband waveform of OFDM signal defined by equation (4.6).

Case 2: Induced Cyclostationary Signature present in OFDM signal

When induced cyclostationary signatures are inserted into the OFDM signal, the elements of vector \mathbf{q} are no longer independent but there exists a definite correlation structure between them. To find this correlation structure we consider the following model of the OFDM signal which is a modification of equation (4.11) assuming that $x(k)$ is the OFDM source symbol excluding the cyclic prefix and where the time index k is limited to one OFDM symbol period.

$$x(k) = \frac{1}{\sqrt{N_c}} \sum_{n=0}^{N_c-1} d(n) e^{j\frac{2\pi n k}{N_c}}, \quad k = 0, 1, \dots, N_c - 1 \quad (4.18)$$

where $d(k)$ are the data symbols from the output of a M-ary QAM mapper. The symbols $d(k)$ are independent and identically distributed with a power of σ_d^2 . Suppose that we induce cyclostationary signature in $x(n)$ by ensuring that last M subcarriers are modulated by the same stream of data as the first M subcarriers. Now, we can write $x(n)$ as

$$x(k) = \frac{1}{\sqrt{N_c}} \left[a_M^k + b_{N_c-2M}^k + c_M^k \right] \quad (4.19)$$

where, $a_M^k = \sum_{n=0}^{M-1} d(n)e^{j\frac{2\pi n k}{N_c}}$, $b_{N_c-2M}^k = \sum_{n=M}^{N_c-M-1} d(n)e^{j\frac{2\pi n k}{N_c}}$ and $c_M^k = \sum_{n=N_c-M}^{N_c-1} d(n)e^{j\frac{2\pi n k}{N_c}}$ are denote

three subsets of the IFFT output vector of lengths M, N_c-2M and M respectively. The vector of samples of $x(k)$ over one OFDM symbol duration can be written as

$$\mathbf{x} = \begin{bmatrix} a_M^0 + b_{N_c-2M}^0 + c_M^0 \\ a_M^1 + b_{N_c-2M}^1 + c_M^1 \\ \vdots \\ a_M^{N_c-1} + b_{N_c-2M}^{N_c-1} + c_M^{N_c-1} \end{bmatrix} \text{ and hence, the covariance matrix of } \mathbf{x} \text{ can be written as}$$

$$\Sigma_x = E\{\mathbf{x}\mathbf{x}^H\} = E \left\{ \begin{bmatrix} a_M^0 + b_{N_c-2M}^0 + c_M^0 \\ a_M^1 + b_{N_c-2M}^1 + c_M^1 \\ \vdots \\ a_M^{N_c-1} + b_{N_c-2M}^{N_c-1} + c_M^{N_c-1} \end{bmatrix} \begin{bmatrix} a_M^0 + b_{N_c-2M}^0 + c_M^0 & \cdots & a_M^{N_c-1} + b_{N_c-2M}^{N_c-1} + c_M^{N_c-1} \end{bmatrix}^* \right\}$$

The dimensions of this co-variance matrix are $(KN_c) \times (KN_c)$. Each element of this covariance matrix can be derived by individually taking the expectation of each term. The complete derivation for the matrix Σ_x is given in the Appendix B. The general term of the matrix is derived as

$$t(l_1, l_2) = \frac{\sigma_x^2}{N_c} \left[\left(W^{\frac{(l_2-l_1)(M-1)}{2} + l_1 M} \right) \cdot (1 + W^{-(l_1+l_2)M}) \frac{\sin\left(\frac{2\pi(l_2-l_1)M}{2N_c}\right)}{\sin\left(\frac{2\pi(l_2-l_1)}{2N_c}\right)} \right] \quad (4.20)$$

Here $t(l_1, l_2)$ denotes the term in the l_1 -th row and l_2 -th column of the matrix Σ_x where l_1, l_2 denote any time indices from 0 to N_c-1 and $W = e^{-\frac{j2\pi}{N_c}}$. The variance of the OFDM signal is equal to the power of the input QAM symbols i.e. $\sigma_x^2 = \sigma_d^2$. In the case of $l_1=l_2=l_0$, the above term reduces to

$$t(l_0, l_0) = \frac{\sigma_x^2}{N_c} \left[N_c + 2M \cos\left(\frac{2\pi l_0 M}{N_c}\right) \right] \quad (4.21)$$

The vector \mathbf{x} is same as the vector \mathbf{q} used in this section earlier, as both are used to define a vector of samples of OFDM within one symbol time. Using the entries of the matrix Σ_x , the co-variance matrix Σ_s can be written as $\Sigma_s = \mathbf{T}\Sigma_x\mathbf{T}^H$.

As a result, under the hypothesis H_1 , the co-variance matrix of the received vector \mathbf{r} becomes

$$\mathbf{Q} = \sigma_w^2\mathbf{I} + \Sigma_s = \sigma_w^2\mathbf{I} + \sigma_x^2\mathbf{T}\mathbf{T}^H$$

Thus, the distribution of \mathbf{r} under H_1 becomes[21]

$$p(\mathbf{r} | H_1) = \frac{1}{\pi^N \det(\mathbf{Q})} \exp(-\mathbf{r}^H \mathbf{Q}^{-1} \mathbf{r}), \quad (4.22)$$

Hence, the optimal Neyman-Pearson test for detection of CP-OFDM can be defined as,

$$\begin{aligned} \Lambda_{optimal} &= \log \left(\frac{p(\mathbf{r} | H_1)}{p(\mathbf{r} | H_0)} \right) \\ &= \log \left(\frac{\frac{1}{\pi^N \det(\mathbf{Q})} \exp(-\mathbf{r}^H \mathbf{Q}^{-1} \mathbf{r})}{\frac{1}{\pi^N \sigma_w^{2N}} \exp\left(-\frac{\|\mathbf{r}\|^2}{\sigma_w^2}\right)} \right) \\ &= \log \left(\frac{\sigma_w^{2N}}{\det(\mathbf{Q})} \right) - \mathbf{r}^H \left(\mathbf{Q}^{-1} - \frac{1}{\sigma_w^2} \mathbf{I} \right) \mathbf{r} \end{aligned} \quad (4.23)$$

This test statistic is also the optimal time domain test for cyclostationarity in a CP-OFDM signal. Axell and Larsson in [21] state that there is no closed form expression for the distribution of this test statistic. Hence the threshold for the test statistic $\eta_{optimal}$ must be computed empirically. When no cyclic prefix is present in the signal, then $\mathbf{Q} = \frac{1}{\sigma_w^2 + \sigma_x^2} \mathbf{I}$

becomes a $\text{KN}_c \times \text{KN}_c$ diagonal matrix. In this case the optimal Neyman-Pearson test reduces to an energy detector which follows a chi-square distribution and the formulae for its probability of false alarm and probability of detection can be found as described earlier in section 4.2 and section 2.1.

$$\Lambda_{equiv} = \sum_{i=0}^{N-1} |r_i|^2 \quad (4.24)$$

4.5.3. Simulation Results for Optimal Detection in OFDM

An OFDM signal is simulated with number of subcarriers $N_c=32$, and cyclic prefix length $N_{cp}=8$. Cyclostationarity is induced by mapping the first M subcarriers onto the last M subcarriers. The corresponding value of p is equal to N_c-M . Signal variance σ_x^2 is varied between 1 to 0.01 and noise variance σ_w^2 is chosen as unity. Thus, the SNR range of received OFDM signal is from 0dB to -20 dB. 4-QAM modulation is used to produce the source symbols. The simulation is carried out for 400 received data symbols meaning thereby 10 complete OFDM symbol durations are used for sensing. To find and compare the probability of detection achieved by using energy detector and optimal detectors for cyclic prefix and the induced cyclostationarity, their corresponding Neyman-Pearson test statistics are constructed from the received symbols. For the case when no signal is being transmitted, 1000 Monte Carlo runs are conducted and a threshold $\eta_{optimal}$ is derived, such that the false alarm probability is limited to 0.05. Consequently, at each SNR value, average probability of detection is computed for all three detectors by calculating the average rate of detection over 1000 simulation runs. A comparison of the detection probability achieved in the 0 to -20dB SNR range, achieved by the three detectors, is shown in figures 4.14 and 4.15 for the cases of $M=3$ and 5.

From the figures 4.14-4.15, it can be clearly seen that the proposed optimal test statistic for detection of induced cyclostationary signature provides progressively better probability of detection than both cyclic prefix and energy detector. Also, there is around 1.5 dB SNR loss by using the energy detector instead of the optimal induced cyclic feature detector.

In this chapter, we have discussed various spectrum sensing techniques for OFDM and their performance in OFDM. OFDM exhibits weak cyclostationarity even in the presence of cyclic prefix and providing excess bandwidth by using raised cosine pulse shaping can enhance the peaks in the cyclic autocorrelation function of OFDM. We have shown the efficacy of FRESH filter based detection over cyclostationary detection in spectrum sensing for OFDM. Finally, induced cyclostationarity in OFDM is introduced and an optimal detector is derived for the same. Simulation results show the improved performance of the optimal detector as compared to energy detector and optimal time domain detector for cyclostationarity.

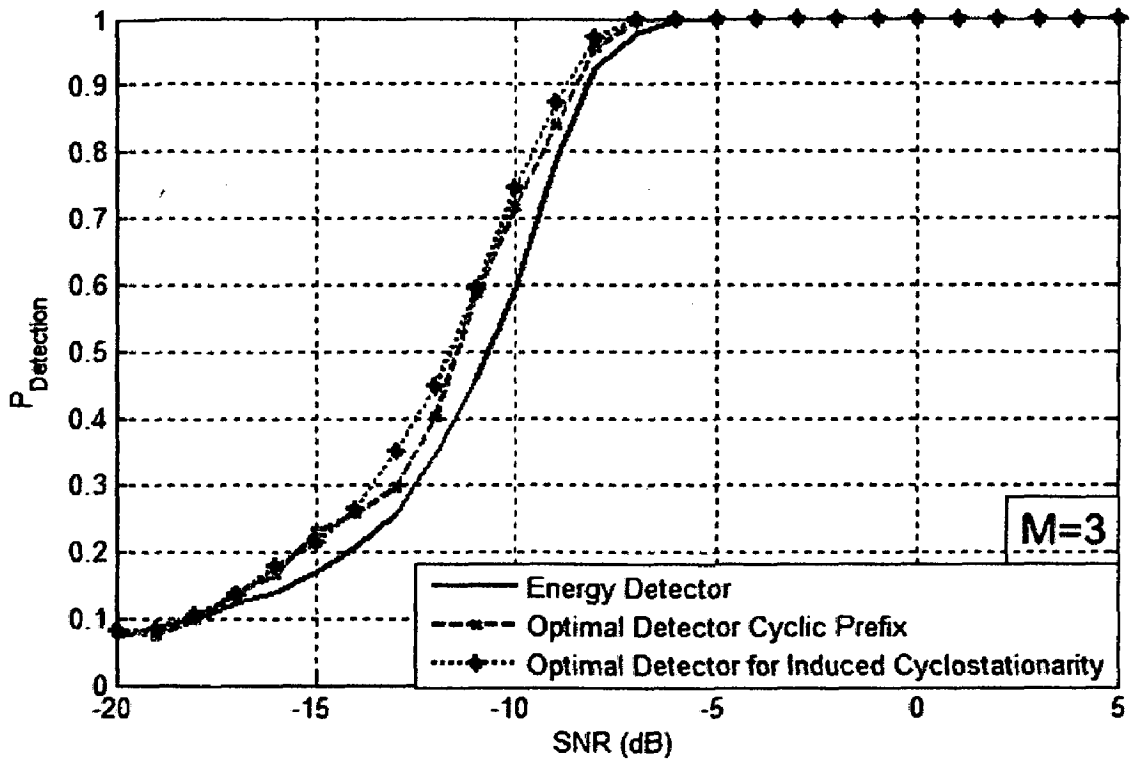


Figure 4.14: Comparison of probability of detection curves for energy detection and optimal detectors for cyclic prefix and induced cyclostationarity in CP-OFDM for 400 samples and $M=3$.

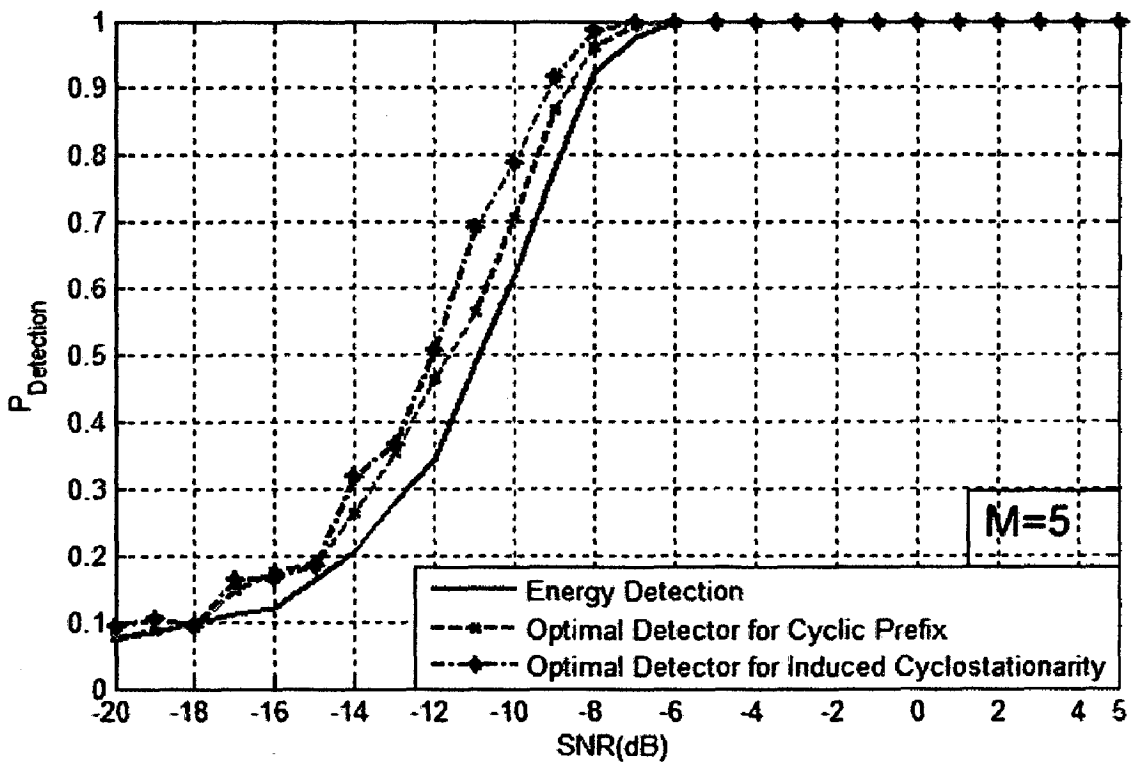


Figure 4.15: Comparison of probability of detection curves for energy detection and optimal detectors for cyclic prefix and induced cyclostationarity in CP-OFDM for 400 samples and $M=5$.

Chapter 5

Conclusion and Future Work

This thesis attempts to study the emerging topic of spectrum sensing in cognitive radio. It presents a comparative analysis of three spectrum sensing techniques viz. energy detection, cyclostationary detection and FRESH (FREquency SHift) filter based detection. As energy detection is widely used and suffers from many limitations, the contribution of this thesis is to develop cyclostationary spectrum sensing techniques to robustly detect a signal in the low SNR regime. It presents the application of FRESH filters for spectrum sensing and presents simulation results to substantiate the claim that FRESH filter based detection can outperform other detection techniques in single carrier AWGN environments. For the multicarrier environment, this thesis develops an optimal detector for induced cyclostationarity in cyclic prefixed OFDM, and verifies its superior performance over energy and cyclostationary detection techniques through simulation. A chapter-wise list of conclusions is provided below.

Chapter 1 presents an overview of the properties of cognitive radio such as adaptability and reconfigurability etc. and various tasks a cognitive radio must perform. It explains the importance of spectrum sensing in a primary user-secondary user context and introduces various techniques used for spectrum sensing such as energy detection and cyclostationary detection and highlights their advantages and deficiencies.

A comparative analysis between energy detection and cyclostationary detection in terms of their detection performance and robustness is presented in Chapter 2. Theoretical results are presented with derivation and it is seen that energy detector is non-robust below the SNR-wall due to noise distribution uncertainty. Inherent cyclostationarity is present in all modulated signals at different cyclic frequencies which can be used for their detection. Through a simulation example, it is shown that a BPSK signal exhibits strong cyclic peaks in its conjugate cyclic autocorrelation function and spectral correlation density at twice the carrier frequency. For the same signal, using a sub-optimal sum test statistic, it is seen that

energy detection performs better than cyclostationary detection upto -15 dB but with 1dB noise uncertainty it becomes highly non-robust and fails to detect the signal below -7dB.

Chapter 3 explores the application of frequency shift filtering for spectrum sensing. First, structure of FRESH filter using LCL filtering is shown and the basic theory of cyclic Wiener filtering is presented. Then adaptive implementations using LMS and RLS algorithms are discussed and the optimal step size parameter is chosen experimentally. Simulation results show that the excess MSE decreases with increasing number of frequency shift branches. A 6 branch blind adaptive FRESH filter is constructed to detect a BPSK signal in AWGN using both baud rate and carrier related cyclostationarity and the sub-optimal sum test of Chapter 2 is applied on the CAF of the frequency shift filtered BPSK signal. The average detection performance achieved is better than both cyclostationary detection and energy detection technique, with the RLS based adaption giving better results than its LMS counterpart. It is also shown that BA-FRESH filters need more samples to converge in the presence of high power interference.

In Chapter 4, we extend the application of spectrum sensing techniques to OFDM and find that it is more challenging due to absence of cyclostationarity in OFDM. In order to preserve cyclostationarity, a cyclic prefix must be inserted at the beginning of the OFDM symbol. The low magnitude CAF peaks due to cyclic prefix can be accentuated by using pulse shaping to provide excess bandwidth. Using this OFDM signal and the sum test statistic, it is observed that FRESH filter based detection performs better than simple cyclostationary detection, but is similar to the worst case of energy detector. Following this, we present an optimal time domain test for cyclostationarity to detect the cyclic prefix in OFDM. Induced cyclostationarity is introduced in OFDM signal and an optimal detector for detecting induced cyclic features is developed. Simulation results show that the proposed detector outperforms the energy detector and optimal detector for cyclic prefixed OFDM.

Future Work

The thesis presents results that LAPTIV filters can be used for improved spectrum sensing in AWGN environments. These results can be extended to interference scenarios by improving upon the blind adaption process. Since trained FRESH filters offer excellent interference rejection properties [2], [26], using a suitable desired signal may result in better performance for BA-FRESH filters. Using a local generated training signal similar to the transmitted signal is a possible option as its SCD peaks will be congruous with the SOI. The performance

of spectrum sensing with FRESH filters can be improved by using the optimal test for cyclostationarity proposed by Giannakis in [33]. For OFDM, the proposed optimum detector can be extended to the case of unknown noise variance by using a GLRT (Generalised Likelihood Ratio Test) based approach and it can be compared with the existing techniques. Filter bank multicarrier scheme has been proposed by Boroujeny in [48] as an alternative to OFDM and he argues that such filter banks can provide higher spectral efficiency and low sideband levels than OFDM. Due to excellent filtering properties of FBMC (Filter Bank Multi Carrier) systems, they can possibly be used for spectrum sensing in a cognitive radio context, and a comparison with the techniques discussed in this thesis will be a topic for further work.

Appendix A

Cyclic Frequencies in Digital Modulated Signals

A real QAM signal can be written as

$$d(t) = c(t) \cos(\omega_0 t) + s(t) \sin(\omega_0 t) \quad (\text{A.1})$$

and $c(t)$ can be written as,

$$c(t) = \sum_{r=-\infty}^{\infty} c_r p(t - rT_0 - t_0) \quad (\text{A.2})$$

where $p(t)$ is the pulse shape with keying rate $1/T_0$. For the most general case of M-ary QAM signal the amplitude of $d(t)$ can take M different values

$$|a_r| = \sqrt{c_r^2 + s_r^2} \quad (\text{A.3})$$

with the corresponding phase shifts

$$\angle a_r = -\tan^{-1} \left(\frac{s_r}{c_r} \right) \quad (\text{A.4})$$

For this general signal $d(t)$ the spectral correlation function is given by [2]

$$\begin{aligned} S_{dd}^{\alpha}(f) = & \frac{1}{4} \sum_{n=-1,1} [S_{cc}^{\alpha}(f + nf_0) + S_{ss}^{\alpha}(f + nf_0)] + ni[S_{sc}^{\alpha}(f + nf_0) - S_{cs}^{\alpha}(f + nf_0)] \\ & + \frac{1}{4} \sum_{n=-1,1} [S_{cc}^{\alpha+2nf_0}(f) - S_{ss}^{\alpha+2nf_0}(f)] + ni[S_{sc}^{\alpha+2nf_0}(f) + S_{cs}^{\alpha+2nf_0}(f)] \end{aligned} \quad (\text{A.5})$$

where $f_0 = \omega_0 / 2\pi$ and

$$S_{cc}^{\alpha}(f) = \frac{1}{T_0^2} P(f + \alpha/2) P^*(f - \alpha/2) \times \sum_{r,s=-\infty}^{\infty} S_{cc}^{\alpha-r/T_0}(f - s/T_0 + r/2T_0) e^{-j2\pi\alpha t_0} \quad (\text{A.6})$$

in which $P(f)$ is the Fourier transform of $p(t)$ and $\tilde{c}(t)$ is any time-series with $\tilde{c}(rT_0) = c_r$.

An analogous expression for $S_{ss}^\alpha(f)$ can be derived by assuming the relation

$$s(t) = \sum_{r=-\infty}^{\infty} s_r q(t - rT_0 - t_0) \quad (\text{A.7})$$

When the data c_r and s_r come from a stationary time series, then (A.6) can be rewritten as

$$S_{cc}^\alpha(f) = \frac{1}{T_0^2} P(f + \alpha/2) P^*(f - \alpha/2) \times \sum_{r,s=-\infty}^{\infty} S_{\tilde{c}\tilde{c}}^0(f - s/T_0 + \alpha/2) e^{-j2\pi\alpha t_0} \quad (\text{A.8})$$

for $\alpha = k/T_0 \forall$ integers k , and $S_c^\alpha \equiv 0$ for all other values of α . also if c_r is a white sequence with variance σ_c^2 then,

$$S_{cc}^\alpha(f) = \frac{\sigma_c^2}{T_0^2} P(f + \alpha/2) P^*(f - \alpha/2) e^{-j2\pi\alpha t_0} \quad (\text{A.9})$$

In addition if c_r and s_r are statistically independent zero-mean time series then,

$S_{cs}^\alpha(f) \equiv S_{sc}^\alpha(f) \equiv 0$ and the equation (A.5) reduces to

$$S_{dd}^\alpha(f) = \frac{1}{4} \sum_{n=-1,1} [S_{cc}^\alpha(f + nf_0) + S_{ss}^\alpha(f + nf_0) + S_{cc}^{\alpha+2nf_0}(f) - S_{ss}^{\alpha+2nf_0}(f)] \quad (\text{A.10})$$

For AM signals purely stationary amplitude $c(t)$, the above equation can be reduced further by making $s(t) = 0$.

$$S_{dd}^\alpha(f) = \begin{cases} \frac{1}{4} S_{cc}(f) & \alpha = \pm 2f_0 \\ \frac{1}{4} (S_{cc}(f + f_0) + S_{cc}(f - f_0)) & \alpha = 0 \end{cases} \quad (\text{A.11})$$

and $S_{dd}^\alpha(f) \equiv 0$ for all other values of α . For a BPSK signal, with $T_0 f_0$ irrational, (A.10) can be substituted with (A.9) to yield

$$S_{dd}^{\alpha}(f) = \frac{\sigma_{\epsilon}^2}{4T_0} [P(f + f_0 + \alpha/2)P^*(f + f_0 - \alpha/2) + P(f - f_0 + \alpha/2)P^*(f - f_0 - \alpha/2)] e^{-i2\pi\alpha t_0} \quad (\text{A.12})$$

for $\alpha = k/T_0$ and

$$S_{dd}^{\alpha}(f) = \frac{\sigma_{\epsilon}^2}{4T_0} P(f \pm f_0 + \alpha/2)P^*(f \pm f_0 - \alpha/2) e^{-i2\pi\alpha t_0} e^{-[2\pi(\alpha \pm 2f_0)t_0 + 2\phi_0]} \quad (\text{A.13})$$

for $\alpha = \mp 2f_0 + k/T_0$. The parameter ϕ_0 is introduced for the sake of generality. i.e.

$$d(t) = c(t) \cos(\omega_0 t + \phi_0) \quad (\text{A.14})$$

On the other hand, for a balanced QPSK signal (with $S_{cs}^{\alpha}(f) \equiv S_{cs}^{\alpha}(f) \equiv 0$ and $S_{cc}^{\alpha} \equiv S_{ss}^{\alpha}$) with $T_0 f_0$ irrational, we obtain (A.12) multiplied by 2 for $\alpha = k/T_0$ but $S_d^{\alpha} \equiv 0$ for $\alpha = \mp 2f_0 + k/T_0$.

This shows that an AM signal possess cyclostationarity at $\alpha = \mp 2f_0$ and a QPSK signal possess cyclostationarity at $\alpha = k/T$. A real BPSK signal on the other hand, possesses cyclic peaks at both multiples of T and twice the carrier frequency.

A similar analysis can be performed when complex QAM signals where the envelope of the signal $a(t)$ becomes complex. A summary of the combined results can be stated as :

- (1) Complex representation of AM has no spectral correlation, but it only possesses conjugate spectral correlation related to twice the carrier frequency ($2f_0$).
- (2) Complex representation of balanced QPSK has no conjugate spectral correlation. It only has spectral correlation associate with baud rate and its harmonics (k/T_0).
- (3) Complex representation of BPSK, has both spectral correlation at baud rate and its harmonics as well as conjugate spectral correlation related to twice the carrier frequency.

Appendix B

Derivation of the Co-variance Matrix of the Optimum Detector for Induced Cyclostationarity in CP-OFDM

The OFDM signal $x(k)$ is given by

$$x(k) = \frac{1}{\sqrt{N_c}} \sum_{n=0}^{N_c-1} d(n) e^{j \frac{2\pi n k}{N_c}}, \quad k = 0, 1, \dots, N_c - 1 \quad (\text{B.1})$$

We assume that the source symbols $d(n)$ have been derived from a signal constellation with zero mean and variance σ_d^2 . Another justifiable assumption is that the source symbols are independent and identically distributed (i.i.d.). We introduce cyclostationary signature in $x(n)$ such that last M subcarriers carry the same data as the first M subcarriers. This can be mathematically stated as

$$d(n) = d(n + N_c - M), \quad \forall n \in [0, 1, \dots, M - 1] \quad (\text{B.2})$$

Hence partitioning the signal into three distinct subsets, we can write,

$$x(k) = \frac{1}{\sqrt{N_c}} \left[a_M^k + b_{N_c-2M} + c_M^n \right] \quad (\text{B.3})$$

The data in first and third subset are correlated. We form a vector \mathbf{x} of length N_c with elements $x(0) \dots x(N_c-1)$. The covariance matrix of this matrix is given by

$$\Sigma_{\mathbf{x}} = E\{\mathbf{xx}^H\} = E \left\{ \begin{bmatrix} a_M^0 + b_{N_c-2M}^0 + c_M^0 \\ a_M^1 + b_{N_c-2M}^1 + c_M^1 \\ \vdots \\ a_M^{N_c-1} + b_{N_c-2M}^{N_c-1} + c_M^{N_c-1} \end{bmatrix} \begin{bmatrix} a_M^0 + b_{N_c-2M}^0 + c_M^0 & \cdots & a_M^{N_c-1} + b_{N_c-2M}^{N_c-1} + c_M^{N_c-1} \end{bmatrix}^* \right\} \quad (\text{B.4})$$

Let the element at the l_1 -th row and l_2 -th column of the $N_c \times N_c$ matrix $\Sigma_{\mathbf{x}}$ be denoted by

$t(l_1, l_2)$. Assume $W = e^{\frac{j2\pi}{N_c}}$. Then $t(l_1, l_2)$ can be written as

$$t(l_1, l_2) = E \left\{ [a_M^{l_1} + b_{N_c-2M}^{l_1} + c_M^{l_1}] [a_M^{l_2} + b_{N_c-2M}^{l_2} + c_M^{l_2}]^H \right\} \quad (\text{B.5})$$

where $E\{\cdot\}$ denotes expectation and the operator H denotes Hermitian. This term is made up of nine product terms. Owing to the independence of source symbols, any product term involving two different source symbols will yield an expectation value of 0 as the source symbols are independent and zero mean, hence uncorrelated. This means that, the terms in a_M^k and c_M^k can correlated among each other because of induced correlation structure, but none of them correlated with $b_{N_c-2M}^k$. This leaves us with 5 product terms. We tackle each term separately.

$$\begin{aligned} E \left\{ (a_M^{l_1}) \cdot (a_M^{l_2})^* \right\} &= \frac{1}{N_c} E \left\{ \left(\sum_{n=0}^{M-1} d(n) W^{-nl_1} \right) \left(\sum_{n=0}^{M-1} d^*(n) W^{+nl_2} \right) \right\}, \\ &= \frac{1}{N_c} \sum_{n=0}^{M-1} W^{n(l_2-l_1)n} E \left\{ d(n) d^*(n) \right\}, \\ &= \frac{\sigma_d^2}{N_c} \sum_{n=0}^{M-1} W^{n(l_2-l_1)n}. \end{aligned} \quad (\text{B.6})$$

$$\begin{aligned} E \left\{ (b_{N_c-2M}^{l_1}) \cdot (b_{N_c-2M}^{l_2})^* \right\} &= \frac{1}{N_c} E \left\{ \left(\sum_{n=M}^{N_c-M-1} d(n) W^{-nl_1} \right) \left(\sum_{n=M}^{N_c-M-1} d^*(n) W^{+nl_2} \right) \right\} \\ &= \frac{1}{N_c} \sum_{n=M}^{N_c-M-1} W^{n(l_2-l_1)n} E \left\{ d(n) d^*(n) \right\} \\ &= \frac{\sigma_d^2}{N_c} \sum_{n=M}^{N_c-M-1} W^{n(l_2-l_1)n} \end{aligned} \quad (\text{B.7})$$

$$\begin{aligned}
E\{(c_M^{l_1}).(c_M^{l_2})^*\} &= \frac{1}{N_c} E\left\{\left(\sum_{n=N_c-M}^{N_c-1} d(n)W^{-nl_1}\right)\left(\sum_{n=N_c-M}^{N_c-1} d^*(n)W^{+nl_2}\right)\right\} \\
&= \frac{1}{N_c} \sum_{n=N_c-M}^{N_c-1} W^{n(l_2-l_1)n} E\{d(n)d^*(n)\} \\
&= \frac{\sigma_d^2}{N_c} \sum_{n=N_c-M}^{N_c-1} W^{n(l_2-l_1)n}
\end{aligned} \tag{B.8}$$

$$E\{(a_M^{l_1}).(c_M^{l_2})^*\} = \frac{1}{N_c} E\left\{\left(\sum_{n=0}^{M-1} d(n)W^{-nl_1}\right)\left(\sum_{n=N_c-M}^{N_c-1} d^*(n)W^{+nl_2}\right)\right\}, \tag{B.9}$$

Substitute, $k = N_c - M$, in the second summation

$$E\{(a_M^{l_1}).(c_M^{l_2})^*\} = \frac{1}{N_c} E\left\{\left(\sum_{n=0}^{M-1} d(n)W^{-nl_1}\right)\left(\sum_{k=0}^{M-1} d^*(k+(N_c-M))W^{+kl_2} \cdot W^{+N_c l_2} \cdot W^{-Ml_2}\right)\right\}, \tag{B.10}$$

Since, $W^{N_c l_2} = 1$, $d^*(k+(N_c-M)) = d^*(k)$ and $d(n)d^*(n) = 0$ for $n \neq k$ hence,

$$\begin{aligned}
E\{(a_M^{l_1}).(c_M^{l_2})^*\} &= \frac{W^{-Ml_2}}{N_c} \sum_{n=0}^{M-1} W^{n(l_2-l_1)n} E\{d(n)d^*(n)\} \\
&= \frac{W^{-Ml_2} \sigma_d^2}{N_c} \sum_{n=0}^{M-1} W^{n(l_2-l_1)n}
\end{aligned} \tag{B.11}$$

$$E\{(c_M^{l_1}).(a_M^{l_2})^*\} = \frac{1}{N_c} E\left\{\left(\sum_{n=N_c-M}^{N_c-1} d(n)W^{-nl_1}\right)\left(\sum_{n=0}^{M-1} d^*(n)W^{+nl_2}\right)\right\}, \tag{B.12}$$

Substitute, $k = N_c - M$, in the first summation

$$E\{(c_M^{l_1}).(a_M^{l_2})^*\} = \frac{1}{N_c} E\left\{\left(\sum_{k=0}^{M-1} d(k+(N_c-M))W^{-kl_1} \cdot W^{-N_c l_1} \cdot W^{Ml_1}\right)\left(\sum_{n=0}^{M-1} d^*(n)W^{+nl_2}\right)\right\}, \tag{B.13}$$

Since, $W^{-N_c l_1} = 1$, $d(k+(N_c-M)) = d(k)$ and $d(n)d^*(n) = 0$ for $n \neq k$ hence,

$$\begin{aligned}
E\{(c_M^i)(a_M^j)^*\} &= \frac{W^{Ml_1}}{N_c} \sum_{n=0}^{M-1} W^{n(l_2-l_1)n} E\{d(n)d^*(n)\} \\
&= \frac{W^{Ml_1} \sigma_d^2}{N_c} \sum_{n=0}^{M-1} W^{n(l_2-l_1)n}
\end{aligned} \tag{B.14}$$

Adding equations (B.6), (B.7), (B.8), (B.11) and (B.14) we get

$$t(i, j) = \frac{\sigma_d^2}{N_c} \left\{ \sum_{n=0}^{N_c-1} W^{(l_2-l_1)n} + \left(\sum_{n=0}^{M-1} W^{(l_2-l_1)n} \right) (W^{Ml_1} + W^{-Ml_2}) \right\} \tag{B.15}$$

For the case when $l_1=l_2$, the diagonal term $t(i,j)$ can be found by modifying (B.15) to

$$t(l_1, l_1) = \frac{\sigma_d^2}{N_c} \left\{ N_c + 2M \cos\left(\frac{2\pi Ml_1}{N_c}\right) \right\} \tag{B.16}$$

For the general case when $l_1 \neq l_2$, the term in (B.15) can be simplified to

$$t(l_1, l_2) = \frac{\sigma_d^2}{N_c} \left\{ \frac{W^{(l_2-l_1)N_c} - 1}{W^{(l_2-l_1)} - 1} + \left(\sum_{n=0}^{M-1} W^{(l_2-l_1)n} \right) (W^{Ml_1} + W^{-Ml_2}) \right\}, \tag{B.17}$$

Since $W^{(l_2-l_1)N_c} = 1$, hence the first term becomes zero. The second term can be simplified to

$$\begin{aligned}
t(l_1, l_2) &= \frac{\sigma_d^2}{N_c} \left\{ \frac{W^{(l_2-l_1)M} - 1}{W^{(l_2-l_1)} - 1} (W^{Ml_1} + W^{-Ml_2}) \right\}, \\
&= \frac{\sigma_d^2}{N_c} \left\{ \left(\frac{W^{\frac{(l_2-l_1)M}{2}}}{W^{\frac{(l_2-l_1)}{2}}} \right) \left(\frac{W^{\frac{(l_2-l_1)M}{2}} - W^{-\frac{(l_2-l_1)M}{2}}}{W^{\frac{(l_2-l_1)}{2}} - W^{-\frac{(l_2-l_1)}{2}}} \right) (W^{Ml_1} + W^{-Ml_2}) \right\}, \\
&= \frac{\sigma_d^2}{N_c} \left\{ W^{\frac{(l_2-l_1)(M-1)}{2} + Ml_1} (1 + W^{-M(l_2+l_1)}) \left(\frac{2j \sin\left(\frac{2\pi(l_2-l_1)M}{2N_c}\right)}{2j \sin\left(\frac{2\pi(l_2-l_1)}{2N_c}\right)} \right) \right\} \tag{B.18} \\
t(l_1, l_2) &= \frac{\sigma_d^2}{N_c} \left\{ W^{\frac{(l_2-l_1)(M-1)}{2} + Ml_1} (1 + W^{-M(l_2+l_1)}) \frac{\sin\left(\frac{2\pi(l_2-l_1)M}{2N_c}\right)}{\sin\left(\frac{2\pi(l_2-l_1)}{2N_c}\right)} \right\}
\end{aligned}$$

Using the general term $t(i,j)$, the covariance matrix of the signal $x(n)$, Σ_x can be constructed.

Bibliography

- [1] R. Tandra and A.Sahai, "SNR Walls for Signal Detection," *IEEE J. of Sel. Topics Signal Process.*, vol.2, no.1, pp. 4-17, Feb. 2008.
- [2] W.A. Gardner, "Cyclic Wiener filtering: theory and method," *IEEE Trans. on Commun.*, vol.41, no.1, pp. 151-163, Jan. 1993.
- [3] I.F. Akyildiz, Lee Won-Yeol, M.C. Vuran, and S. Mohanty, "A survey on spectrum management in cognitive radio networks," *IEEE Communications Magazine*, vol.46, no.4, pp. 40-48, Apr. 2008.
- [4] S. Haykin, "Cognitive radio: brain-empowered wireless communications," *IEEE J. Sel. Areas Commun.*, vol. 23, no. 2, pp. 201- 220, Feb. 2005.
- [5] Federal Communications Commission, " Spectrum Policy Task Force ," Rep. ET Docket, no. 02-135, Nov. 2002.
- [6] J. Mitola, "Cognitive radio: An integrated agent architecture for software defined radio," Ph.D. Dissertation, Royal Inst. Technol. (KTH), Stockholm, Sweden, 2000.
- [7] J. Mitola, V. Bose, B.M. Leiner, T. Turletti, and D. Tennenhouse, "Guest Editorial software radios," *IEEE J. Sel. Areas Commun.*, vol. 17, no. 4, pp. 509-513, Apr. 1999.
- [8] J. Mitola and G.Q. Maguire, "Cognitive radio: Making software radios more personal," *IEEE Pers. Commun.*, vol. 6, no. 4, pp. 13–18, Aug. 1999.
- [9] D.J. Thomson, "Spectrum estimation and harmonic analysis," *Proc. IEEE*, Sept. 1982. vol. 70, no. 9, pp. 1055- 1096.
- [10] D.Cabric, A. Tkachenko, and R.W. Broaderson, "Experimental Study of Spectrum Sensing based on Energy Detection and Network Cooperation," in *Proc. ACM 1st Int. Workshop on Tech. and Policy for Accessing Spectrum (TAPAS '06)*, New York, NY.
- [11] M. Oner and F. Jondral, "Cyclostationarity based air interface recognition for software radio systems," in *IEEE Radio and Wireless Conf.*, 19-22 Sept. 2004, pp. 263- 266.
- [12] J. Lunden, V. Koivunen, A. Huttunen, and H.V. Poor, "Collaborative Cyclostationary Spectrum Sensing for Cognitive Radio Systems," *IEEE Trans. Signal Process.*, vol. 57, no. 11, pp. 4182-4195, Nov. 2009.
- [13] T. Yucek and H. Arslan, "A survey of spectrum sensing algorithms for cognitive radio applications," *IEEE Communications Surveys & Tutorials*, vol. 11, no. 1, pp. 116-130, First Quarter 2009.

- [14] D. Cabric, S. Mishra, and R. Brodersen, "Implementation issues in spectrum sensing for cognitive radios," in *Proc. Asilomar Conf. Signals, Syst. Comp.*, Nov. 2004, Pacific Grove, CA, vol. 1, pp. 772–776.
- [15] E. Blossom, "GNU radio: tools for exploring the radio frequency spectrum," *Linux Journal*, vol. 2004, no. 122, June 2004.
- [16] M. Ettus, "Universal software radio peripheral." [Online]. Available: "www.ettus.com".
- [17] M. McHenry, E. Livsics, T. Nguyen, and N. Majumdar, "XG dynamic spectrum sharing field test results," in *Proc. IEEE Int. Symp on New Frontiers in Dynamic Spectrum Access Networks*, Dublin, Ireland, Apr. 2007, pp. 676–684.
- [18] I. F. Akyildiz, W. Y. Lee, M. C. Vuran, and S. Mohanty, "NeXt generation/dynamic spectrum access/cognitive radio wireless networks: A survey," *Computer Networks*, vol. 50, issue 13, 15 Sept. 2006, Pages 2127-2159.
- [19] H. Urkowitz, "Energy detection of unknown deterministic signals," *Proc. IEEE*, vol. 55, no. 4, pp. 523- 531, Apr. 1967.
- [20] H. Tang, "Some physical layer issues of wide-band cognitive radio systems," in *Proc. 1st IEEE Int. Symp. New Frontiers in Dynamic Spectrum Access Networks (DySPAN '05)*, pp.151-159, 8-11 Nov. 2005.
- [21] E. Axell and E.G. Larsson, "Optimal and Sub-Optimal Spectrum Sensing of OFDM Signals in Known and Unknown Noise Variance," *IEEE J. Sel. Areas Commun.*, vol. 29, no. 2, pp. 290-304, Feb. 2011.
- [22] A. Sahai, N. Hoven, and R. Tandra, "Some fundamental limits on cognitive radio," in *Proc. 42nd Allerton Conf. Commun., Control, and Computing*, Monticello, Illinois, Oct. 2004, pp. 1-11.
- [23] A. Fehske, J. Gaeddert, and J.H. Reed, "A new approach to signal classification using spectral correlation and neural networks," in *1st IEEE Int. Symp. New Frontiers in Dynamic Spectrum Access Networks (DySPAN '05)*, 8-11 Nov. 2005, pp. 144-150.
- [24] W. A. Gardner, "An introduction to cyclostationary signals," in *Cyclostationarity in Communications and Signal Processing*, pp. 1 - 90, NY :IEEE Press, 1994.
- [25] J. Whitehead and F. Takawira, "Blind adaptive multiuser detection for periodically time varying interference suppression [DS-CDMA system applications]," *IEEE Wireless Commun. and Networking Conf.*, 13-17 Mar. 2005, vol.1, pp. 273- 279.
- [26] J. Adlard, "Frequency Shift Filtering for Cyclostationary Signals," Ph.D. Dissertation, University of York, 2000.

- [27] C. Cordeiro, K. Challapali, D. Birru, and N. S. Shankar, "IEEE 802.22: the first worldwide wireless standard based on cognitive radios," *1st IEEE Int. Symp. on New Frontiers in Dynamic Spectrum Access Networks (DySPAN '05)*, 8-11 Nov. 2005, pp. 328-337.
- [28] F.F. Digham, M.S. Alouini, and M.K. Simon, "On the energy detection of unknown signals over fading channels," in *IEEE Int. Conf. Commun., 2003 (ICC '03)*, 11-15 May, vol.5, pp. 3575- 3579.
- [29] E.W. Weisstein, "Marcum Q-Function." [Online]. Available: "<http://mathworld.wolfram.com/MarcumQ-Function.html>".
- [30] W. S. Jeon, D. G. Jeong, J. A. Han, G. Ko, and M. S. Song, "An efficient quiet period management scheme for cognitive radio systems," *IEEE Trans. Wireless Commun.*, vol. 7, no. 2, pp. 505-509, Feb. 2008.
- [31] S. Shellhammer and R. Tandra, "Performance of the power detector with noise uncertainty," in IEEE 802.22-06/0134r0, July 2006. [Online]. Available: "http://ieee802.org/22/Meeting_documents/2006_July/22-06-0134-00-0000Performance-of-the-power-detector-with-Noise-Uncertainty.ppt".
- [32] J. Wang, T. Chen, and B. Huang, "On spectral theory of cyclostationary signals in multirate systems," *IEEE Trans. Signal Process*, vol. 53, no. 7, pp. 2421- 2431, Jul. 2005.
- [33] A.V. Dandawate and G.B. Giannakis, "Statistical tests for presence of cyclostationarity," *IEEE Trans. Signal Process.*, vol. 42, no. 9, pp. 2355-2369, Sep. 1994.
- [34] S. Haykin, *Adaptive Filter Theory*, 4th ed. Delhi, India: Pearson, 2007.
- [35] W.A. Gardner, "Representation and estimation of cyclostationary processes," Ph.D. Dissertation, Dep. elec. Comput. Eng., Univ. Massachusetts, Amherst, MA, 1972. [Online]. Available: "<http://www.dtic.mil/cgi-bin/GetTRDoc?AD=AD753125&Location=U2&doc=GetTRDoc.pdf>".
- [36] O.A. Y. Ojeda and J. Grajal, "Adaptive-FRESH filters for compensation of cycle-frequency errors," *IEEE Trans. Signal Process.*, vol. 58, no. 1, pp. 1-10, Jan. 2010.
- [37] W.A. Gardner and S. Venkatraman, "Performance of optimum and adaptive frequency-shift filters for co-channel interference and fading," in *Proc. 24th Annu. Asilomar Conf. Signals, Syst., Comput.*, Pacific Grove, CA, Nov. 5-6, 1990, pp. 242-247.

- [38] J. Zhang, K.M. Wong, Q. Jin, and Q. Wu, "A new kind of adaptive frequency shift filter," in *1995 Int. Conf. on Acoustics, Speech, and Signal Process., 1995 (ICASSP-95)*, 9-12 May, vol. 2, pp. 913-916.
- [39] J. Zhang, K.M. Wong, Z.Q. Luo, and P.C. Ching, "Blind adaptive FRESH filtering for signal extraction," *IEEE Trans. Signal Process.*, vol. 47, no. 5, pp. 1397-1402, May 1999.
- [40] J. Whitehead and F. Takawira, "Low complexity constant modulus based cyclic blind adaptive multiuser detection," in *7th AFRICON Conf. in Africa (AFRICON 2004)*, 17-17 Sept. 2004, vol. 1, pp. 115-120.
- [41] O.A. Y. Ojeda and J. Grajal, "Cyclostationarity-based signal separation in interceptors based on a single sensor," in *IEEE Radar Conf. (RADAR '08)*, May 2008, pp. 1-6.
- [42] H. Saggarr and D.K. Mehra, "Cyclostationary Spectrum Sensing in Cognitive Radios Using FRESH Filters," presented at *ICEIT National Conf. on Advances in Wireless Cellular Telecom.*, 14-15 Apr. 2011, New Delhi, India.
- [43] K. Fazel and S. Kaiser, "Implementation Issues," in *Multi-Carrier and Spread Spectrum Systems*, West Sussex, England: Wiley, 2003, pp. 15-23.
- [44] D. Vučić, M. Obradović, and D. Obradović, "Spectral correlation of OFDM signals related to their PLC applications," in *Proc. 6th Int. Symp. Power-Line Commun. (ISPLC '02)*, Athens, Greece, Mar 27-29, 2002.
- [45] Yakun Hu and Dapeng Wu, "Frequency shift filter-based multi-carrier transceiver," *Wireless Communications and Mobile Computing*, 30 Mar 2011 [Online]. Available: "<http://onlinelibrary.wiley.com/doi/10.1002/wcm.1119/full>".
- [46] J.G. Proakis, *Digital Communications*, 4th ed. New York, NY: McGraw Hill, 2011.
- [47] P.D. Sutton, K.E. Nolan, and L.E. Doyle, "Cyclostationary Signatures in Practical Cognitive Radio Applications," *IEEE J. Sel. Areas Commun.*, vol.26, no. 1, pp. 13-24, Jan. 2008.
- [48] B. F. Boroujeny, "OFDM Versus Filter Bank Multicarrier," *IEEE Signal Processing Magazine*, vol. 28, no. 3, pp. 92-112, May 2011.